Analysis of Hockey Blade Dynamic Behavior using Digital Image Correlation (DIC)

By

Adrien Gerbé

Department of Mechanical Engineering McGill University Montréal, Québec, Canada

A thesis submitted to McGill University in partial fulfillment of the requirements of the Degree of Masters in Engineering (M.Eng).

December 2016

© Adrien Gerbé 2016



The student enjoying the Japanese culture and mountains.

Photo taken at the top of Rusutsu Resort, on the island of Hokkaido, Japan, in March 2015.

Acknowledgements

I would first like to thank my parents, Brigitte and Olivier. Thank you for pushing me to do what I love and for always believing in me. I would have never made it this far without your support and I will be forever grateful. I love you both very much.

I would also like to thank Dr. Larry Lessard for giving me the opportunity to work on such an interesting project. Thank you for your advice and input, it has been greatly appreciated. A particular thank you to Dr. David Pearsall for allowing me to work with the Ice Hockey Research Group (IHRG). The financial support and the weekly feedback and meetings allowed me to stay focused on the task at hand. Thank you as well to Dr. Luc Mongeau and the Canadian Foundation for Innovation (CFI) thanks to whom the DIC equipment was made available to me.

A big thank you to our beloved lab mate turned Research Assistant, Philippe Renaud. Your help with all the testing sessions was invaluable and I definitely wouldn't have been able to do this without you. Thank you as well to Burnett Johnston for introducing me to the art of DIC. I would also like to thank all of the students who were present in the IHRG lab on a regular basis: Jaymee, Spencer, Dan, Dave, Other Dan and Aleks. Thank you for coping with me when no walking was allowed during the testing sessions. It's been a pleasure to work alongside all of you and you've managed to make the lab a fantastic place to work in.

Last but not least, I would like to thank all of my friends for supporting me throughout this endeavor. It wasn't always easy but it's thank to you all that I managed to pull through. You were always available for awesome trips, bike rides, park laps or touring adventures and it has helped me keep my sanity.

Abstract

Hockey stick manufacturers are constantly working on improving the handling and shooting performance of their sticks. Although the effects of shaft properties on shot outcome are relatively well understood, little research has been done focusing specifically on the behavior of the hockey stick blade during a shot. The geometry and construction of the blade affect the stick feel perceived by players, and is expected to influence blade displacement and deformation when undergoing impact with a hockey puck. It is for these reasons that a precise and reliable method is needed to study the dynamic behavior of the hockey blade during actual shots. In this research, the three-dimensional digital image correlation (3D-DIC) was used to study blade behavior throughout slap shot events. Six highlevel hockey players took slap shots with four sticks with different blade and construction combinations and images of the blade were recorded using high-speed cameras. The images were processed to obtain displacement and strain data for each blade during dynamic testing, and the displacement accuracy and strain resolution of the system were assessed through static testing. Statistically significant differences between blade types were identified for shot velocity and maximum strain values. Moreover, the strain along the blade length was found to be significantly lower than the shear strain and strain along the height of the blade. Significant differences between subjects were also found, which emphasizes the effect of subject technique and variability between shots.

Résumé

Les manufacturiers de bâtons de hockey travaillent constamment à améliorer la performance des bâtons au niveau des tirs et du maniement. L'influence des propriétés du manche du bâton sur les résultats d'un tir sont assez bien connues; malgré cela, peu de recherche consacrée spécifiquement au comportement de la palette durant un tir a été réalisé. La géométrie et la construction de la palette ont une influence sur la sensation ressentie par le joueur lors du maniement du bâton, et devrait donc aussi affecter la déformation et le déplacement de la palette lors d'un tir. C'est pour ces raisons qu'une méthode fiable et précise est requise pour étudier le comportement dynamique de la palette lors de tirs. Pour ce faire, la technique de corrélation d'image en trois dimensions (3D-DIC) fut utilisée dans cette étude pour analyser la palette lors de lancers frappés. Six joueurs de hockey de haut calibre ont exécuté des lancers frappés avec quatre bâtons possédant des palettes avec différentes constructions et géométries. Les images ont été captées avec des caméras haute-vitesse et les images ont été traitées pour obtenir des données sur le déplacement et la déformation de la palette. La précision du système a été mesurée au travers de tests statiques. Des différences statistiquement significatives entre types de palettes ont été identifiées au niveau de la vitesse des tirs et de la contrainte maximale. De plus, la contrainte de la palette sur sa longueur est plus importante que la contrainte de cisaillement ou la contrainte sur la hauteur. Des différences significatives ont aussi été identifiées entre sujets, ce qui met l'emphase sur les effets de la technique et la variabilité entre chaque tir.

Table of Contents

Acknowle	edgen	nents	II
Abstract	•••••		III
Résumé .	•••••		IV
Table of (Conte	nts	V
List of Fig	gures .		X
List of Ta	bles		XII
1. Intr	roduct	tion	1
1.1.	The E	volution of the Ice Hockey Stick	1
1.2.	Digita	Il Image Correlation (DIC)	3
1.3.	Motiv	vation	5
1.4.	Objec	tives	5
1.5.	Thesis	s Organization	6
2. Lite	erature	e Review	7
2.1.	Hocke	ey Stick Design	7
2.1.1	l. 7	The Slap Shot	7
2.1.2	2. [NHL Requirements and Regulations	9
2.1.3	3.	Shaft Design	11
2.3	1.3.1.	Geometry	11
2.3	1.3.2.	Construction	12
2.:	1.3.3.	Shaft Static Properties	14
2.3	1.3.4.	Shaft Dynamic Properties	16

2.1	.4.	Blade Design	18
2	2.1.4.1.	Geometry	19
2	2.1.4.2.	Construction	20
2	2.1.4.3.	Blade Static Properties	22
2	2.1.4.4.	Blade Dynamic Properties	22
2.1	.5.	Finite Element Analysis	24
2	2.1.5.1.	Current Models	24
2	2.1.5.2.	Limitations	25
2.2.	Three	e-Dimensional Digital Image Correlation (3D-DIC)	26
2.2	.1.	Principle	26
2.2	.2.	Camera Selection	29
2.2	.3.	Speckle Pattern	31
2	2.2.3.1.	Pattern Selection	31
2	2.2.3.2.	Pattern Application	32
2.2	.4.	Stereoscopic Arrangement	33
2.2	.5.	Technique Validation	36
3. Im	naging	System	38
3.1.	Imag	ging Hardware and Stereoscopic Arrangement	38
3.1	.1.	Camera System	38
3.1	.2.	Support Frame	40
3.1	.3.	Lenses and Field of View	41
3.1	.4.	Stereo Angle	43
3.1	.5.	Lighting	44
3.2.	Data	Collection and Pre-Processing	47
3.3.	Svste	em Calibration	47

	3.4.	Sum	mary	50
4.	San	nple	Preparation for DIC	52
	4.1.	Stick	c Characteristics	52
	4.2.	Spec	ckle Pattern Theory	54
	4.2.1	1.	Calculations	54
	4.2.2	2.	Speckle Pattern Generator	56
	4.3.	Pilot	t Testing	56
	4.3.1	1.	Static Testing	56
	4.3.2	2.	Dynamic Testing	60
	4.4.	Арр	lication of Speckle Pattern	62
	4.4.1	1.	Spray Paint Tests	63
	4.4.2	2.	Stencil Fabrication	64
	4.4.3	3.	Speckle painting	66
	4.5.	Disc	ussion	67
5.	Sta	tic Te	esting	69
	5.1.	Stick	s Static Testing Apparatus	69
	5.1.1	1.	Stick Support	71
	5.1.2	2.	Blade Deformation	72
	5.1.3	3.	Displacement Measurement	73
	5.2.	Test	ing Procedure	74
	5.3.	Data	a Processing & Results	75
	5.3.1	1.	Measured Out-of-Plane System Accuracy	76
	5.3	3.1.1.	Dial Gauge Orientation Vector	76
	5.3	3.1.2.	Point Displacement Vector	80

	5.3.1.3.	Measured out-of-plane system accuracy results	81
	5.3.2.	VIC-3D Measured System Accuracy	83
	5.3.2.1.	Displacement Accuracy	83
	5.3.2.2.	Strain Resolution	86
	5.3.3.	VIC-3D Calculated System Accuracy	87
	5.4. Disc	ussion	89
_	D	. Taskin a	0.1
6.	Dynami	c Testing	91
	6.1. Part	icipants and Equipment	91
	6.1.1.1.	Participants	91
	6.1.1.2.	Equipment Tested	92
	6.2. Test	ing Setup	92
	6.3. Test	ing Procedure	94
	6.3.1.	Paperwork	94
	6.3.2.	Warm-Up	95
	6.3.3.	Dynamic Trials	95
	6.3.3.1.	Systematic Calibration	95
	6.3.3.2.	Data Collection	96
	6.3.3.3.	Data Pre-Processing	96
	6.4. Data	Processing	97
	6.4.1.	VIC-3D Processing	97
	6.4.2.	Matlab Processing	100
	6.4.3.	Statistics	101
		ılts	
	6.5.1.	Visual Representation	
	6.5.2.	Displacement Error	104

	6.5.3.	Shot Velocity	105
	6.5.4.	Blade Velocity	106
	6.5.5.	Strain Values	108
	6.5.5.1.	Maximum strains	108
	6.5.5.2.	Strain Delay	110
	6.5.5.3.	Correlation with puck and blade velocity	112
6.	6. Disc	ussion	112
7.	Conclusi	ion	115
7.	1. Futu	re Work	116
Refe	erences		117
Арр	endix A: S	Static Testing Detailed Results	122
aaA	endix B: P	Pre-Screening Questionnaire and Consent Form	126

List of Figures

Figure 1.1: Bauer Vapor 1X ice hockey stick [4]	1
Figure 2.1: The phases of the slap shot motion [6]	9
Figure 2.2: NHL regulations for ice hockey stick dimensions [26]	10
Figure 2.3: Sample composite hockey stick shaft cross-section	12
Figure 2.4: Bauer Vapor APX hockey stick shaft construction [7]	13
Figure 2.5: Hockey stick shaft major and minor axis [6]	15
Figure 2.6: Hockey blade geometrical characteristics [36]	19
Figure 2.7: Bauer Vapor APX hockey stick blade construction [7]	21
Figure 2.8: Stereo vision schematic [13].	27
Figure 2.9: Camera orientation diagram [48].	34
Figure 2.10: Stereo angle representation	34
Figure 2.11: Effect of stereo angle and lens focal length on strain measurements [39]	36
Figure 3.1: Photron FASTCAM MC2 cube cameras and processor [52]	39
Figure 3.2: Support frame and cameras	41
Figure 3.3: Influence of stereo angle on FOV	44
Figure 3.4: Lighting arrangement	46
Figure 3.5: Calibration image.	48
Figure 4.1: Blade patterns P1 (top) and P2 (bottom)	54
Figure 4.2: Image capture of 4mm speckle pattern during static testing.	57
Figure 4.3: Comparison of AOI and data point coverage	59
Figure 4.4: Test speckle patterns using modified spray nozzle	64
Figure 4.5: Speckle pattern stencil	65

Figure 4.6: Blade with base coat and stencil prior to speckle painting	66
Figure 4.7: Final blade with speckle pattern.	67
Figure 5.1: Static testing setup	70
Figure 5.2: Static testing blade displacement applicator.	72
Figure 5.3: Stick with displacement applicator and dial gauge for static testing	74
Figure 5.4: Blade and reference plane initial frame processed data	77
Figure 5.5: Reference plane data points metric node export.	78
Figure 6.1: Dynamic testing setup	93
Figure 6.2: VIC-3D representation of the tensile strain along the X-direction (ϵ_{xx}) for b	olade
P1-CB1	. 102
Figure 6.3: Tensile strain along the X-direction (ϵ_{xx}) for blade P1-CB1 plotted using Ma	ıtlab
	. 103
Figure 6.4: Average blade velocity through a slap shot for each stick tested	. 107

List of Tables

Table 4.1: Blade geometric properties	53
Table 4.2: Speckle static testing results	58
Table 4.3: Speckle dynamic testing results	62
Table 5.1: Measured out-of-plane system accuracy results	82
Table 5.2: VIC-3D measured system displacement accuracy results	85
Table 5.3: VIC-3D measured system strain resolution	86
Table 5.4: VIC-3D calculated system displacement accuracy	88
Table 6.1: Displacement error Sigma averaged for each stick	05
Table 6.2: Average shot velocity per stick10	05
Table 6.3: Average blade velocity at puck impact per stick10	80
Table 6.4: Maximum strain values averaged for each stick	09
Table 6.5: Statistical results for comparison of strain types1	10
Table 6.6: Strain delay between frame at puck impact and frame at maximum strain 1	11

1. Introduction

Ice hockey is a team sport mainly practiced in the northern hemisphere in countries where winter is usually accompanied by colder temperatures allowing for outdoor ice skating. In Canada in particular, it is very popular across the country both at the professional and amateur levels. From local leagues to professional teams playing in the National Hockey League (NHL), the desire to perform has led to a great evolution in almost all aspects of the game, including training, coaching as well as design and manufacturing of equipment used to practice the sport [1].

1.1. The Evolution of the Ice Hockey Stick

In order to play ice hockey, different types of equipment are required. These can be divided into three main categories: protective equipment, skates and sticks. Protective equipment regroups everything that is used to protect the player from impacts; from helmets to shin guards, and gloves to shoulder pads. The ice hockey skates are used to ensure players' locomotion on the ice, allowing for acceleration, gliding and stopping on the low friction surface. The hockey stick is the final essential piece of equipment as it allows for handling of the puck, enabling the player to pass and shoot in order to achieve the objective of scoring goals against the opposing team [1-3].



Figure 1.1: Bauer Vapor 1X ice hockey stick [4].

The ice hockey stick has an "L" shaped geometry, as illustrated in Figure 1.1, and is made of a combination of a shaft and a blade which are connected together in the "hosel" area via either a one-piece construction, or a two-piece construction involving a hollow shaft and tapered blade glued together [5].

Hockey sticks were initially made of a wooden construction with the shape of the stick being carved out of a single piece of wood [6]. By the 1920s, two-piece sticks began appearing on the market and soon became the norm [7]. Manufacturers began experimenting with various materials, and through the 1950s players saw the apparition of wooden stick constructions combined with fiberglass coatings to increase strength of shafts and blades. At that point, the important characteristics of the hockey sticks were limited to weight and geometric specifications of both shaft and blade [3]. In the 1960s, some players began experimenting with blade geometry by heating the blades and introducing a curvature. This allowed for better puck handling and shooting, increasing shot precision and velocity [3, 8]

By the end of the 1980s, as manufacturing methods improved and the interest for lighter and stiffer sticks came about, hockey sticks gradually transformed and aluminum made its mark as the best suited material for the shaft construction, combining stiffness and lightness [2, 9, 10].

In the last decades, the development of composite materials has led to their application in a wide variety of fields, including the sports industry, and in particular ice hockey equipment manufacturing. Composite materials are now found in protective equipment, skates and sticks, which has had a great impact on the performance and design possibilities associated with these products. These new materials allow for new complex stick structures to be developed, combining rectangular shell construction for the shaft with sandwich

construction for the blade. Moreover, the introduction of composite materials permits fine tuning of a multitude of parameters, catering precisely to players needs and preferences.

With ever-growing diversity in constructions and geometries of hockey sticks, and especially hockey stick blades, the need for efficient and accurate ways to simulate hockey stick behavior has kept growing. Finite Element Analysis (FEA) models have been developed in order to accelerate the Research & Development (R&D) process [11, 12], but a major part of stick design still relies on prototype testing by professional athletes, which can prove both time consuming and inconsistent. A new technique to study blade behavior throughout a dynamic event is therefore needed in order to better the understanding of the effects of blade construction and geometry on its dynamic behavior, and possibly increase the reliability of FEA models.

1.2. Digital Image Correlation (DIC)

Digital Image Correlation (DIC) is a non-contact, image-based technique used to obtain full-field measurements of samples. This technique allows for precise shape measurements as well as the study of the mechanical behavior of materials undergoing deformation. The first developments in the field of image-based measurements came with the introduction of the photogrammetry technique around 1850 [13]. With improvements in the field of photography and the introduction of digitized images in the 1960s, the first investigations into DIC made their apparition, initially with the goal of extracting positional information from aerial photographs through a combination of photogrammetry and vision-based algorithms. At first, the developments in the DIC technique were led by particular interests for the technology in fields of research such as medicine and microscopy. Despite the

progress made with DIC in the 1960s and 1970s, the engineering applications of the technique remained limited due to the great interest in new laser measurement technologies such as laser speckle photography and interferometry. However, the difficulties encountered with the laser technologies combined with great developments in DIC led researchers in the field of experimental solid mechanics to investigate the technique for deformation measurements. In 1983, Sutton et al. [14] were the first to conduct experiments and combine numerical algorithms with recorded images to prove the feasibility of what is known nowadays as 2D-DIC. Through the following years, numerous studies continued in the same direction to validate the use of 2D-DIC for translational and rotational rigid body motion measurements [15] as well as deformation in solids [16]. Further work was done up to now to improve the speed and reliability of the process through improvements in the algorithms used with the technique.

Despite the strength of the 2D-DIC technique, an important source of error remains and is associated with the influence of out-of-plane displacements on the accuracy of the 2D measurements [13]. In order to account for this type of error associated with material behavior such as buckling, the introduction of a three-dimensional measurement technique was necessary. Prior to the development of 2D-DIC, photogrammetry had been used extensively to quantify shape and motion of sample objects, and the idea of combining this technique with the principles of DIC was introduced gradually between 1970 and 1990 [13]. In 1993, two studies were published proposing similar techniques to study three-dimensional deformation of objects using a stereo-vision system capturing images of samples with a grid pattern [17] or a random speckle pattern [18]: modern 3D-DIC was born. As for the 2D-DIC, the three-dimensional technique has evolved ever since to improve its

speed and robustness and allow for applications to fluid mechanics for example, and can also be used to accurately track an object undergoing rigid body motion.

3D-DIC is now used for a number of applications ranging from material characterization [19] to the improvement of numerical simulation models for aerospace applications [20].

1.3. Motivation

The primary motivation for this research was to apply a new technique to study the dynamic behavior of a hockey blade undergoing dynamic deformation. With increasingly complex sandwich construction for hockey blades, it would be a significant step in hockey stick design research to be able to correctly assess blade behavior and identify differences based on blade construction and geometry. This would allow for the optimization of hockey blade design in order to obtain the desired characteristics required for athletes playing different positions in the hockey game. Moreover, the data collected can prove useful to improve the current FEA models. Since the blade motion throughout a shot varies from shot to shot and from player to player, having a databank of shots where the blade can be tracked through space would allow for a more accurate and realistic simulation of a shot.

1.4. Objectives

The objectives of this project were to investigate the feasibility of applying DIC to study dynamic blade behavior while ensuring this technique could be applied in the hockey stick manufacturing industry. This would be achieved through the following steps:

a. Determine a fast, reliable and repeatable method to prepare blade samples for DIC.

- b. Determine the accuracy of the DIC apparatus through blade static testing.
- c. Determine the feasibility of capturing good quality images of hockey stick blade motion using high-speed cameras.
- d. Compare the error associated with the static and dynamic tests to ensure quality of the dynamic data.
- e. Study the effects of blade construction and geometry on dynamic behavior of the hockey stick blade throughout a slap shot task.

1.5. Thesis Organization

In order to fulfill the objectives listed above, as well as to maintain coherence in the work achieved, this thesis is divided into the following chapters. Chapter 2 is a review of the literature relevant to ice hockey stick design and DIC techniques. In this chapter the characteristics of hockey stick shaft and blade will be explained and an overview of the DIC principles and important considerations for successful application of the technique will also be detailed. Chapter 3 discusses the imaging system setup and its calibration as well as the preliminary processing of images obtained. Chapter 4 details the work behind the preparation of the blade samples, from determining the right speckle pattern for DIC to applying it on the different blades. Chapter 5 provides details on conducting the static testing, the data processing and the associated results. Chapter 6 describes the dynamic testing, going over the methods used to obtain the data and interpretation of the results. Finally, Chapter 7 provides a conclusion and a review of the major contributions as well as future work to consider.

2. Literature Review

In order to successfully achieve the objectives detailed in section 1.4, it is important to understand what has been done both in hockey stick and DIC research. A good understanding of current hockey sticks characterization methods and knowing the limits of FEA dynamic models is required. Moreover, the extensive research done in the field of DIC will prove useful in order to optimize the apparatus used for static and dynamic testing of the sticks.

2.1. Hockey Stick Design

The design of hockey sticks takes into account a multitude of factors from regulations set in place by the NHL to feedback from athletes, and considers the work done by numerous researchers in the field. The following section is a comprehensive literature review of the work that has been done in the field of hockey stick design and manufacturing, and includes an overview of the intricacies of the slap shot technique, the restrictions in stick geometry at the competitive level, the important aspects in designing blades and shafts and a look at the Finite Element modeling of an ice hockey slap shot.

2.1.1. The Slap Shot

The hockey stick is used by the player as an extension to his arms and hands, allowing him to manipulate the puck as desired to pass, receive or shoot the puck, as well as steal the puck from the opposite team's players [1]. The main focus of scientific studies has been directed towards shooting skills as they are the primary means of scoring goals in a game and have a strong influence on the overall performance of a player [21]. A multitude of

factors can influence the outcome of a shot, including forces exerted by the player, bladepuck contact time, stick velocity, stick bending, stick stiffness, stick mass and the efficiency in energy transfer from elastic energy from shaft loading to kinetic energy of the puck [22, 23].

The two most commonly used shooting techniques are the slap shot and the wrist shot. Numerous studies have used a variety of techniques to measure puck velocity, including high speed cameras, light traps, accelerometers and radar guns, with values ranging from 22 to 44 m.s⁻¹ for the slap shot and 13 to 22 m.s⁻¹ for the wrist shot [1].

Wu et al. directly analyzed the slap and wrist shot techniques by looking at the maximum vertical force applied by the stick on the ice as well as the maximum bending of the stick during a shot. It was found that the shaft bending angle and vertical force applied was greater for the slap shot than for the wrist shot [24].

The technique of the slap shot involves grasping the hockey stick with two hands, one at the butt end of the stick and the other 40 to 60 cm below, and creating a rapid rotational and translational motion from side to side similar to a pendulum path [6]. Refer to Figure 2.1 below for a visual representation. The motion can be divided into six phases: backswing, downswing, preloading, loading, release and follow-through [2, 6, 24, 25]. The most interesting phases relating to blade behavior occur when the stick is in contact with the ice, from preloading to release of the puck, as the stick is rapidly loaded and deforms to a great extent.

By confirming the presence of greater impact forces and shaft deformation in the slap shot compared to the wrist shot, this lead to the conclusion that studying the slap shot dynamic motion should lead to greater differences in blade behavior compared to the wrist shot. Therefore, the following sections of this literature review will focus on information related to the slap shot task relevant to this study.

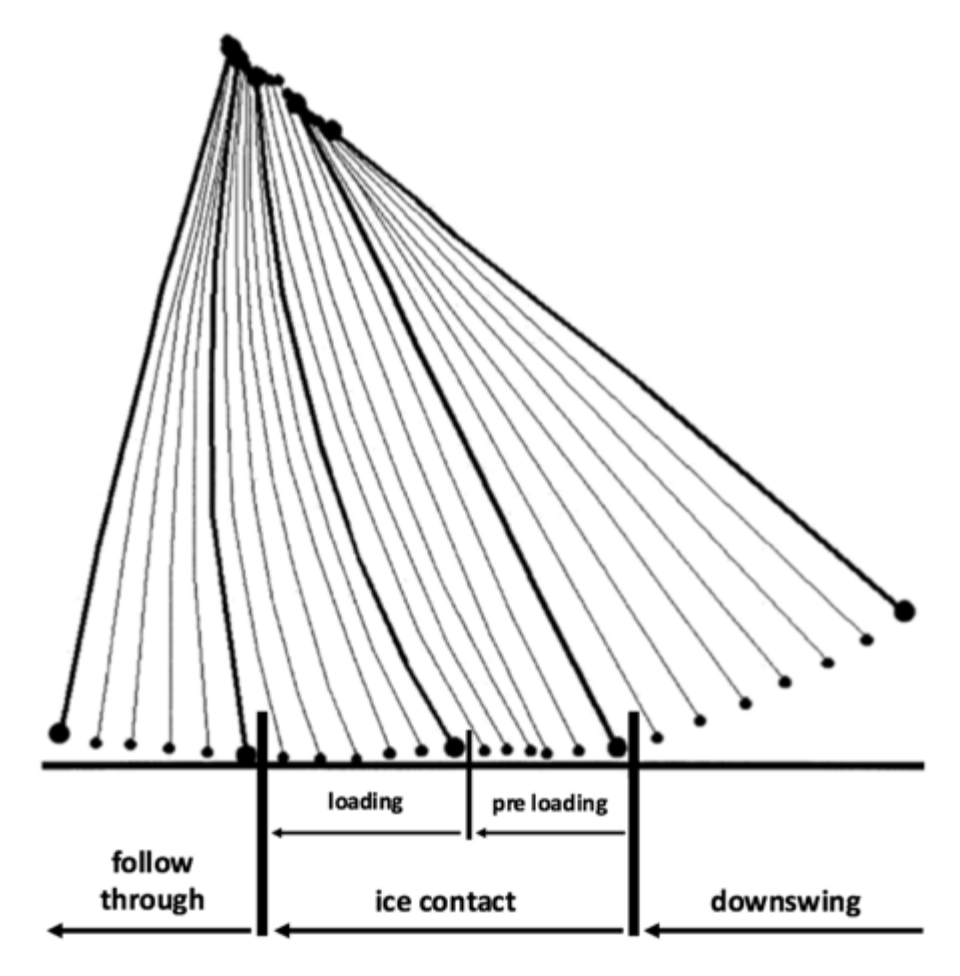


Figure 2.1: The phases of the slap shot motion [6].

2.1.2. NHL Requirements and Regulations

Every year the National Hockey League (NHL) publishes its Official Rulebook, where the rules and regulations of the game are stated, with which high-level athletes must comply [26]. This encompasses rules of play but also strict requirements regarding the player's equipment. In terms of a player's hockey stick, the relevant regulations, illustrated in Figure 2.2 below, are as follows:

- Stick must be made of a material approved by the NHL (includes carbon fiber and a multitude of foams).
- Shaft must have a maximum length of 63 inches (160 cm).
- Blade must have a maximum length of 12.5 inches (31.75 cm).
- Blade must have a height between 2 and 3 inches (5.08 and 7.62 cm).
- The curvature of the blade must not exceed 0.75 inch (1.9 cm).

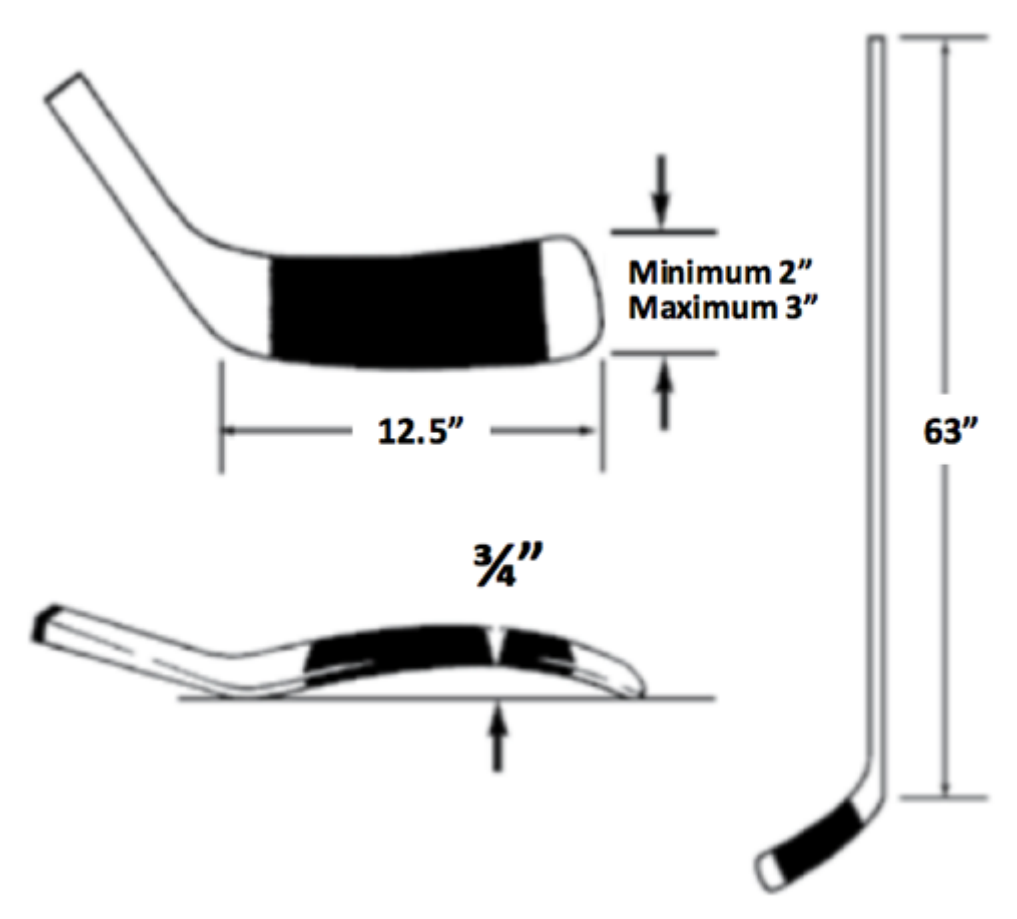


Figure 2.2: NHL regulations for ice hockey stick dimensions [26].

These regulations are used to ensure players' safety as well as to avoid unfair advantages. The shaft and blade specifications can be modified in terms of material, stiffness, wall structure, coating and color. The geometrical restrictions for the blade are such that customization of the blade geometry to the player's preference remains possible.

These regulations regarding hockey stick design may vary depending on the league in which an athlete may play, but manufacturers tend to follow these guidelines as it is a recognized standard across the globe.

2.1.3. Shaft Design

An essential part of the hockey stick is the design of the hockey stick shaft. Although this study focuses on blade behavior, a lot more research has been done on shaft properties. The research that has been done relating to shaft design properties can prove insightful in terms of static and dynamic testing and its applications to blade design.

2.1.3.1. <u>Geometry</u>

The general geometry of the shaft is a beam of rectangular cross-section. Its length limitations have been mentioned previously, but the size of the cross-sectional area is up to the manufacturer's discretion. It must be easy to hold in the hand while wearing hockey gloves, and must be beveled at the corners to prevent injuries [26].

The shaft has been reported to have a thickness between 19 and 25 mm (minor axis) and a width between 28.6 and 30 mm (major axis) [1-3, 11]. Modern composite shafts are hollow, and the wall thickness varies between manufacturers, and can be modified to obtain a desired shaft stiffness.

To improve handling and cater to players' preferences, the walls of the shaft can be designed to have concave, convex or straight geometry. To further customize the stick and increase players' performance, the shaft can be tapered in certain locations and the thickness of the walls can be modified to alter the location of the kick point along the stick (point of maximum deflection of the shaft during a shot) [27]. The effects of these changes on stick

dynamic behavior are not fully understood, and manufacturers rely on players' feedback to fine tune the stick characteristics.

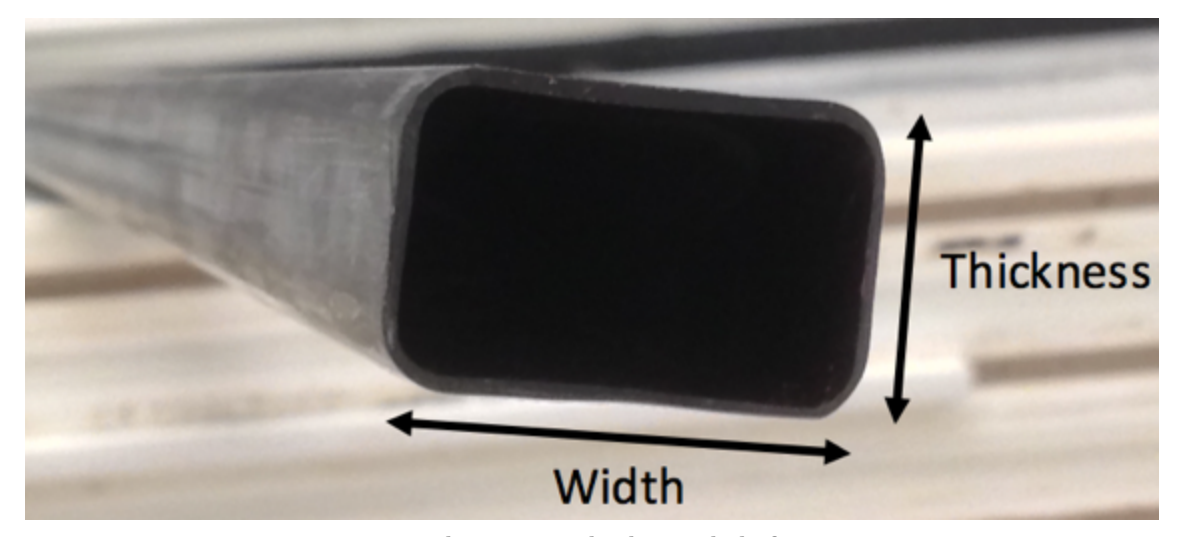


Figure 2.3: Sample composite hockey stick shaft cross-section.

2.1.3.2. <u>Construction</u>

The construction of a composite shaft varies between each manufacturer, as well as between models of a same manufacturer. Most companies have proprietary designs and the details are rarely released to the public. It is known however that most modern high-end hockey sticks are one-piece composite sticks made of carbon, Kevlar, graphite (low modulus carbon fibers) or fiberglass fibers with a polymer resin [27, 28]. This type of construction allows for lighter and stiffer shafts, while allowing for customization to any player's specification, particularly at the professional level. Composite shafts are also more durable and better maintain their properties over the life of the stick compared to regular wood construction. Moreover, the use of composite materials enables manufacturers to obtain less variability during manufacturing, which isn't the case with natural materials [27-29].

Figure 2.4 shows an example of shaft construction for a Bauer high-end composite hockey stick [7]. It is assumed that most manufacturers use similar constructions, varying the number of plies and their orientation (referred to as ply layup), the materials used as well as geometric properties of the shaft.

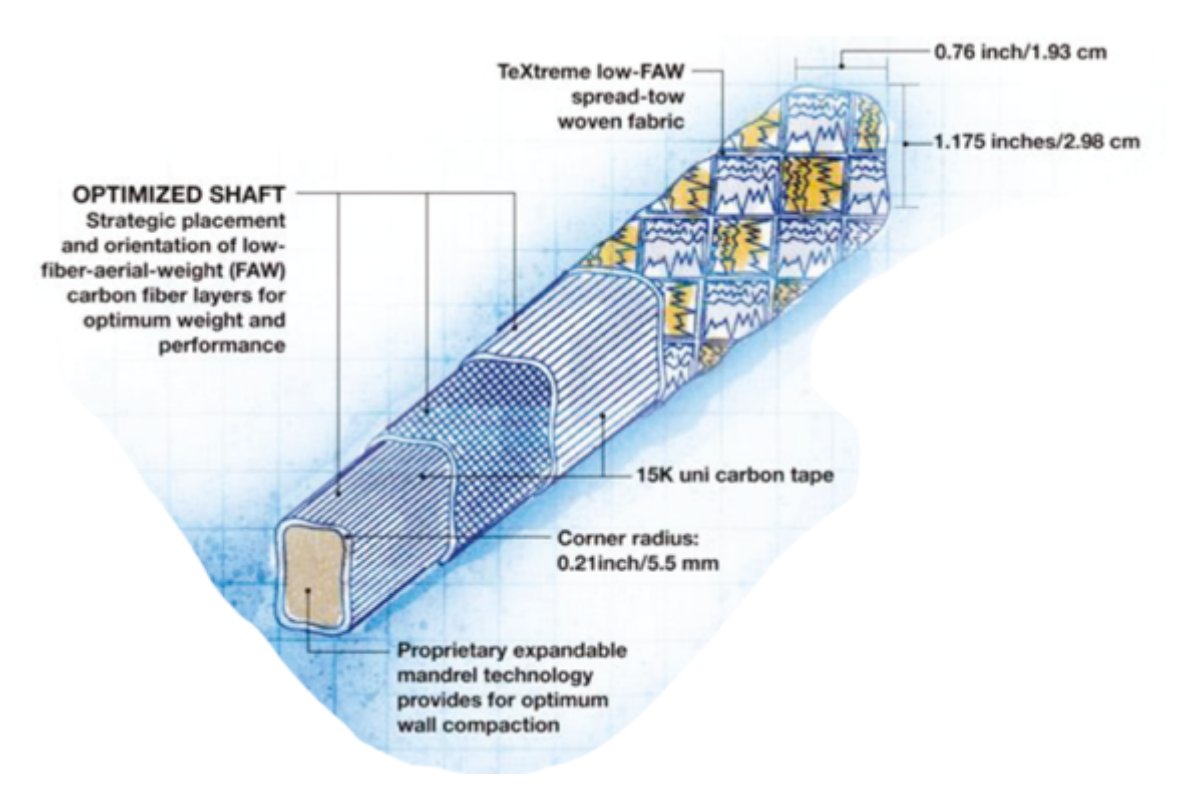


Figure 2.4: Bauer Vapor APX hockey stick shaft construction [7].

For this particular model, the shaft is made of carbon fiber unidirectional prepreg tape, with varying orientation of the prepreg layers with respect to one another. The number of layers and their orientation varies throughout the stick to be able to control its bending properties. The prepreg tape is said to have high strength, standard modulus and low fiber aerial weight, and is supplied by Mitsubishi (Chiyoda-ku, Tokyo, Japan). The outer layer of the stick is made of a material known as FAW100 TeXtreme© Spread Tow fabric. It is a spread-tow woven fabric manufactured by Oxeon AB (Borås, Sweden), which is impregnated with a proprietary resin system called eLASTech. This resin system is specific to Bauer and

is said to be a toughened epoxy resin incorporating carbon nanotubes and thermoplastic nanoparticles [7].

Although dating back to the release of the Bauer Vapor APX hockey stick in 2011, the current high-end sticks from Bauer still incorporate eLASTech resin and TeXtreme© fabric [4]. Despite improvements made in stick design and construction, the shaft construction detailed above is still relevant and representative of the current hockey sticks available on the market, with materials and proprietary designs varying between manufacturers.

2.1.3.3. Shaft Static Properties

One of the most common properties used to characterize hockey sticks is the shaft linear stiffness, commonly referred to as shaft "flex". The flex rating of a stick corresponds roughly to the amount of force, measured in pounds force (lbf), required to deflect a stick by 1 inch along the shaft major axis in a three-point bending test (refer to Figure 2.5 below for visual representation of the major and minor axis of the hockey shaft). The flex value of a stick can range anywhere from 40 to over 110, and is chosen by the player depending on weight, height, style of play and personal preference [30]. No specific standard restricts manufacturers when determining the flex ratings of the sticks, meaning that for a similar flex rating the actual shaft stiffness might differ slightly.

Behrmann et al. have studied the static properties of two sticks with similar flex ratings coming from different manufacturers. They have come to the conclusion that the two sticks did not have similar bending properties despite their close flex ratings (87 and 90 flex) [31].

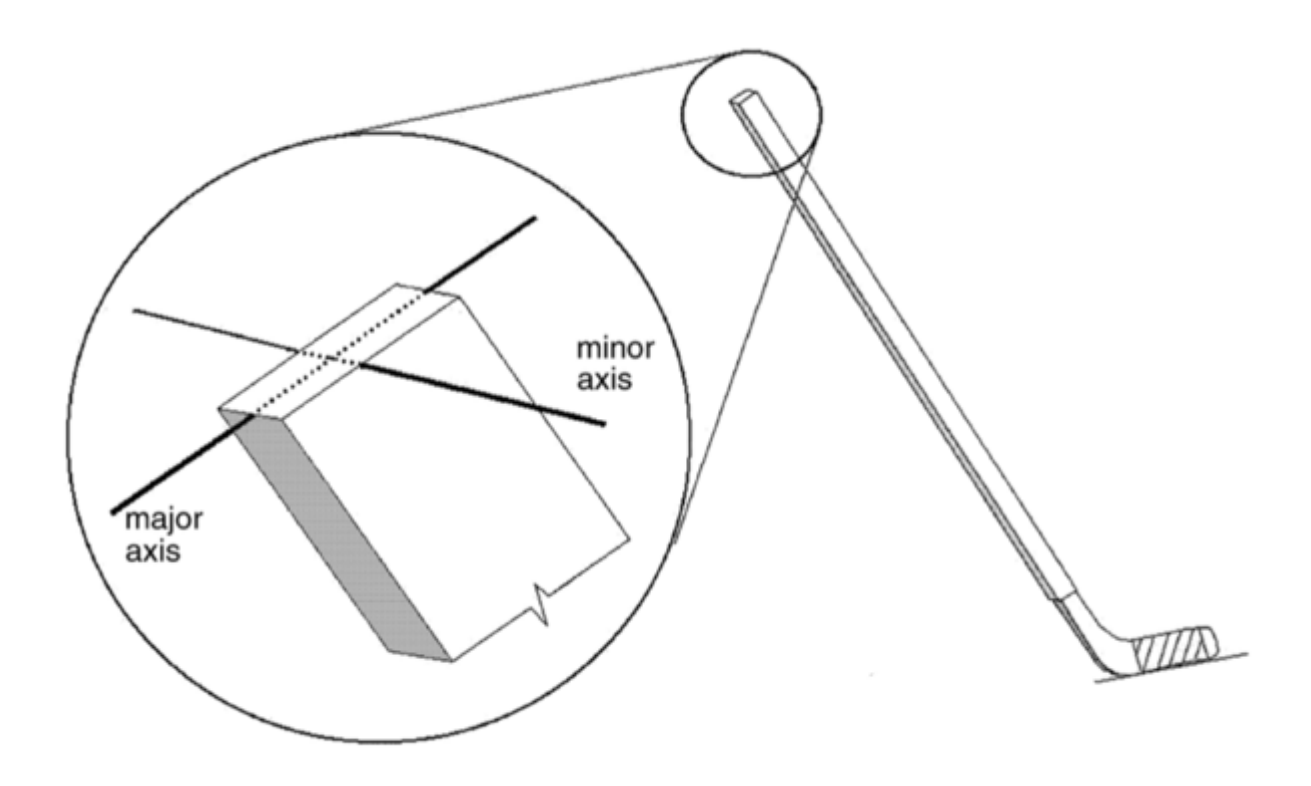


Figure 2.5: Hockey stick shaft major and minor axis [6].

A number of studies have looked at shaft linear stiffness in one way or another, whether for simple characterization of hockey sticks or to study the effects of shaft stiffness on dynamic properties of the hockey stick. Two techniques have been used: the cantilever beam method [9, 28, 31-33] and the three-point bending test [6, 24]. Both techniques have allowed for determining the distinction between shaft linear stiffness based on material and flex ratings. They are both valid, but since this type of testing has not been standardized, the comparison between studies is hard to achieve. Nevertheless, the following conclusions can be extracted:

- No significant differences in shaft linear stiffness exist depending on material, as all shafts can be manufactured to obtain a specific linear stiffness [9, 10].
- Despite inconsistencies in linear stiffness properties across manufacturers, the "flex" rating of a stick still gives a good estimate of shaft stiffness [33].

Another shaft property which has been studied, but to a lesser extent, is the torsional characteristic. The rotational stiffness of the shaft can be of great importance to the overall stick behavior due to the "L" shape of the stick. A few studies have investigated the torsional properties of the hockey stick shaft, arriving to the following conclusions:

- Composite shafts have the greatest rotational stiffness compared to aluminum shafts (2nd greatest) and wooden shafts [10, 28].
- Composite shafts' linear stiffness does not correlate to rotational stiffness [31].

The relationship between static properties of the hockey stick shaft and dynamic behavior is still not fully understood. The "stick feel" perceived by players is hard to characterize as it combines many proprioceptive senses related to stick dynamic behavior and influential factors that have yet to be identified.

2.1.3.4. <u>Shaft Dynamic Properties</u>

While some correlations between shaft static testing and stick performance can be found, studying the dynamic properties of the shaft would lead to more interesting results. Since the flex rating of the shaft is an important factor for many players, studying the effect of shaft linear stiffness on dynamic deformation of the shaft throughout a shot has been the subject of interest of many studies.

Dating as far back as 1976, Roy and Doré studied the effects of shaft linear stiffness on the dynamic behavior of the hockey stick in wrist and slap shots. They identified differences in maximum flexion of the shafts depending on shot type and shaft linear stiffness characteristics [34].

More recently, Pearsall et al. investigated the matter using high-speed video recording and reflective markers, testing four sticks with varying linear stiffness. The use of this

technology allowed for the identification of differences in peak angular deflection of the shaft and time to peak deformation depending on shaft stiffness [6].

Using a similar experimental setup, Wu et al. studied the effect of player skill on the dynamic deformation of the shaft during a standing slap shot, highlighting that skilled players were able to bend the stick more than unskilled players [24]. Similarly, Villaseñor et al. used high-speed video to study stick movements and deformation throughout a standing slap shot task; they were able to estimate the bending and recoil (unbending) phases of the shaft, showing differences in timing and duration of shaft bending and recoil phases depending on player skills [25]. These two studies show that shooting technique has an important effect in shot outcome, which cannot be neglected.

In order to increase data accuracy and identify shaft deformation characteristics not possible with high speed video, Magee et al. developed a portable strain measurement system to measure shaft strain deformation during dynamic stick handling tasks [35]. Bending and torsional strain along the major axis were measured both on and off-ice with consistent strain profiles, confirming robustness of the technique. Hannon et al. used a similar strain gauge instrumented stick, in combination with reflective markers and infrared motion capture cameras, to study the shaft dynamic strain profile and the effect of shaft stiffness and player skills [23]. Similar conclusions to previous studies were reached, and the point of maximum deflection of the shaft was identified to be close to the lower hand.

Shafts made of composite materials being stiffer than wooden ones, the subject of shaft vibration has become increasingly relevant to the field of hockey stick design. It has been claimed by players that the increased stiffness of composite shafts leads to a poor "stick feel" [27], which is undesirable and reduces the player's ability to efficiently control the puck.

Anderson et al. conducted a modal analysis of several wood and composite sticks, reporting lower first bending mode natural frequencies for wooden sticks, which are said to provide a better "feel". This gives some insight into a possible correlation between low bending frequency and improved stick "feel", which could be relevant to blades as well [27].

Finally, it is of great interest for manufacturers to replicate as realistically as possible the dynamic behavior of a slap shot through semi-static testing in a laboratory setting. Worobets et al. tried to tackle this problem by analyzing stick deformation through a standing slap shot task and replicating shaft maximum deformation on a workbench while measuring applied forces. The information extracted was used to calculate the energy stored, lost and returned by the shaft, and no correlation with shaft stiffness was found [32].

The most important factor mentioned in these research papers has been the effect of player skill and technique on shaft dynamic behavior, showing high variability between players. Despite some general trends being highlighted (i.e., stiffer shaft means less deformation), the intricate relationship between shaft construction and the effects on dynamic behavior is still not fully understood.

2.1.4. Blade Design

In a similar manner to shaft design, the design of the blade plays an important role in the performance of a hockey stick. The blade geometry can be modified to adapt to players' preferences and style of play. Modern hockey blade construction is more complex than the shaft since a number of different materials can be used for the blade core. This poses an interesting design challenge with numerous possibilities when it comes to material selection and layout within the blade structure. Both blade geometry and construction ultimately affect the stick "feel" perceived by the player.

2.1.4.1. Geometry

As mentioned in section 2.1.2, the NHL sets regulations regarding the maximum and minimum dimensions of the hockey blade. Despite these restrictions, there are many geometrical characteristics of the blade that can be altered to improve puck handling and shooting. Roy & Doré studied the geometrical characteristics of 14 different hockey sticks and identified variations in blade length and height ranging from 4 to 14%, and as high as a 50% difference for blade curvature [3].

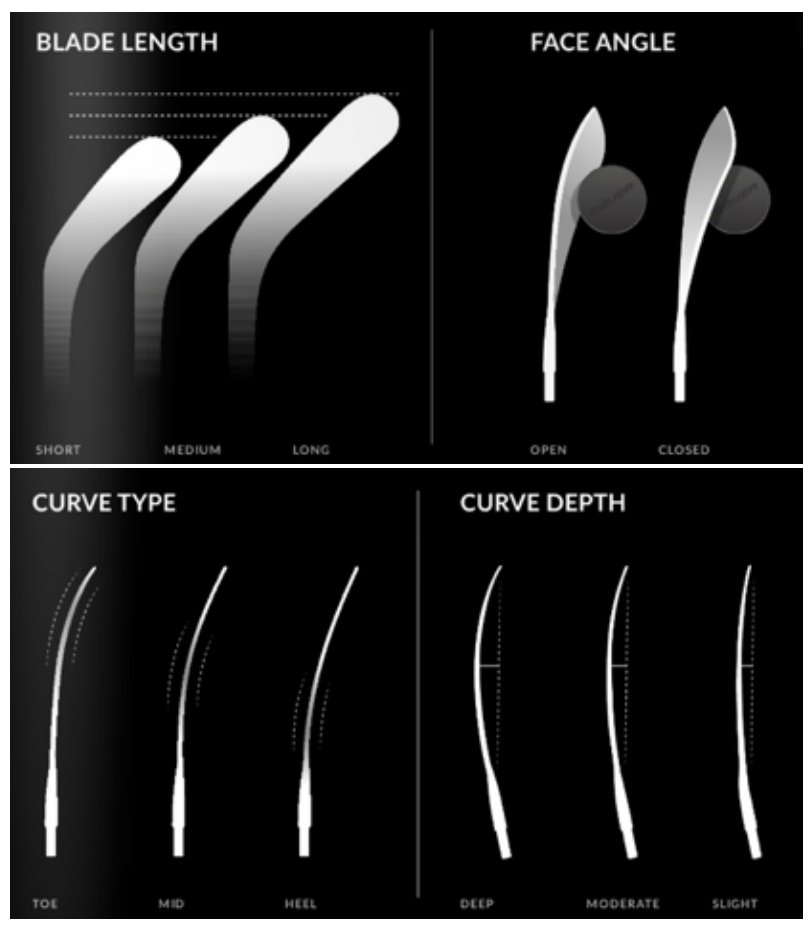


Figure 2.6: Hockey blade geometrical characteristics [36].

The blade geometry (or "blade pattern") is characterized by the blade length, the face angle (open to closed), the curve type (from heel to toe), the depth of the curve (0 to 1.9 cm) and the shape of the toe (round or square) (refer to Figure 2.6 above) [1, 36].

Blade patterns are specific to manufacturers and have an important effect on the feel and behavior of the stick.

2.1.4.2. <u>Construction</u>

As is the case for shaft construction, the blade construction varies between manufacturers as well as between blade patterns and stick models from the same manufacturer. It is important to note that only a few scientific studies have focused on blade design and its effect on stick behavior, which leads to a lack of literature regarding blade construction characteristics. Moreover, the fact that most designs are proprietary information further reduces the amount of information publicly available. The most relevant information can be found on manufacturers' websites and in certain sports magazines; in both cases, no specific details are revealed.

It is known, however, that composite blades are made of a sandwich construction. The outer shell is usually made of a similar material as the shaft, namely carbon, Kevlar, graphite or fiberglass fibers with a polymer resin. The blade core can be made of different types of foam, epoxy, plastic and silicon combinations and the layout of the core material can be modified to obtain different blade properties [7, 22]. This type of construction allows for customization of the blade properties but also involves a complex design process where the effects of the different materials are not perfectly understood.

Figure 2.7 below shows an example of blade construction for a Bauer high-end composite hockey stick [7]. As for the shaft construction, it is assumed that most

manufacturers use a similar type of construction, varying the materials, ply layup and geometric properties of the blade. For this model, the outer shell of the blade is made of the same materials as the shaft, a combination of carbon fiber unidirectional prepreg tape inner layers with an outer layer of TeXtreme© Spread Tow fabric. The blade core is made of two different types of foam: a low-density polymethacrylimide (PMI) foam used in low impact locations, namely the heel of the blade and the shaft-blade intersection, and a high density epoxy foam with high shear strength for the regions of the blade that experience puck impacts [7].

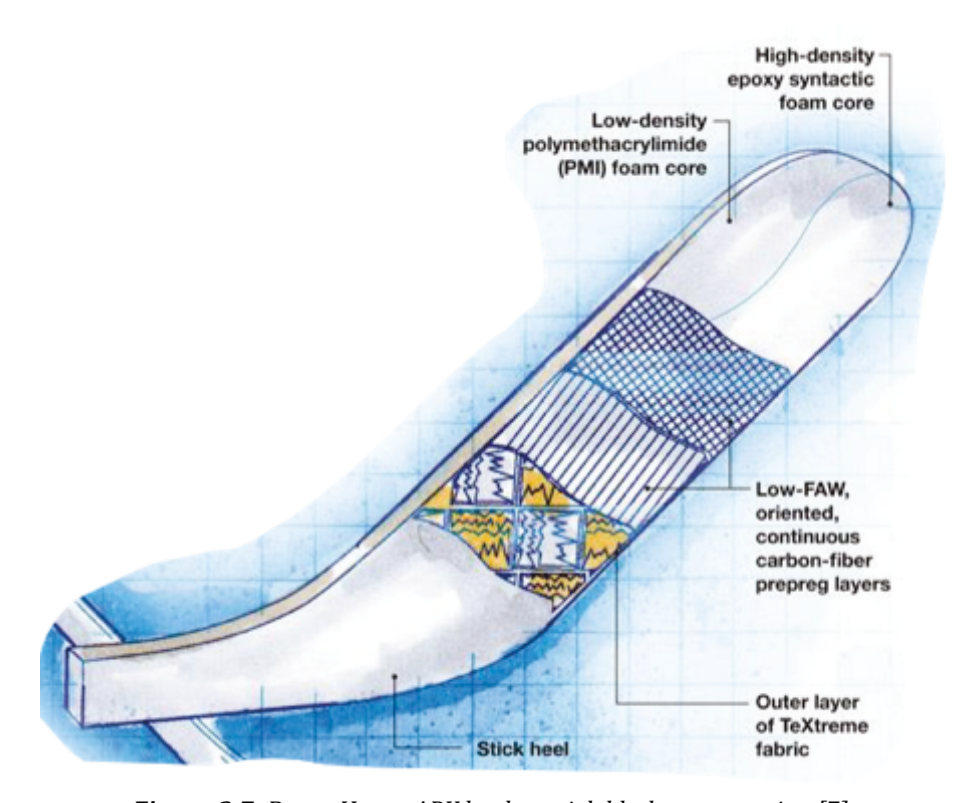


Figure 2.7: Bauer Vapor APX hockey stick blade construction [7].

Although this information dates back to 2011, the current Bauer hockey sticks still incorporate TeXtreme© fabric and are said to have new and improved foam cores [4]. The blade construction detailed above is still representative of the current blade constructions, with slight differences in materials used for the blade core.

2.1.4.3. <u>Blade Static Properties</u>

The static properties of blade have not been investigated to a great extent in literature, and it is not particularly well understood how these relate to blade dynamic behavior and the feeling perceived by the player.

Behrmann et al. and Kays & Smith have included the blade in their static measurements of shaft stiffness and came to the conclusion that the linear stiffness of the entire stick was typically twice as high at the heel compared to the toe of the blade [31, 33]. These two studies give a slight insight into the influence of the blade properties, but are not sufficient to draw any significant conclusions.

In a paper detailing their work to develop a numerical simulation of a hockey slap shot, Kays & Smith used a three-point bending test to determine the bending stiffness of three fiberglass blades. They found that the blade stiffness was about a third of the shaft stiffness, at 5kN.m⁻¹ and 15kN.m⁻¹ respectively [11].

Simard et al. investigated the static properties of both shaft and blade for composite and wooden hockey sticks. Similar values as Kays & Smith were found for the composite blade stiffness (5 kN.m⁻¹). The torsional properties of the blade were also investigated by applying a torsion load to the blade with the heel clamped. The composite blades were reported to have lower torsional stiffness than the shafts, with 20 – 22 versus 68 – 106 Newtons per degree-of-rotation respectively [28].

2.1.4.4. <u>Blade Dynamic Properties</u>

A number of studies have taken an in-depth look at the blade and its behavior throughout a slap shot, focusing on blade-puck contact times, the effects of impact location,

the movement of the puck along the blade, the ground forces involved as well as the blade orientation and velocity throughout the stages of a slap shot.

To identify blade-puck contact times, researchers have resorted to video analysis, electrical circuits on the blade, tape on the blade and chalk on the puck as well as accelerometers within the puck. Throughout these investigations, it has been reported that the blade-puck contact time is between 30 to 45 ms [25, 29, 33]. It is also interesting to note that three studies have reported that the blade-puck contact was not continuous, noticing that there can be anywhere from one to four "bounces" of the puck along the blade prior to its release from the stick [25, 28, 33]. Villaseñor et al. have reached the conclusion that the blade-puck contact time has a strong influence on the maximum velocity of a shot [25].

The location where the puck impacts the blade has also been hypothesized to influence the outcome of a shot. Kays & Smith showed that the impact affected the puck velocity, and that puck velocity increased when the puck impacted the blade closer to the toe [33]. Moreover, Simard et al. have shown that on top of "bouncing" multiple times, the puck will travel between 170 to 210 mm along the blade [28]. The combination of puck "bounce" and translation along the blade can explain in part why the importance of puck impact location is hard to quantify, and that an ideal puck impact location has yet to be determined.

The forces applied to the blade have also been investigated, and two similar studies used force platforms to study both vertical and horizontal forces at the blade-ground interface during a slap shot. It was highlighted that high-level players and stiffer shafts had a tendency to generate more vertical force [6, 24].

Using high speed video, markers on the back of the blade, a puck instrumented with an accelerometer and a force platform, Lomond et al. conducted an in-depth study investigating

specifically the blade behavior throughout a slap shot and the effect of player skill. For elite players, the blade velocity had a tendency to decrease between initial ice contact through to puck impact, but increased significantly before leaving the ice. Moreover, there were significant differences in blade orientation patterns between elite and recreational players [22].

No clear conclusions can be extracted from the limited amount of work done on the study of hockey blade properties. This highlights the need for further investigation into the effects of geometry and construction on blade dynamic behavior.

2.1.5. Finite Element Analysis

Numerical simulations and techniques such as Finite Element Analysis (FEA) have become incredibly valuable in the design process of many products, including hockey sticks. As with most of the design process of the stick, FEA models and research in the field remains confidential and specific to each manufacturer.

2.1.5.1. Current Models

To the author's knowledge, only two studies publicly available have tackled the task of creating numerical models to simulate a hockey slap shot [11, 12]. For both models, information extracted from studies relating to static and dynamic properties of hockey sticks were used as well as stick motion throughout a shot.

The numerical simulation involves creating a stick model representing as best as possible the geometry of an actual shaft and blade, including the complex tapers in the hosel region (see Figure 1.1). The static properties of the stick such as shaft and blade stiffness as well as bending frequency need to be measured and the model tuned to match these

measurements as precisely as possible. A puck model also needs to be developed and the ice surface defined.

The dynamic nature of a slap shot involves complex interactions between stick, ice and puck. The motion of the stick can be recorded quite accurately using high speed cameras and trackers, giving information on stick velocity and trajectory. The forces applied between blade and ground have been measured using force plates [6, 24] and hand grip forces have been investigated as well [37, 38]; these can be used as reference input in terms of force application on the stick.

2.1.5.2. Limitations

The hockey slap shot involves a lot of variability between players as well as from shot to shot for the same player. This makes it complicated to duplicate the event in the form of a numerical simulation. In order to have a more accurate representation of the ice hockey slap shot, a number of dynamic shooting studies would have to be combined together. The use of high speed video with markers on the stick and blade, alongside strain gauges and force transducers on the stick, force plate beneath the artificial ice surface, radar gun to measure puck velocity and precise static measurements of the stick properties would be required for accurate comparison of the numerical model with reality. The amount of influential factors involved with such testing makes it hard to develop an accurate representation of the motion that can be validated with dynamic measures.

The influence of material selection for the blade core is hard to predict due to the complex geometry and characterization of the materials. Creating an accurate finite element model of the blade remains a challenge to this day.

This highlights the need for a technique to be developed to improve these models through testing of different blade geometries and construction to further expand the knowledge on the subject and improve the overall performance of hockey sticks.

2.2. Three-Dimensional Digital Image Correlation (3D-DIC)

Three-dimensional digital image correlation is a powerful technique as it allows for displacement and deformation measurements without physical contact with the sample. This is especially useful in the case of impact testing such as a hockey slap shot, as other tools like strain gauges tend to break or separate from the sample under such rapid loading. The following section investigates the main considerations for a successful 3D-DIC study, including the basic principles of the technique and the importance of the speckle pattern and stereoscopic arrangement. Moreover, a brief overview of the validation of the 3D-DIC technique will be discussed including its application to moving samples.

2.2.1. Principle

The basic principle behind 3D-DIC is the use of two cameras capturing simultaneous images of a sample on which a particular pattern has been applied. Through the use of advanced algorithms and sequential images of the sample undergoing testing, its deformation and displacement can be quantified, derived from the changing aspects of the speckle pattern.

One of the drawbacks of images captured using cameras is the transformation of a three-dimensional object into a two-dimensional projection. This leads to a loss of the third dimension, crucial to the study of out-of-plane motion. Similar to human vision, a way to

recover the 3D position of a point is the use of a second camera setup in a stereoscopic arrangement and focused on the same object.

As can be seen in Figure 2.8 below, despite the projection of points Q and R to a single point P on the left camera image, the use of a second camera C' allows for the differentiation of these two points through the capture of the second image from a different perspective [13].

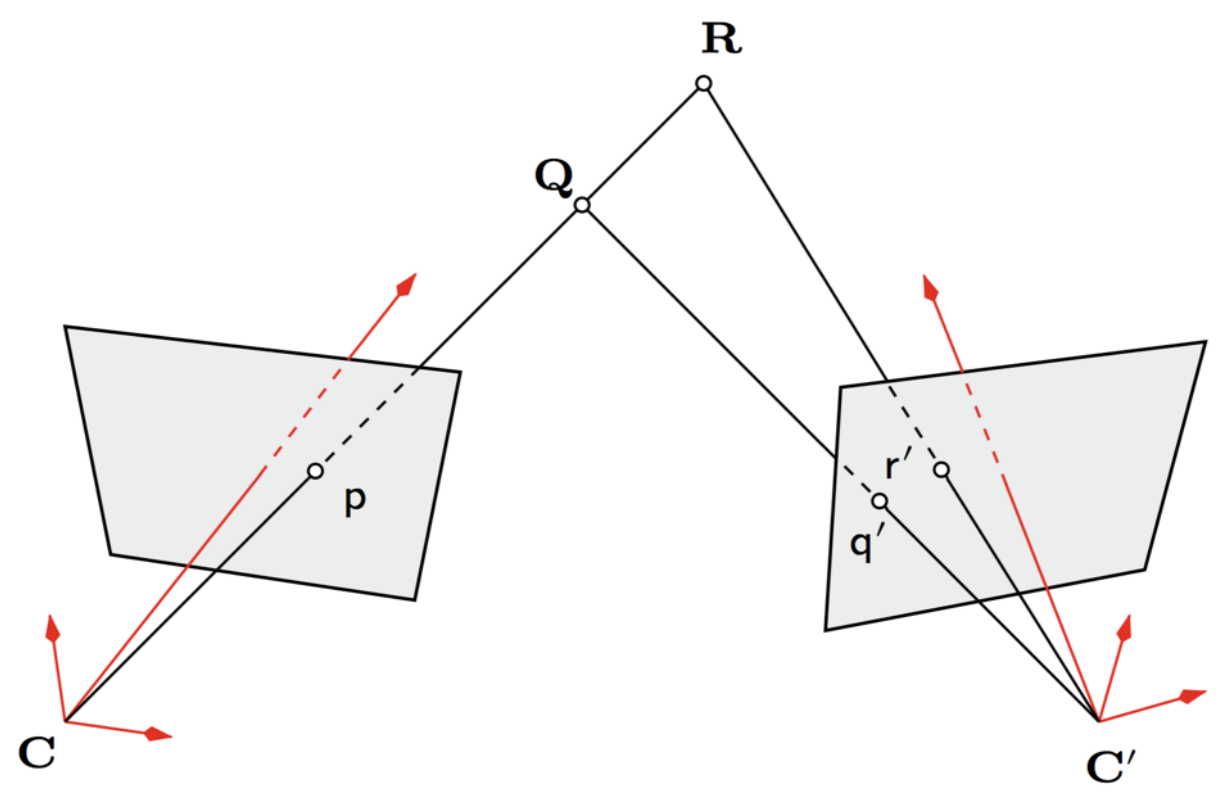


Figure 2.8: Stereo vision schematic [13].

By being able to extract the three-dimensional location of points, it is possible to track an object and its displacement and deformation from a number of sequential images. Although this simple example with two unique points is easy to process, it can become quite challenging to track the displacements of a greater number of data points along a homogeneous surface.

The use of a pair of cameras in a stereoscopic arrangement along with a calibration grid with known specifications allows for 3D reconstruction of the scene within the FOV of the cameras. By calibrating the system using a calibration grid, a reference frame and scale is determined allowing for 3D reconstruction of the undeformed sample based on the first captured image. The processing of the following images of the sample then considers the initial size and shape of the sample to determine its displacement and deformation throughout the dynamic test.

The use of specific patterns on the surface of the sample being studied is key to a successful image correlation, as one of the important principles behind the technique is the tracking of unique features within the captured images. Digital images of the sample are recorded by assigning numerical values to each pixel within the camera sensor (grey value from 0 for black to 255 for white) and the images are then imported into the software for further processing. An area of interest (AOI), within which the image correlation will be carried out, is defined on the image of the undeformed sample and used as reference for subsequent analysis. The AOI is then divided into smaller regions called subsets, within which unique arrangements of pixels can be identified based on their grey value and location with respect to one another. Any deformation or displacement within a subset is averaged to its center to create a data point, and the chosen step size defines the number of pixels separating each of the data points.

Based on the reference image, the sample is studied and possible matches in pixel groups are identified by assigning similarity scores determined by a correlation function [39]. The correlation function is usually based on a sum of the squared differences for the selected pixels [40]. Assuming that the cameras remain fixed, the location and shape of these

unique groups of pixels, combined with the initial 3D reconstruction of the sample, give information on the displacement and deformation of the sample from one image to the next.

As can be expected, the camera and speckle pattern selection, as well as stereoscopic arrangement, all have an important influence on the results of 3D-DIC.

2.2.2. Camera Selection

Due to the fast blade motion encountered in a hockey slap shot, the use of high-speed digital cameras is required for this study. High-speed cameras have been used in a number of studies and have been proven as reliable, particularly for high-speed complementary metal-oxide semiconductor (HS-CMOS) models [41].

There is a great difference in hardware complexity between HS-CMOS and ultra-high-speed intensified charge-coupled device (UHS-ICCD) cameras. The latter usually involves a number of optical elements such as a beam-splitter, numerous fiber optic bundles and photo-multiplier plates, which tend to increase the error in image reconstruction, in turn affecting DIC results. On the other hand, HS-CMOS cameras have relatively simple construction and the main source of error results from lens distortions (also present in UHS-ICCD cameras) which can usually be removed through system calibration [42]. Although the errors associated with UHS-ICCD cameras can be reduced through thorough calibration and correction steps, the variability in displacement and strain is reported to be ten and twenty times higher, respectively, than with HS-CMOS cameras [43].

A HS-CMOS camera is most appropriate for this study as the capture rate should not need to exceed 10,000 frames per second (FPS). This would allow for more accurate images while reducing the cost of the equipment.

The resolution of the DIC system is directly dependent on the field of view (FOV) of the cameras based on lens selection, since data processing relies on pixel information. It has been shown that the system resolution can be as low as ± 0.01 pixel, relating to anywhere from micrometer to centimeter precision depending on the chosen FOV [42, 44]. The resolution of the camera sensor is also important, as it will influence the pixel density in each image captured. The greater the number of pixels, the greater is the pixel density for a similar FOV. Therefore, cameras with higher resolution – $1024 \times 1024 \times 512 \times 512 \times 512$ pixels for example – are preferable, as they allow for increased system accuracy.

Similarly, the error associated with data processing is linked to the quality of the captured images. Obtaining good quality images with sharp details and high contrast can prove to be quite challenging due to the short exposure times (as low as 1 microsecond for HS-CMOS cameras) required with high-speed imaging [41]. Such short exposure times are associated with a need for powerful lights, as high as 1000W, which need to be closely monitored due to the great amount of heat generated [20]. Moreover, the depth of field within which the captured image is in focus is crucial to image quality, particularly for a moving sample. Lenses with fixed focal lengths ranging from 19 to 200 mm have been used successfully and have been shown to provide good quality images [13].

Extensive pilot testing is therefore required to assess the optimal FOV and lens characteristics for this particular study, and can only be determined through trial and error while keeping in mind the general guidelines mentioned above.

2.2.3. Speckle Pattern

A key element of DIC is the quality of the speckle pattern applied on the sample. Once the cameras and FOV have been determined, there are a number of features that need to be considered when creating a speckle pattern: speckle size and density, color contrast, edge sharpness and pattern application technique.

2.2.3.1. <u>Pattern Selection</u>

The most common type of pattern used for DIC is a speckle pattern, which consists of a uniform background, usually white, with a random pattern applied on top, usually black. The objective is to obtain a high contrast in order to accurately identify unique features on the sample. It is important that the pattern be non-repetitive and exhibit no particular orientation in order to obtain accurate full-field measurements in all directions [45].

When deciding upon a specific speckle pattern, it is important to consider the resolution and FOV of the cameras. These two factors will determine the appropriate speckle size needed for correct sampling of the surface. The general rule of thumb dictates that speckle size should represent at least 3 by 3 pixels in the recorded images [13]. A correct speckle size allows for deformation within the speckle to be accurately identified. An approximate speckle size of 3 by 3 pixels has been proven to lead to accurate results in at least two studies [40, 46] and is given as a guideline in support material from a leading DIC equipment manufacturer [45]. Equations to calculate speckle size for specific accuracy and FOV requirements are also given [13] and can be used to calculate an initial guess for speckle size. Choosing a speckle size that is too big can lead to a lack of accuracy in the measurements due to increased subset size. On the other hand, speckles that are too small can lead to

misrepresentation of the deformation of the specimen, a phenomenon known as aliasing [45].

Another important factor is the speckle density, which influences the number of speckles within each subset of the AOI. A subset which is too small can prevent the identification of unique patterns, while a subset too big could lead to erroneous results due to homogenization of the data within a large area of the sample [46]. Once again, a general rule of thumb dictates that each subset should contain at least 3 by 3 speckles [13]. This is supported by studies relating to speckle pattern size and subset selection [40, 46].

In all cases, the emphasis is put on the need for pilot testing to ensure adequate speckle size and subset dimensions to match the specific study and test conditions.

2.2.3.2. Pattern Application

The application of the speckle pattern onto the surface of the test sample can be a rather complicated task. A number of techniques are available for pattern application, depending on the speckle size and nature of the test sample. Such techniques include the use of spray paint, toner, lithography, printing, marker or stencils [45]. The use of black anodizing has also been reported in the case of aluminum plates as test samples for impact testing [41].

The use of toner and lithography is usually associated with small specimens (smaller than 12 mm), which would not be suitable for the study a full hockey blade measuring up to 30cm in length. The printing of speckle patter on vinyl sheet has been successful, but can lead to inaccurate results if the vinyl dissociates from the sample surface [45]. The use of ink, placed with a marker, has also led to great results [47], but can become time consuming for

larger samples and wouldn't be applicable in an industrial context where numerous samples need to be tested regularly.

The use of spray paint is by far the most successful technique, but has the drawback of requiring multiple attempts to achieve the desired pattern [40, 46]. The surface is usually painted with a white base coat, and the speckle pattern applied by modifying the spray nozzle or adjusting the pressure applied.

The most promising technique involves the use of a stencil and spray paint, as it allows for the application of a very specific speckle pattern on large samples and allows for consistent speckle pattern application [45].

The type of paint used is important to consider in order to reduce reflection of light on the surface of the sample. Light reflection will create bright spots in the images, which will prevent the correct representation of the speckle pattern. In order to reduce glare in images, the use of matte paint is suggested [13].

2.2.4. Stereoscopic Arrangement

The stereoscopic arrangement of the cameras, which refers to their orientation with respect to each other, is specific to every experimental setup. It can be determined through pilot testing and the optimal setup will vary from one study to another.

The influence of the stereoscopic arrangement on the accuracy of a DIC system has not been the subject of many studies. It is, however, important to keep in mind the effects of camera orientation with respect to the sample and its expected motion when preparing the stereoscopic setup. If sample motion is expected, it is crucial that the sample remain within

the FOV of each camera throughout the test and that the images captured are not blurry due to a limited depth of field.



Figure 2.9: Camera orientation diagram [48].

The orientation of a camera is defined by three angles: pan, tilt and roll angles (refer to Figure 2.9 above). When cameras are arranged side-by-side, the stereo angle is related to the pan angle of each camera, and represents the angle between the line of sight of each camera, as seen in Figure 2.10 below.

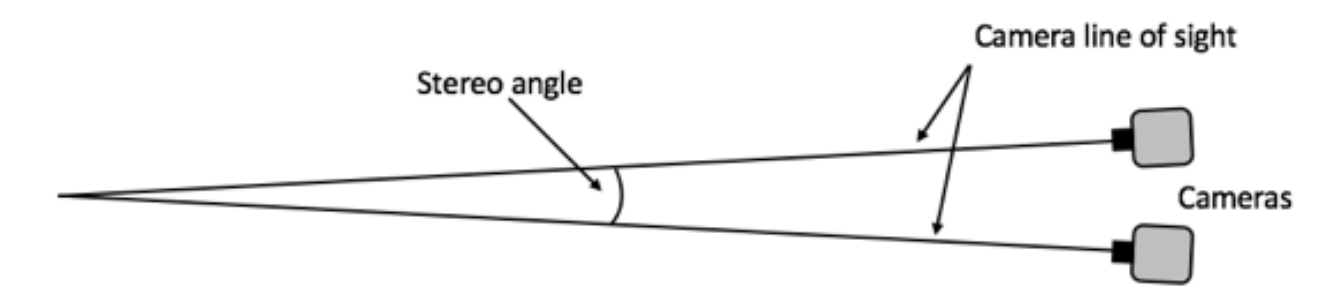


Figure 2.10: Stereo angle representation.

There are guidelines available to ensure accurate measurement, but they are not restrictive and any setup that falls outside of these guidelines can still lead to a successful DIC study. It is suggested that the tilt and roll angles of the two cameras should be as close as possible, and that the cameras be attached in a way that prevents them from moving during testing. Moreover, no modifications should be made to the camera arrangement or focal settings once the system has been calibrated [13].

Finally, a stereo angle between 10° and 30° has been proven to lead to accurate measurements, but smaller or greater angles can still be used at the expense of out-of-plane and in-plane sensitivity, respectively. Increasing out-of-plane sensitivity is directly linked to decreasing in-plane accuracy, and vice-versa. It is important to note that in-plane noise is said to cause 200 times more error than out-of-plane noise, meaning that a good compromise between out-of-plane and in-plane sensitivity needs to be found based on the test setup [13].

The graph presented in Figure 2.11 [39] gives a good approximation of the effects of stereo angle on standard deviation in strain measurements. As mentioned previously, any stereo angle greater than 10° gives good accuracy with any lens. It is interesting to keep in mind that for a lens with focal length greater than 37 mm, the use of a stereo angle below 10° reduces the accuracy of the strain measurements only by a factor of 2, as compared to 5 for smaller focal length. The error associated with the use of a small stereo angle, if deemed necessary based on laboratory setting, could be compensated in part by the use of a longer focal length lens.

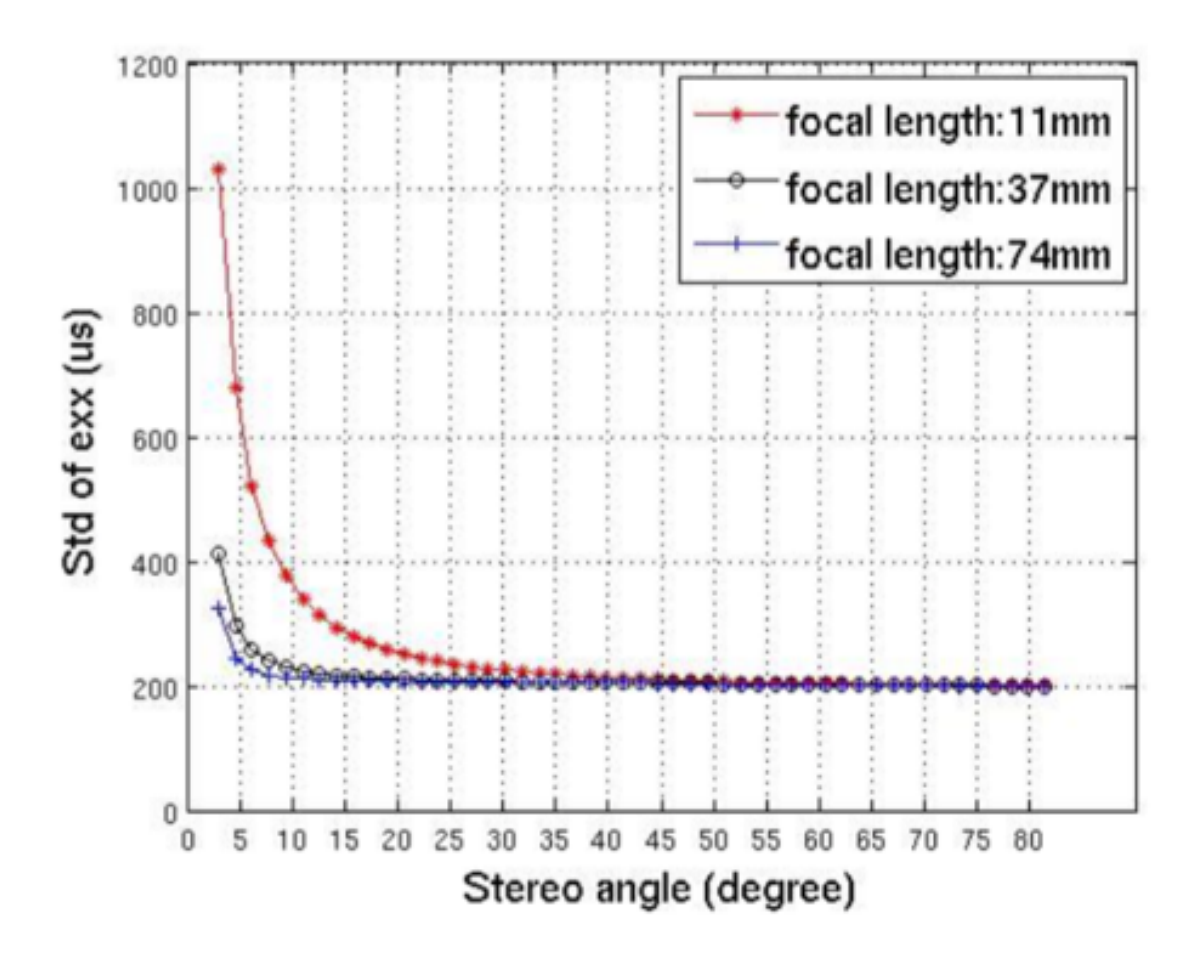


Figure 2.11: Effect of stereo angle and lens focal length on strain measurements [39].

2.2.5. Technique Validation

A number of studies have investigated the validity and accuracy of 3D-DIC regarding both displacement and strain measurements.

It has been reported that the displacement accuracy of a system can range anywhere from 1% to 6% of a pixel depending on camera type and speckle pattern selection [19, 20, 49]. Robert et al. also investigated the displacement resolution (systematic displacement error) by analyzing multiple images of the same undeformed sample and comparing the

results extracted from DIC software. The agreement between values is said to be around 0.5% of a pixel [19]. Moreover, Kirugulige et al. highlighted that neither the amount nor the direction (in-plane versus out-of-plane) of the displacement affected the accuracy of the results, with similar standard deviation results in all test cases [49].

The in-plane strain accuracy related with 3D-DIC study has been reported to be in the range of 30 to 100 micro strain, and had excellent agreement with strain gauge measurements [50, 51]. The work of Robert et al. also proved interesting regarding strain resolution (systematic strain error), as it was highlighted that the size of the strain filter used (relating to the virtual strain gauge length) had a great impact on the resolution of the system. The greater the strain filter (synonym with greater virtual strain gauge size), the smaller the standard deviation, ultimately reaching 0 for a virtual gauge length covering the length of the AOI. The order of magnitude of the strain resolution was identified to be around 10 micro strain, while accuracy was around 100 micro strain [19].

DIC studies involving impact tests can prove challenging when the vibrations transfer to the cameras. Any changes in the camera orientation after calibration needs to be accounted for as it can affect results. Coordinate transformation method, camera orientation recalibration method and image registration method are different techniques that have been proven as successful in mitigating the effects of camera vibrations [41, 43].

3. Imaging System

The imaging system used for this study needs to satisfy a number of conditions based on the dynamic nature of a slap shot, the laboratory conditions and the variability and time constraints present with human testing. The following section discusses the challenges associated with hardware selection, stereoscopic setup, system calibration and data collection.

3.1. Imaging Hardware and Stereoscopic Arrangement

With blade-puck contact times of 30 to 40 ms, the use of high-speed cameras is essential. The rectangular shape of a hockey blade also imposes certain restrictions regarding camera FOV, and as with any high-speed video, correct lighting needs to be determined.

3.1.1. Camera System

Based on the work done in the field of high-speed DIC, the use of HS-CMOS cameras was deemed sufficient. Although any pair of cameras can be used to conduct a DIC study, the synchronization of the cameras is crucial to proper imaging, and a ready-to-use system is ideal to avoid dealing with timing delays. Available within the Department of Mechanical Engineering was a high speed camera system consisting of all the required elements to conduct a 3D-DIC study. The system was acquired via funding from the Canadian Foundation for Innovation (CFI), and was graciously lent by Professor Luc Mongeau for this study. The Photron FASTCAM MC2 10K system (Photron USA, Inc., San Diego, CA) was used and consists of the following elements:

- Two monochrome cube cameras: 10K model, CMOS sensor, lens C-mount.
- Processor module with 7m cables for camera-processor connection.
- Photron FASTCAM Viewer (PFV) software with Gigabit Ethernet PC interface.



Figure 3.1: Photron FASTCAM MC2 cube cameras and processor [52].

The cube cameras are ideal for this type of study as they are small enough (35 x 35 x 33.3 mm) to be mounted almost anywhere, and feature a metallic outer frame with a threaded hole that can be used to attach the cameras to a support frame. The single CMOS sensor with 10 μ m pixels allows for good image quality, avoiding image inaccuracies usually found with UHS-CCD cameras. The presence of a C-mount for lens attachment proved useful as most lenses available within the Department are C-mount compatible and do not require any specific adapters. Last, but not least, the recording speed and resolution of the system is adapted to the dynamic problem at hand. With high blade velocity and short blade-puck

contact times expected with slap shots, a camera with recording speeds up to 10,000 frames per second (FPS) is needed. Although the camera resolution could be higher, 512×512 pixels and 512×96 pixels resolution at minimum and maximum recording speeds, respectively, is sufficient to provide accurate results.

The processor, used to synchronize the two cameras, proved easy to setup, and the 7m cables enable sufficient distance between the shooting location and the computer to avoid any accidents. The Photron system also comes with its own software, the Photron FASTCAM Viewer (PFV) version 3.3.9 (Photron USA Inc., San Diego, CA), which allows instant visualization of the cameras' FOV through a Gigabit Ethernet connection to the computer. This proved extremely useful when it came the time to adjust the FOV and exposure of the cameras and to immediately review the images captured during static and dynamic testing. Moreover, the PFV software allows for control over the camera recording speed and shutter speed, which affects the inter-frame timing and quality of the images captured.

3.1.2. Support Frame

In order to ensure stability of the cameras during testing, an aluminum frame was built, and onto which the two cameras mentioned previously were attached. The frame is 1 foot in height, 2 feet in width and 1 foot in depth, and made out of 1-inch aluminum t-slot extrusions. Locking pivots are used to secure the cameras to the frame, they can be moved from side-to-side and allow for tilt and pan adjustment of the cameras to obtain the desired camera orientation. The height of the support frame is calculated so that when the cameras are attached to it and aimed towards the location of the blade, the cameras are normal to the

back of the blade's surface. As mentioned in DIC literature, it is preferable to have the cameras line of sight normal to the sample surface.

The support frame was set on the floor of the lab, away from the artificial ice surface, to reduce the transmission of vibrations from stick impacts. Two 25 kg weights were also added on top of the frame to prevent frame motion and reduce vibrations. Pilot testing showed that the test setup was adequate and no major motion of the cameras was noticed during slap shots.

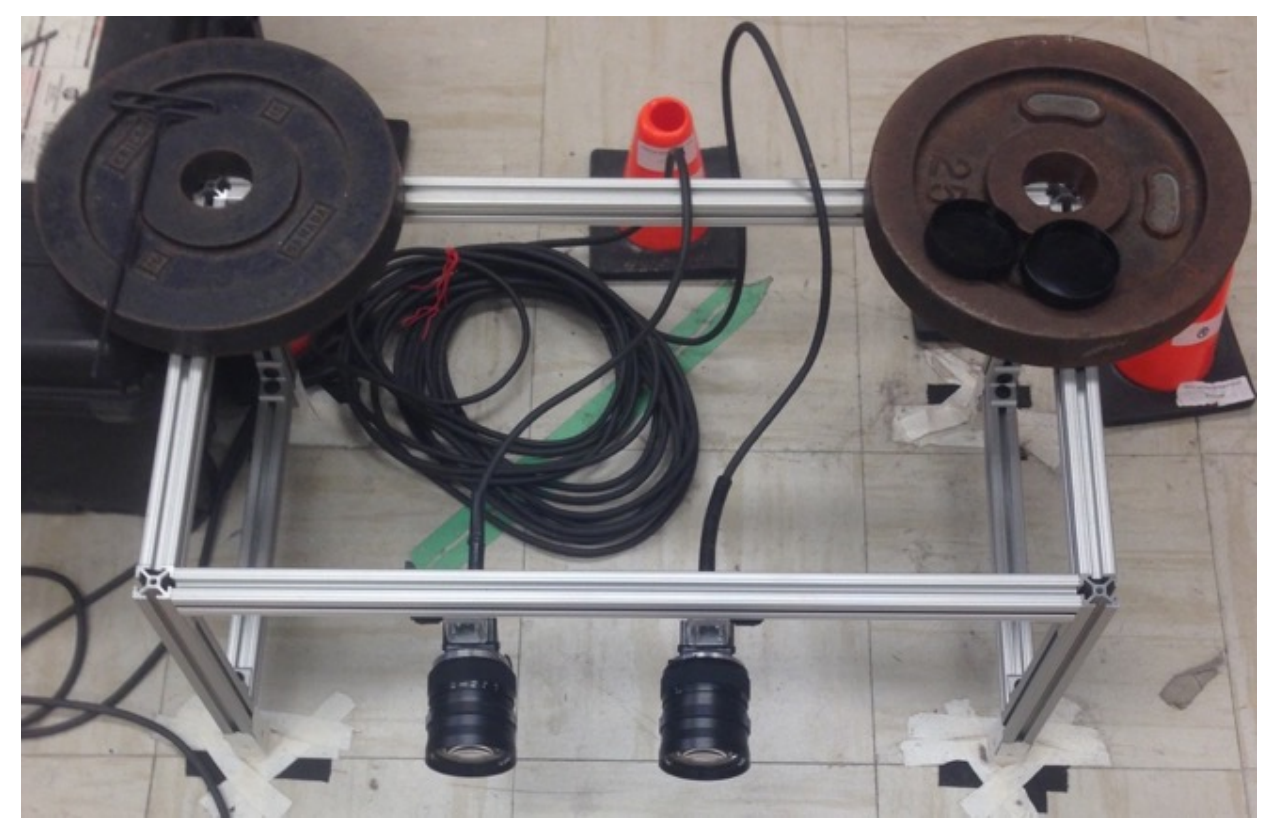


Figure 3.2: Support frame and cameras.

3.1.3. Lenses and Field of View

The lens desired characteristics are based on a few key factors identified during the literature review. It is necessary to consider: the focal length and whether it is fixed or adjustable, the depth of field properties and the aperture limits of the lenses. It is also

preferable to have two identical lenses to simplify the fine-tuning of the stereoscopic setup and ensure correct calibration can be achieved.

The main focus of the lens pilot testing was to find a lens that would allow the blade to be within the FOV of the cameras throughout a shot, from ice impact all the way past puck impact. It is important that the cameras be far enough from the shot location to avoid any impacts from either the puck or the stick during dynamic testing. Moving the cameras away from the shot location also reduces the propagation of vibrations to the cameras, which can affect results. Finally, due to the dimensions of the laboratory where testing was taking place, the cameras could not be placed more than five meters away from the shot location.

In terms of image quality, fixed focal length lenses are preferable as they are known to provide sharper images. The depth of field also has to be long enough so that non-blurry images can be captured throughout the blade motion. A wide range in aperture adjustability is also preferable to ensure adequate contrast and lighting of the images can be obtained.

A number of different lenses combinations were tested, varying from 12.5 to 108 mm, fixed and variable focal length, all with adjustable aperture. A 50 mm fixed focal length lens was initially tested and provided a good FOV with a sharp image. A 12.5-75 mm adjustable focal length lens was set at approximately 50 mm focal length and was tested. It provided lower image quality than the fixed focal length lens. An 18-108 mm lens was also tested but was shown to provide a poor depth of field, unable to focus on the required region.

A combination of two Navitar 50 mm, fixed focal length, f0.95 lenses was found to work well within the testing environment and provided an adequate FOV for both cameras. The wide range of aperture (f 0.95 - f 16) allows for great control of the exposure of the images and enables the use fast shutter speeds. Moreover, the depth of field of the lenses is sufficient,

giving non-blurry images on a distance of around 40 cm, which is required to capture sharp images of the blade throughout a shot.

With this lens combination, the FOV measured approximately 33 cm in width and height at full resolution, with the cameras located approximately 3 meters away from the puck location. The FOV is slightly larger than the length of a blade and is appropriate as it allows the blade to move slightly from side-to-side while remaining within the FOV. Due to the variability always present with human testing, a FOV too restrictive proved detrimental to data collection as difference in technique and blade motion meant part of the blade would go out of the FOV. Since the height of a blade measures only about a third of its length, reducing the height of the FOV is possible in order to increase the capture rate of the cameras. At 2000 FPS, the cameras record at the full 512 x 512 pixels resolution, while increasing the recording speed to 4000 FPS cuts down resolution in half in the vertical direction, giving an effective resolution of 512 x 256 pixels. At 4000 FPS recording speed, the FOV is 33 cm wide by 16.5 cm high. This smaller FOV remains adequate and allows for successful capture of the blade motion from ice impact to after puck impact. This setup gives an effective magnification factor of 1.6 pixels/mm.

3.1.4. Stereo Angle

Due to the motion of the blade, only a small range of stereo angles ensures that the blade remains within the FOV throughout the shot. As illustrated in Figure 3.3 below, increasing the stereo angle reduces the length of the region where the blade is within the FOV of both cameras. Even though a stereo angle within the 10° to 30° range is desirable, it is hard to achieve in the case of a dynamic slap shot as the blade travels away from the

cameras. Through preliminary dynamic tests, the optimal orientation of the cameras was found and later determined, through system calibration, to be between 3° and 5°. This variability in stereo angle is due to changes made in the stereoscopic arrangement to adapt to certain technique differences between subjects.

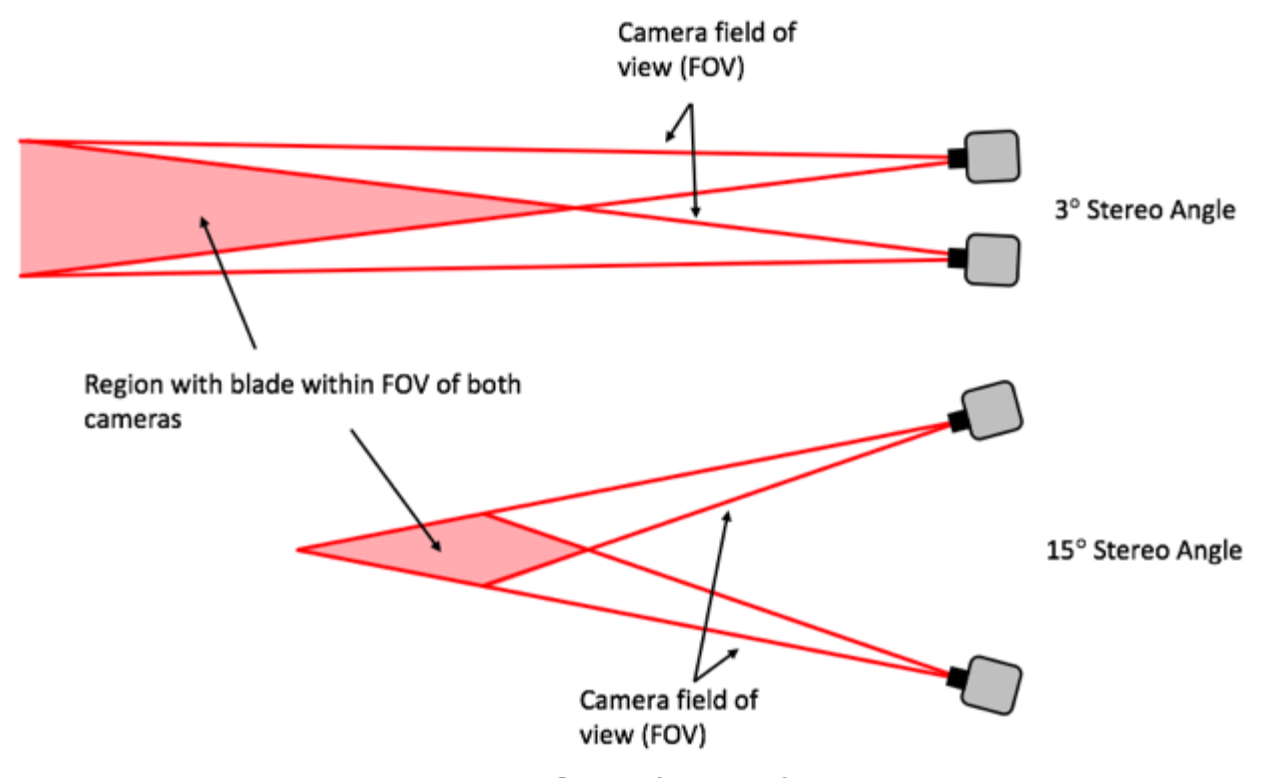


Figure 3.3: Influence of stereo angle on FOV.

If we consider the effects of stereo angle and lens selection, shown in Figure 2.11, we can see that with a 50 mm lens and a 3° to 5° stereo angle, a strain accuracy between 300 μ s and 400 μ s can be expected. This is not as optimal as the 200 μ s minimum, but is sufficient to correctly identify the deformation of the hockey blade during a slap shot.

3.1.5. Lighting

The use of powerful lights is necessary to obtain good lighting of the sample surface even at high shutter speeds. Due to the fast motion of the hockey blade, having fast shutter

speeds is required to obtain sharp images. Unfortunately, using a fast shutter speed reduces the amount of light than can reach the camera sensor, which can only be compensated by increasing the light projected onto the sample surface.

To provide sufficient lighting, four Lowel Pro 250 Watt adjustable spot/floodlights (Lowel-Light Manufacturing, Hauppauge, NY, USA) and one 1000 Watt Ianiro Varibeam 1000 floodlight (Ianitronic SRL, Mezzolombardo, Italy) were used. The lights are set on the artificial ice surface, between the cameras and puck, without hindering the FOV of the cameras. The lights are at a distance of 0.4 to 1 meter away from the puck, and arranged in a semi-circular pattern to reduce the risk of the stick impacting the lights during a shot. A safe distance for the lights was determined through pilot testing.

The Ianiro floodlight is put further away from the cameras to illuminate the area in its entirety. The four Lowel spot/floodlights are closer to the expected blade trajectory, and the intensity of the light beam (spot light to wider beam) is individually adjusted to ensure even lighting along the sample. It was noticed that increasing the intensity of the lights (spot light) created very bright spots on the sample, which led to poor images. Fine tuning of the lights location and intensity is done to minimize the occurrence of bright spots and have consistent light along the sample throughout the entire blade motion.

It is important to note that the lights were moved between test sessions to accommodate for variations in players' technique and angulation of the blade. Therefore, an exact diagram of lights location and distances cannot be shown. However, Figure 3.4 below is a good representation of the lighting arrangement used throughout testing. Not present in the picture is a fan that was used to dissipate the heat generated by the lights throughout testing.



Figure 3.4: Lighting arrangement.

With this particular light arrangement, the shutter speed of the cameras and aperture of the lenses is finalized. The shutter speed is set to 40 000 Hz (0.025 ms) for calibration images and 28 000 Hz (0.036 ms) for static and dynamic testing. The difference is due to the difference in light reflectivity between the paper of the calibration grid and the matte paint present on the test samples. It is possible to change the shutter speed directly from the PFV software, which prevents handling of the cameras after calibration. The aperture of the lenses varied slightly throughout static and dynamic testing to adapt to the testing conditions and changes in light reflection due to blade motion. However, it remains in a f 1.6 - f 2.8 range.

3.2. Data Collection and Pre-Processing

The data collection is conducted using the PFV software, which allows both images and videos to be recorded simultaneously from both cameras. The data is saved in the selected folder in a specific format determined by the PFV software. Consecutives snapshots, required for system calibrations, are stored in order of capture. Videos can be trimmed and adjusted for exposure and contrast directly using PFV, and the pairs of images can be exported to a variety of formats. In this study, Tag Image File Format (TIFF) is used.

Once the images are saved, they need to be renamed in order to be correctly processed in the DIC software. For this study, the VIC-3D 2012 ver. 2012.2.1 (Correlated Solutions, Inc., Columbia, SC, USA) software was used. Due to the amount of images collected, the renaming of the files was done using the open source software IrfanView ver. 4.38 (Irfan Skiljan, Wiener Neustadt, Austria), which is free for educational use. It allows for batch processing of files, useful when up to 200 images need to be renamed in sequence.

Once the files are renamed, the calibration and testing images can be uploaded into the VIC-3D software for DIC processing.

3.3. System Calibration

Although there are differences in the processing steps for static and dynamic testing, a system calibration is always required. The system calibration process is used to identify the relative position of the cameras with respect to each other and the scaling factor for the experiment. This is an essential step in order to obtain successful DIC results.

In order to have a well-calibrated system in VIC-3D, a calibration grid is used and images of the grid are taken using the pair of cameras. An example of a calibration grid is shown in Figure 3.5 below.

The calibration grid is made of black dots aligned horizontally and vertically. The number and size of the dots as well as spacing between them is chosen depending on the resolution and FOV of the cameras. Three of the dots have a white center, with a certain vertical and horizontal offset between each other, and a given offset from the bottom left dot of the grid. This information defines the calibration grid properties and is used as input in VIC-3D.

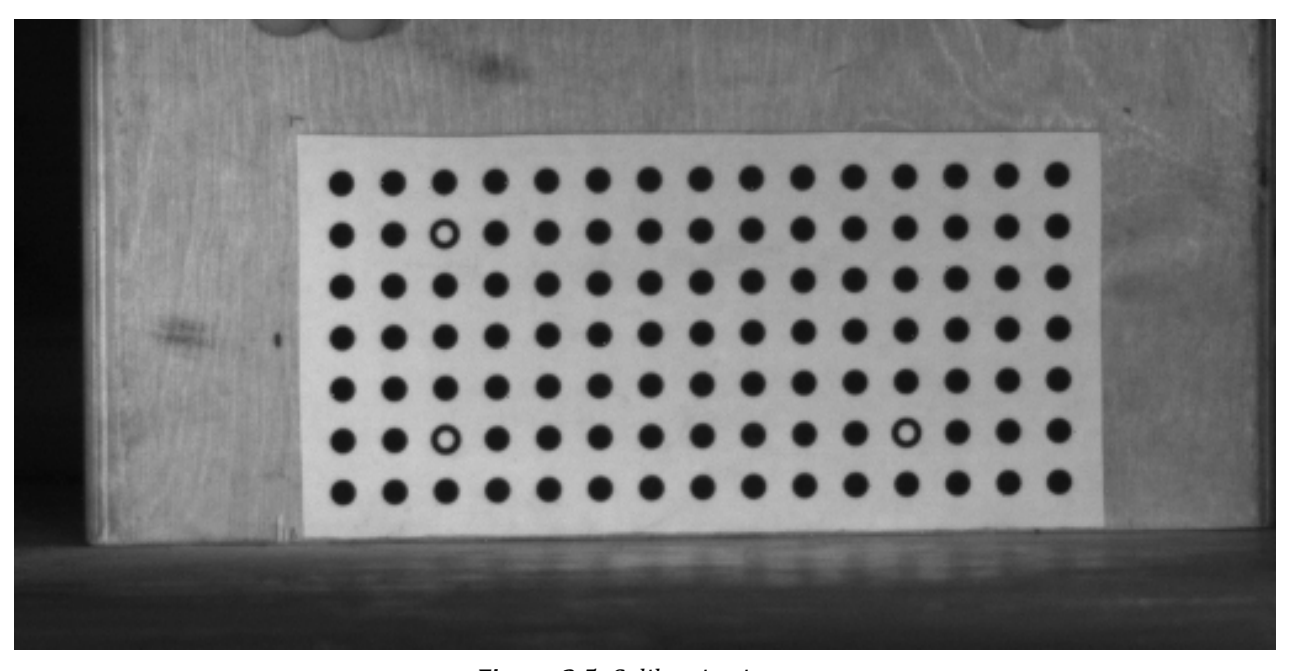


Figure 3.5: Calibration image.

A number of images of the grid are taken, the more the better, using the pair of cameras in their stereoscopic arrangement. The grid needs to be photographed in various positions, changing the angle of the grid surface with respect to the cameras. Based on the different perspective seen from the cameras, the depth and scale of the images can be determined.

The software analyzes the calibration images based on the grid properties and for each image the software attempts to guess the location of the white dots. A pixel error is determined for each of the pictures based on the estimated and actual location of the white dots, and the combination of the images' errors gives a calibration score. The data extracted from the calibration images defines the scaling factor for the experimental setup as well as the orientation and position of the cameras with respect to each other. The data is also used to define the coordinate system of the experimental setup, which is the reference coordinate system for processing of the images from static and dynamic testing.

The calibration grid seen in Figure 3.5 above was made using the Calibration Grid Generator software Version 1.0.1 (Correlated Solutions, Inc., Columbia, SC, USA). It was printed and glued onto a flat wooden surface. The dot spacing, size-to-spacing ratio, number of dots and overall size of the calibration grid was determined through pilot testing by trying a number of calibration grids and studying the calibration results. The following grid properties were chosen for this study as they were found to provide satisfying calibration results:

- Number of dots: 15 horizontal by 7 vertical
- Size-to-spacing ratio: 0.5
- Dot spacing: 13 mm
- Initial white dot offset: 2 horizontal by 1 vertical (white dot offset from bottom left black dot)
- White dots offset: 9 horizontal by 4 vertical (offset to next white dot)

For successful calibration, the calibration score given by the VIC-3D software should be below 0.05 pixel error, and ideally as low as possible. For static and dynamic testing, a maximum calibration error of 0.04 was defined as acceptable and trials with higher

calibration errors were not processed. It is important to note that since the imaging

hardware is not provided by Correlated Solutions, the calibration results cannot be assessed

immediately after the images are taken. Therefore, the calibration process has to be repeated

many times prior to dynamic testing with subjects to ensure that consistent calibration

results can be achieved. Otherwise, the data collected in the dynamic testing cannot be

processed due to calibration errors, which reduces the amount of successful trials.

3.4. Summary

The stereoscopic arrangement used for this study is summarized as follows:

• <u>Cameras:</u> Photron FASTCAM MC2-10K - monochrome

o FOV: 33 cm x 16.5 cm

o Resolution: 512 x 256 pixels

o Magnification factor: $M_T = 1.6$ pixels/mm

Recording Speed: 4000 FPS

Shutter Speed: 0.025 ms - 0.036ms

• Support Frame:

Aluminum: 1' x 2' x 1' (Height x Width x Depth)

Locking pivots for camera attachment

o 2 x 25 kg weights

• Lenses:

Navitar 50 mm fixed focal length

o Aperture: f 1.6 – f 2

50

- Depth of field: ~ 40cm
- Stereo angle: 3° 5°

• <u>Lighting:</u>

- o 4 x Lowel Pro 250 W adjustable spot/floodlight
- o 1 x Ianiro Varibeam 1000 W floodlight

• <u>Calibration grid:</u>

- Number of dots: 15 horizontal 7 vertical
- o Size-to-spacing ratio: 0.5
- o Dot spacing: 13 mm
- o Initial white dot offset: 2 horizontal 1 vertical
- White dots offset: 9 horizontal 4 vertical

• Software:

- o Data collection: Photron Fastcam Viewer (ver. 3.3.9)
- o Data pre-processing: IrfanView (ver. 4.38)
- o DIC: VIC-3D 2012 (ver. 2012.2.1)

4. Sample Preparation for DIC

Based on the specific imaging system and stereoscopic arrangement chosen, the selection and application of the speckle pattern onto the blades is the next consideration in the preparation for this DIC study. This section will present the hockey sticks tested and calculations made to estimate the required speckle pattern properties. The pilot testing done to validate the best pattern will also be discussed along with the technique used to apply the pattern onto the blade surface.

4.1. Stick Characteristics

In order to study the effects of construction and geometry on blade dynamic behavior, four different hockey sticks are used. The shaft characteristics are kept constant while the blade construction and geometry varies between each stick. The same sticks are used for both static testing of the system accuracy and dynamic slap shot tests. A total of eight sticks were provided by Bauer Hockey Inc. (Exeter, NH, USA) to ensure spares were available in case of any stick breaking. Due to the proprietary nature of the information related to blade construction and geometry, the specific blade pattern and construction of the sticks was kept confidential and codes were used to characterize the different blades.

All sticks are the same model of one-piece composite hockey sticks, with identical shaft dimensions and flex rating. The sticks are the Bauer Vapor 1N senior stick with 87 flex. The shafts are 143 cm long and have a cross-section of 29 mm by 19 mm about the major and minor axis respectively (refer to Figure 6 for visual representation of major and minor axis

of the shaft). The shafts are not cut and hockey tape is put on the top end of the shaft and on the front of the blade.

Regarding the blades, two different blades patterns (P1 & P2) and two different constructions (CA & CB) were tested. The blade consisting of blade pattern and construction P1-CB was tested twice to investigate the consistency of the test results and identify the effects of variability associated with human testing. All blades are referred to as a combination of blade pattern and construction, giving the four following blade names: P1-CA, P2-CA, P1-CB-1 and P1-CB-2. The only known details about the blade construction are that construction C1 involves an epoxy core, while C2 is a foam core. The blades were measured and the length, height, thickness, curve depth, face angle and curve type are reported in Table 4.1 below.

Table 4.1: Blade geometric properties.

Blade Pattern	Length [cm]	Height Range [mm]	Thickness Heel - Toe [mm]	Curve Depth [mm]	Face Angle	Curve Type
P1	29	61 – 74	7 – 3	18	Open	Mid-Toe
P2	29	61 – 70	7 – 3	13	Flat	Mid-Heel

The two blades have similar dimensions, but there is a visible difference in face angle, curve depth and curve type (refer to Figure 4.1). The geometrical differences in the two blades have been reported by elite players as a source of noticeable difference in shooting and handling characteristics. Similarly, differences in blade construction have been reported to affect the feel of the stick, but to a smaller extent than blade geometry. It is hypothesized

that these geometrical differences will affect significantly the dynamic behavior of the blades, while the differences in construction will be less evident.



Figure 4.1: Blade patterns P1 (top) and P2 (bottom).

4.2. Speckle Pattern Theory

The use of an appropriate speckle pattern is an essential part of obtaining accurate results in a DIC study. The speckle pattern properties are directly linked to the characteristics of the imaging system and can be determined theoretically. Some pilot testing is still required to ensure the pattern provides satisfying results, and a robust technique to apply the pattern on the sample surface needs to be found.

4.2.1. Calculations

The theoretical calculations of the speckle pattern properties can be used to obtain an estimate of the speckle pattern to be used for a particular imaging system. Based on the work from Sutton et al. [13], information regarding speckle size, subset size and object displacement accuracy can be estimated using parameters obtained from the imaging setup. The following parameters are used or determined in the calculations:

- Magnification factor: $M_T = 1.6$ pixels/mm
- Image displacement accuracy: β_I = 0.01 to 0.04 pixels (smallest to greatest calibration error)
- Object displacement accuracy: β₀
- Image speckle size: ηi
- Object speckle size: η₀
- Subset size: *m* by *m* pixels

The rules of thumb [13] state that the minimum recommended speckle size is 3 by 3 pixels (η_i = 3 pixels) and the minimum recommended subset size 3 by 3 speckles ($m \ge 3*\eta_i$). Using these guidelines, we have the following equations and results:

$$\beta_o = \frac{\beta_i}{M_T} = \frac{\beta_i}{1.6} = 6.25 \text{ to } 25 \text{ } \mu m$$

$$\eta_o \ge \frac{\eta_i}{M_T} \iff \eta_o \ge \frac{3}{1.6} \iff \eta_o \ge 1.875 \, mm$$

This gives a good estimate of the expected object in-plane displacement accuracy, between $6.25\mu m$ and $25\mu m$, and gives an idea of the minimum speckle size to be used, around 2 mm. Since the blade orientation is expected to change during its motion, having slightly bigger speckles than the minimal size will help ensure correct sampling of the speckle pattern during processing. Ultimately, the subset size is determined by the chosen speckle size and will vary between trials depending on blade orientation throughout the images. It is important however to keep in mind that the minimum subset size should not be smaller than 9 by 9 pixels, most likely higher since the average speckle dimension will be higher than the minimum 3 by 3 pixels.

4.2.2. Speckle Pattern Generator

Creating a random pattern with consistent size speckles can be hard to achieve, so is measuring the speckles and determining the minimum speckle size. In order to find a speckle pattern that gives accurate results, it is easier to print a pattern on a piece of paper and glue it to a rigid surface than it is to paint it. The use of the Speckle Generator software ver. 1.0.5 (Correlated Solutions, Inc., Columbia, SC, USA) allows for parameters such as speckle size, density and distribution to be modified, tested and optimized. The use of such software allows to save time and to precisely determine the best speckle pattern properties for any experimental setup, as long as the test samples are not too small.

4.3. Pilot Testing

Using the Speckle Generator software, different speckle patterns were tested first statically and then dynamically to identify the pattern best suited for this specific experiment.

4.3.1. Static Testing

In order to conduct the preliminary testing of the speckle pattern and determine the best pattern for this study, a number of speckle patterns are printed on paper using the Speckle Generator software. Based on the minimum speckle size determined to be 1.875 mm, five speckle patterns with speckle sizes ranging from 2 to 4.5 mm are tested, while speckle density and variation of the pattern are kept constant at 75% and 99%, respectively. Speckle size, speckle density and variation, are the only parameters that can be modified in the

Speckle Generator software. The variation refers to the randomness of the pattern, with 0% variation leading to speckles being aligned in the horizontal and vertical direction.

The speckle patterns are attached to a wooden support and images are taken of the sample undergoing in-plane translation, perpendicular to the FOV of the cameras. The support was moved by about 2 mm increments within a 10 mm range. Since the objective is not to determine the accuracy of the system but rather the pixel error associated with each pattern, the displacement measurements were not investigated at this time. Throughout the various tests the imaging parameters were kept constant.

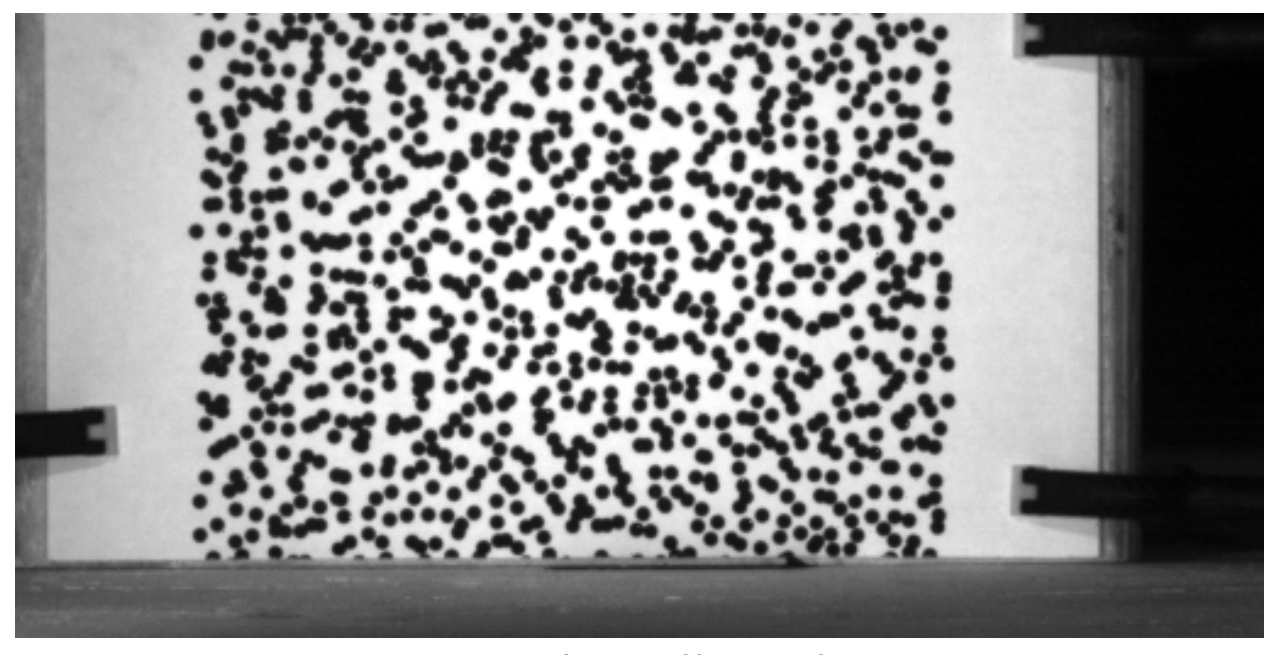


Figure 4.2: Image capture of 4mm speckle pattern during static testing.

For each test, the system was calibrated using the 15×7 calibration grid mentioned in section 3.4. After calibration, a reference image is taken of the support in the same location as the puck would be for a dynamic test. Subsequently, the pattern is moved sideways by specific increments based on marks made on the artificial ice surface. Images are taken at each increment while making sure the sample is kept static for each image.

Once the images have been pre-processed, they are imported into the VIC 3D software, where system calibration is done and the calibration score is recorded. The AOI is defined on the first image, the suggested subset size is used and the images are processed. The processing results are saved and an average pixel error value is calculated for each test. The results are presented in Table 4.2 below.

Table 4.2: Speckle static testing results.

Speckle Size	Calibration Score [pixels]	Subset Size [pixels]	Average Image Error [pixels]	
2 mm	0.015	17 x 17	0.048	
3 mm	0.013	17 x 17	0.010	
4 mm	0.014	21 x 21	0.008	
3.5 mm	0.021	19 x 19	0.010	
4.5 mm	0.018	25 x 25	0.018	
4 mm	0.018	19 x 19	0.013	

As can be seen from Table 4.2, a speckle dimension between 3 and 4 mm led to the smallest image errors for similar calibration scores. Although the 4.5 mm speckle pattern led to a low image error, the suggested subset size is greater than for 3 and 4 mm speckles, which is not desirable.

Every data point is determined as the average of the displacements within the subsets, averaged to its center. This means that the closest data point along the limit of the AOI will be half the subset size away from the edge. Increasing the subset size increases the size of the area along the AOI limit where there are no data points, as seen in Figure 4.3 below. Therefore, it is desirable to have the smallest possible subset size to reduce the distance

along the edge of the AOI where no data is available. A subset size between 17 and 21 pixels, as suggested for the 3, 3.5 and 4 mm speckle patterns, leads to an acceptable size for the region with no data points.

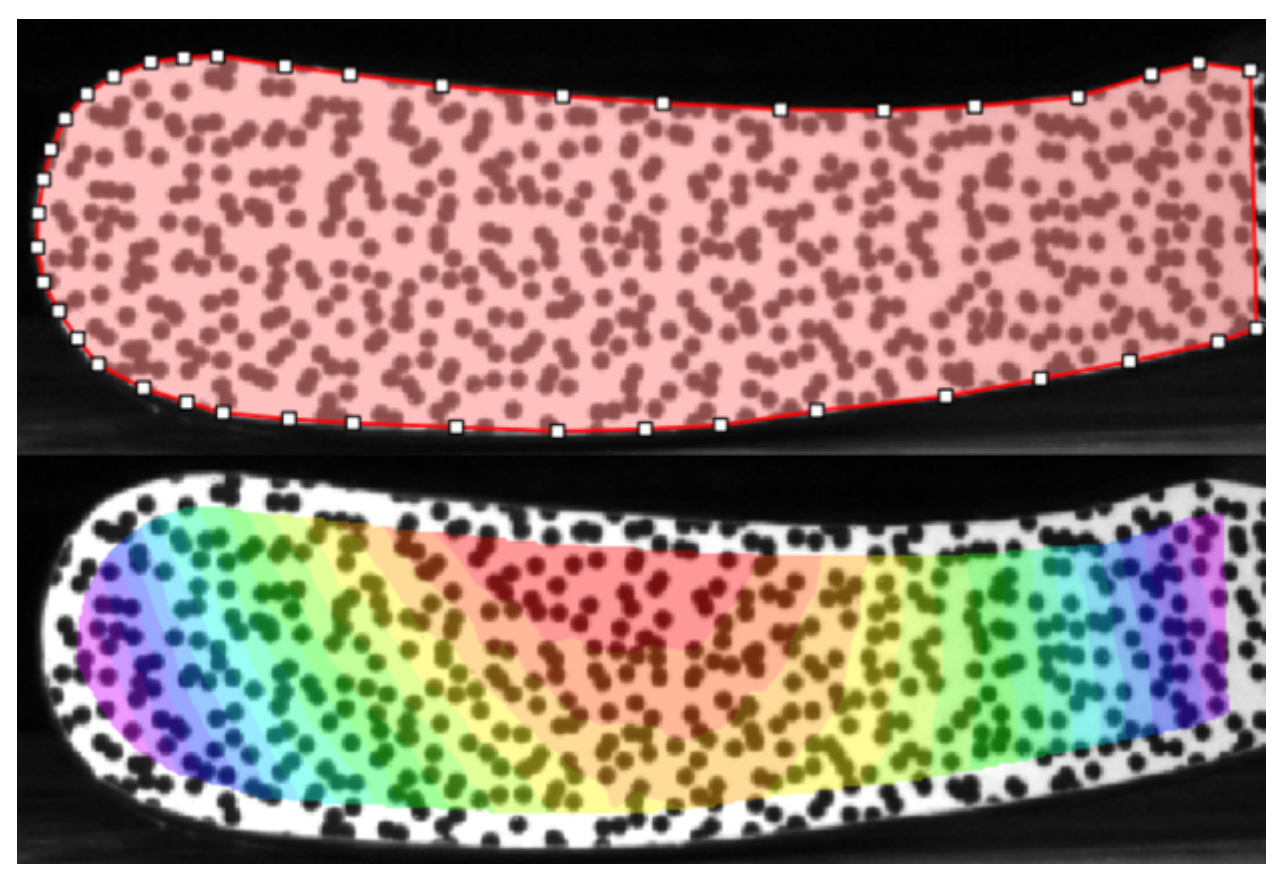


Figure 4.3: Comparison of AOI and data point coverage.

Another 4 mm speckle pattern was made where speckle density and variation were set to 66% and 75%, respectively, in order to assess the influence of speckle density and pattern randomness. The change in these two parameters increases slightly the pixel error associated with the pattern (0.015 pixels error) as well as the suggested subset size (23 x 23 pixels). Since an important feature of a speckle pattern is its randomness, increasing its linearity does not lead to any improvements. Moreover, decreasing the density of the speckle pattern leads to an increase in speckle distance, which requires a bigger subset size. In order to maintain a reasonable subset size, any decrease in density should be compensated by an

increase in speckle size. For these reasons, 75% speckle density and 99% variation, in conjunction with a 3 to 4 mm speckle size, was found to lead to accurate results.

All static testing is done with the speckle pattern surface perpendicular to the line of sight of the cameras. Changing the orientation of the pattern with respect to the cameras reduces the size of the speckles projected onto the captured images. In a similar way, the blade location will influence the effective speckle size in the images and as the blade moves away from the cameras, each speckle appears smaller and covers fewer pixels. Since the blade moves away from the cameras and its orientation is not expected to remain normal to the cameras throughout a shot, a larger speckle size is preferable. This ensures that the minimum speckle size will be achieved regardless of blade orientation and location.

To confirm this approach, some dynamic testing of the speckle patterns is required.

4.3.2. Dynamic Testing

To conduct the preliminary dynamic testing, it is easier to apply a printed speckle pattern onto the blade surface instead of trying to achieve accurate speckle dimensions using spray paint. Using double-sided tape, the speckle pattern to be tested is applied on a stick and a number of test shots are recorded.

The speckle pattern tested had 4 mm speckle size, 75% density and 99% variation, as used in the static testing. The pattern is applied on two sticks with different blade patterns to see if the geometry of the surface influenced the results. Eleven dynamic shots were taken and recorded, along with calibration images for each of the trials, and the captured images were studied to determine the effective speckle size in pixels. The number of good images for a trial ranged from 50 to 100, and the last acceptable image was strongly dependent on

the trajectory of the blade; this trajectory determined when the blade left the FOV of one of the two cameras. The range of out-of-plane displacement of the blade was found to be between 20 and 35 cm from ice impact to the last acceptable image.

There is a noticeable difference in speckle pixel size between the first and last frame of a trial. As the blade moves away, the speckles appear smaller and their average size goes from 5×5 pixels in the first image to 4×4 pixels in the last non-blurry image. Since the speckles should be sampled by at least 3×3 pixels, the use of a 4 mm speckle pattern gives sufficient speckle sampling even with the blade furthest away from the cameras. For this reason, all the dynamic speckle testing was done using a 4 mm speckle pattern.

The subset size used for the processing of each trial is the suggested subset size given by the VIC-3D software, and ranges from 25×25 to 33×33 pixels. The variation in subset size is due to lighting of the sample and the change in blade orientation in the first captured frame, just prior to ice impact, as the initial frame is where the AOI is defined. Although the recommended subset size is slightly bigger than what was found during static testing, this still gives accurate results with data points on the majority of the blade surface.

The blade pattern tested does not have an influence on the quality of the results. The suggested subset size is consistent for both blades, with slight variations for a few trials, and the pixel error associated with the trials did not vary significantly. The average pixel error for all trials was calculated and is shown in Table 4.3 below along with the processing parameters.

The speckle dynamic testing proved successful as it allowed to show that the images captured during dynamic trials could be processed successfully with consistent results and

low pixel error associated with the images. These dynamic tests also confirmed that the 4 mm, 75% density, 99% variability speckle pattern is adapted to this type of dynamic testing. *Table 4.3: Speckle dynamic testing results.*

Stick Number	Trial	Calibration Score [pixels]	Subset Size [pixels]	Average Image Error [pixels]
	1	0.031	33 x 33	0.019
	2	0.034	31 x 31	0.047
1	3	0.033	29 x 29	0.035
1	4	0.035	29 x 29	0.018
	5	0.029	29 x 29	0.030
	6	0.028	25 x 25	0.044
2	1	0.035	27 x 27	0.054
	2	0.026	29 x 29	0.013
	3	0.033	29 x 29	0.022
	4	0.033	29 x 29	0.015
	5	0.028	29 x 29	0.011

4.4. Application of Speckle Pattern

After the speckle pattern parameters were determined and the pilot testing proved successful, the issue of applying the pattern on a hockey blade was tackled. Although the paper pattern technique has proven to work well, the layer of tape and paper on top of the blade might lead to inaccuracies in representing the actual blade surface deformation. It is preferable to use a painted pattern as it has been proven successful in literature and would get rid of the uncertainties associated with a paper pattern.

4.4.1. Spray Paint Tests

Spray paint tests are done to assess the feasibility and repeatability of the speckle painting process. Moreover, it is important to study the toughness of the paint to ensure that it will not come off the blade or crack during the blade-puck impacts.

The first step in painting the speckle pattern is the application of a matte white base coat. White paint is usually used as a primer as it allows for the subsequent paint layers sprayed on top to stand out more. This means that a thin layer of black paint sprayed over the white surface would create more contrast than if white speckles were sprayed over a black base coat.

After the base coat is applied, a can of matte black spray paint is used to create a speckle pattern on the surface. By applying more or less pressure on the spray can nozzle, it is possible to create blobs of paint instead of the usual mist. This is useful in order to obtain the larger speckle size required for this particular study.

Two test blades were first coated with multiple layers of matte white paint, until the surface was even in color and surface finish. Doing multiple thin layers instead of one or two thicker layers allows for a more even surface finish and prevents paint from running. Once the blades were dry, attempts were made to create a pattern with the correct size speckles. The spray nozzle opening was modified and slight pressure was applied to make large blobs of paint. Figure 4.4 below illustrates the patterns that were achieved.

Unfortunately, the speckles that were created using this technique were not big enough. Moreover, avoiding smaller speckles is not possible which leads to a salt and pepper pattern. This is undesirable as it reduces the contrast between the white base and the black speckles, and the small speckles are not big enough to be sampled by an appropriate number

of pixels. The patterns that were made necessitated many trials and the blades had to be recoated at least once to try to obtain a better speckle size and distribution.

This technique is unreliable and time consuming with no certainty regarding the size of the speckles. Since the technique is aimed at testing numerous blades on a daily basis in an industrial setting, another approach was needed to ensure that consistent speckle patterns could be painted on the surface in an efficient way.

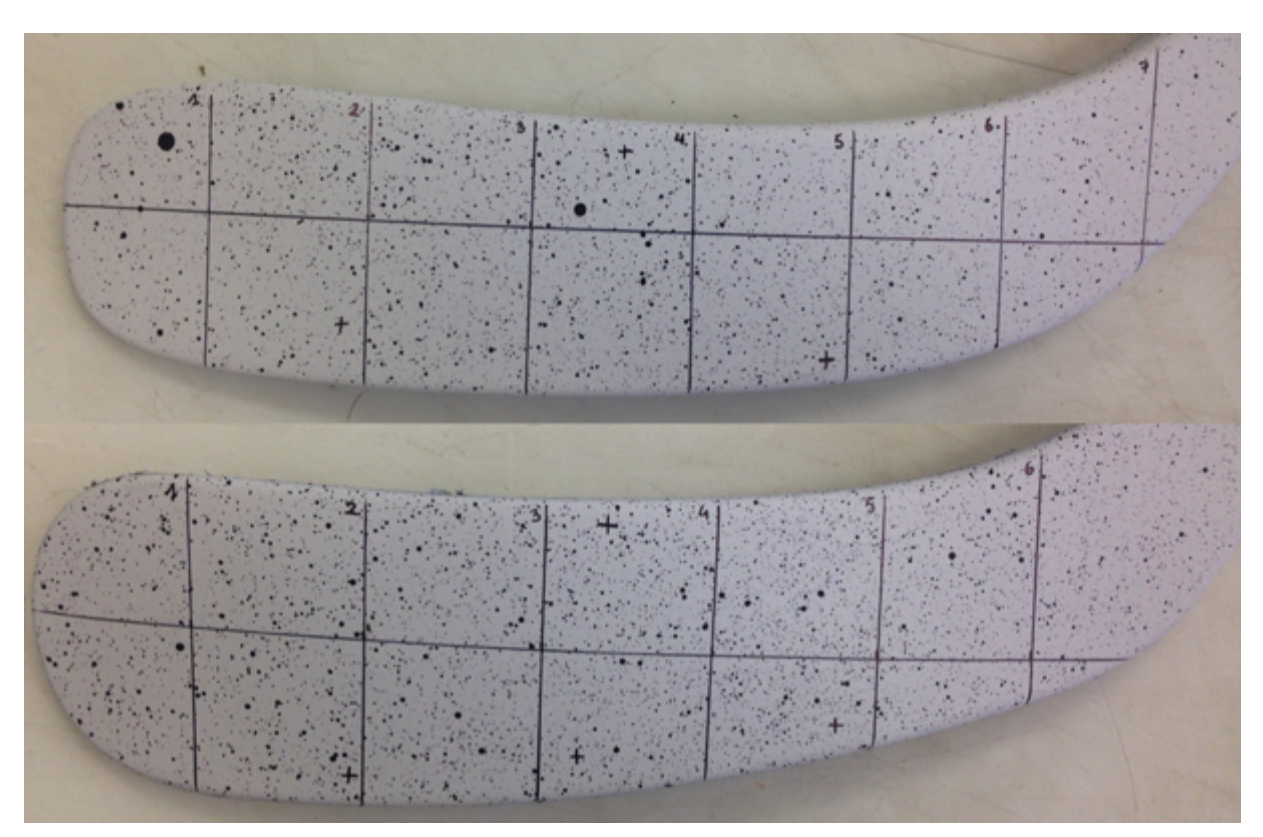


Figure 4.4: Test speckle patterns using modified spray nozzle.

4.4.2. Stencil Fabrication

Due to the large size of the speckles chosen for this study and the ease of creating a speckle pattern using the Speckle Generator software, the use of a stencil is a good alternative. The idea is to generate a speckle pattern and create a two-dimensional CAD

model of it, which can then be laser cut onto a thin acetate sheet. The same speckle pattern used for static and dynamic pilot testing can be painted onto the blade.

The speckle pattern made using the Speckle Generator software is saved as a PDF file and subsequently imported into Rhinoceros ver. 4.0 SR9 (McNeel North America, Seattle, WA, USA) CAD software. The imported PDF file has to be modified slightly to ensure the format would be accepted by the laser printer software, which is compatible with AutoCAD files (Autodesk, Inc., San Rafael, CA, USA).

The material used to create the stencil is a 0.005" thick sheet of Dura-Lar® acetate film (Grafix, Maple Heights, OH, USA). This acetate sheet was chosen as it is flexible enough to match the shape of a blade and is made of a material that can be laser cut without generating toxic fumes. The machine used is a Universal X-660 60 watt CO2 laser cutter (Universal Laser Systems, Inc., Scottsdale, AZ, USA), and the settings were determined by the chief workshop technician, David Speller, to ensure a clean cut without burning of the material. The CAD drawing is sent to print via the laser cutter printing software, and it takes approximately two hours for the stencil to be cut. Constant supervision is necessary to ensure no errors occur during cutting.



Figure 4.5: Speckle pattern stencil.

The stencil fabrication was successful and the finalized stencil is shown in Figure 4.5. Since the acetate sheet is transparent, the picture shows the speckle stencil after it had been used to paint the black speckles on the blade, as the image is more representative.

4.4.3. Speckle painting

Since the stencil does not have an adhesive surface, a way to secure the stencil to the blade is needed. The adhesive used needs to be strong enough for the stencil to adhere to the entire surface of the blade and remain in place during painting. It also has to allow for the stencil to be peeled off without removing any of the white base coat. Finally, the adhesive also has to be applicable to the entire surface of the stencil without covering the speckle holes.



Figure 4.6: Blade with base coat and stencil prior to speckle painting.

After some research, it was found that a spray adhesive would be the ideal material for this particular application. The Krylon® Easy-Tack™ 47020 spray adhesive (Krylon Products Group, Cleveland, OH, USA) was used as it has all the required properties. A thin

layer of adhesive is sprayed on one side of the stencil, left to dry for 10 minutes and the stencil is applied on the blade that has been previously base coated, as shown in Figure 4.6. Thin layers of matte black paint are applied, making sure the paint dries in between each layer. This is done to make sure that there is minimal paint bleeding around the speckle holes in the stencil. The technique proved successful and a finished blade can be seen in Figure 4.7.



Figure 4.7: Final blade with speckle pattern.

4.5. Discussion

The use of a stencil to apply the speckle pattern to the blades is reliable and the painting of the blades required minimal time. With the correct stencils and adhesive, a great number of blades can be painted in a short amount of time. The technique makes for the possibility of applying very specific patterns with consistency and good quality as long as the paint is applied in thin layers at a time and given sufficient time to dry.

Using regular matte paint, which is inexpensive and available in almost any hardware store, has led to great results with no paint cracking during testing and relatively short drying times.

Once the 2D CAD model of the speckle pattern is done, a great number of stencils can be laser cut. This allows the painting of multiple blades at a time if required. In this study, the same stencil was used to paint four of the blades, and no differences in pattern were observed. This shows that the same stencil can be used a number of times as long as new adhesive is applied once the surface is not tacky enough anymore. It is important to keep in mind that with addition of adhesive on the back of the stencil, the distance between blade surface and stencil increases, which could lead to paint bleeding if the stencil is used too many times. This has not been the case in this study but should be considered if deterioration of the speckle pattern quality is observed.

The only apparent drawback to this technique is the range in speckle size that is possible to achieve via laser cutting. Since 4 mm speckles were used for this study, the precision of the laser cutter was sufficient to obtain an adequate pattern. If speckles smaller than 1mm in diameter are required, it is uncertain how precise the pattern obtained would be.

5. Static Testing

Valuable information can be extracted from VIC-3D during data processing to assess the resolution of the system and calculate the accuracy of displacement measurements. It is important, however, to have a method to validate this information by comparing actual displacement measurements to the VIC-3D calculated displacements. This would help assess the system's accuracy and validate the technique and its particular application to this study. Since the strain measurements calculated in VIC-3D are based on the calculated displacements, it is acceptable to compare blade displacement measurements to assess the accuracy of the system. It is also easier to measure the blade displacement instead of the strain since the installation of a strain gauge on top of the speckle pattern would lead to inaccurate DIC results.

The steps taken to conduct the static testing are detailed in this section, including the apparatus used, the testing procedure, the data processing steps and the results obtained.

5.1. Stick Static Testing Apparatus

In order to correctly measure blade displacement while simultaneously capturing images of the blade, three important aspects have to be considered: rigid support for the stick, apply displacement to the blade and measure the blade displacement. It is also important to keep in mind that none of the equipment used for the static testing can be placed between the cameras and the back of the blade, in order to get clear images for DIC processing.

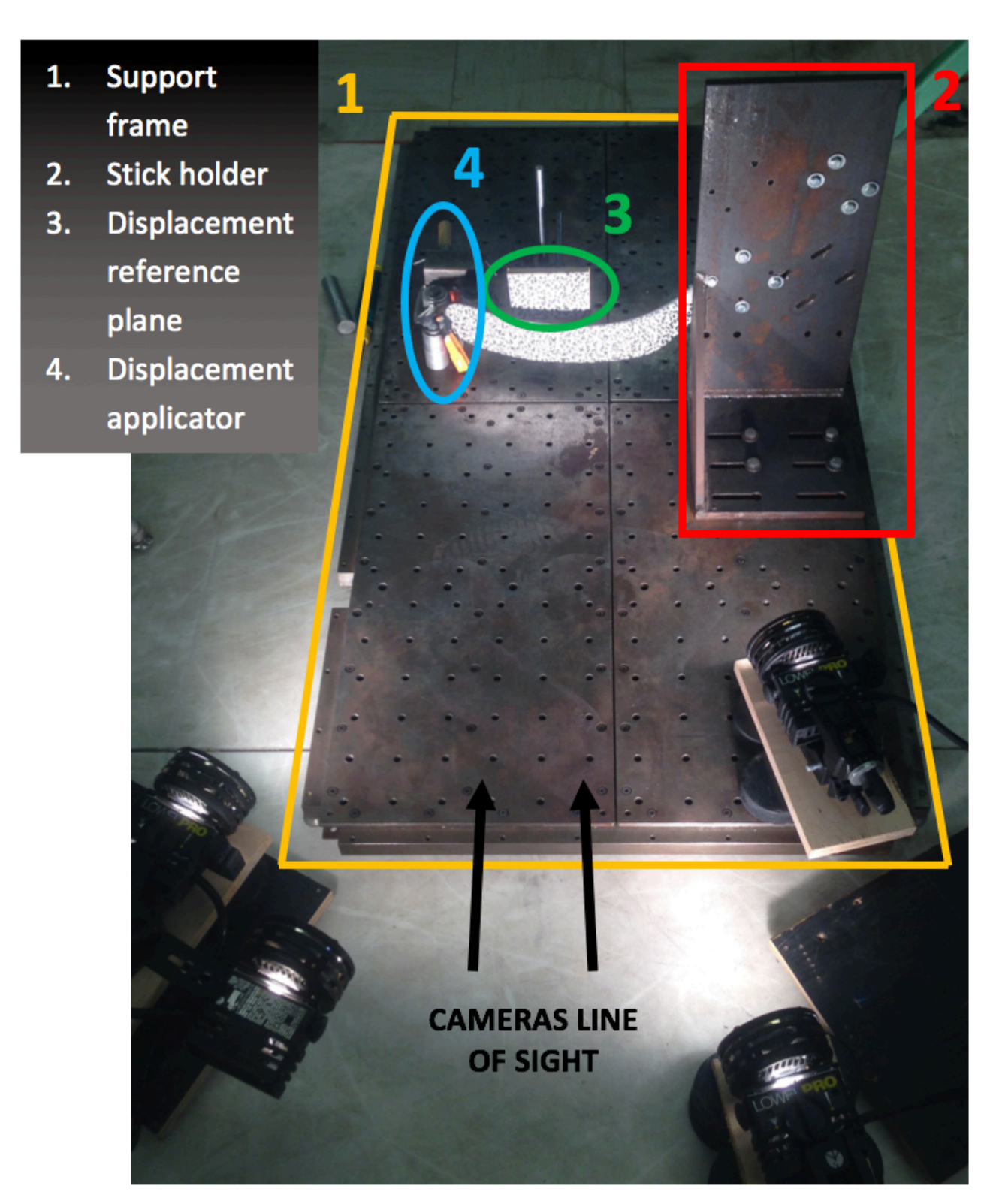


Figure 5.1: Static testing setup.

5.1.1. Stick Support

The stick support structure used in this study was made for a previous study on hockey stick testing. Although it was not designed for this specific study, it provides the required stick support and the heavy base ensures there is no movement between the stick support, the displacement applicator and dial gauge used for displacement measurements.

The support base is 1-meter long by 50 cm wide and has equally spaced threaded holes to attach the stick support structure and other components. The base was assembled and laid down on the artificial ice surface at the same location where the puck would be during a slap shot. This is done to ensure that the static and dynamic testing conditions are the same. The stick holder jig, highlighted in Figure 5.1, is bolted onto the support frame and a test stick is attached to it at two locations near the bottom of the shaft using bolt-on clamps. The stick holder is also made of solid steel and the support flange provides additional support to prevent any deformation of the support.

The tilt angle of the cameras has to be adjusted to compensate for the height of the support base, but the stereo angle is kept the same. The lighting can be adjusted to prevent shading due to the support base and stick holder jig.

As the experimental setup requires the use of a small stereo angle, the out-of-plane displacement error is expected to be noticeably greater than the in-plane error. For this reason, measuring the out-of-plane accuracy of the system is the best way to estimate the system's limitations.

5.1.2. Blade Deformation

To study the out-of-plane accuracy of the system, an arbitrary out-of-plane displacement needs to be applied to the blade. To do so, the blade is deformed and the displacement is measured.

In order to deform the blade, a combination of roller supports and a clutch style bar clamp was used, as can be seen in Figure 5.2. The two rollers support the clamp while the threaded handle allows for the blade's toe to be moved towards or away from the cameras. A reference image is taken of the undeformed blade and the screw is tightened to obtain the desired blade toe displacement. The plastic tip on the screw prevents any damage to the blade. The screw is long enough to provide a displacement range of about 10 mm, and can be set to obtain any desired displacement increment.

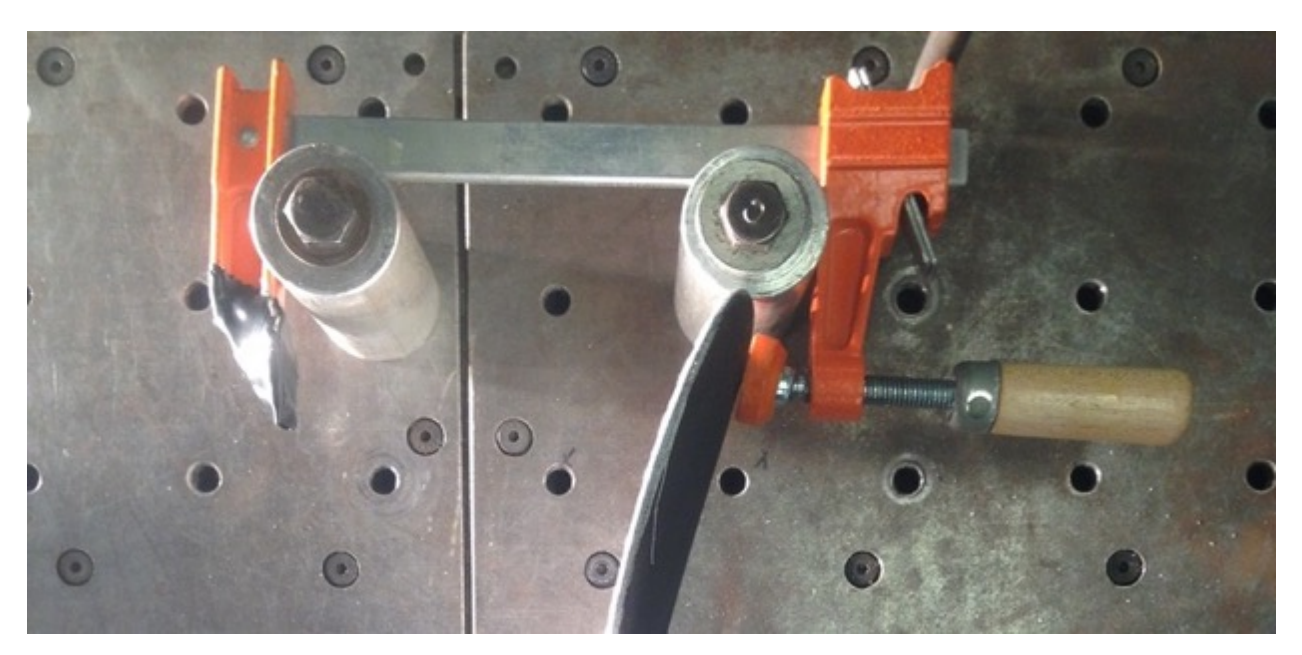


Figure 5.2: Static testing blade displacement applicator.

Figure 5.2 illustrates how the blade displacement is applied at the tip. For this particular case, the deformation applied generates blade displacement towards the cameras.

A similar setup was made to generate blade displacement away from the cameras to identify the effect of the displacement direction on the results.

5.1.3. Displacement Measurement

Once a certain displacement is applied, the issue of correctly measuring the blade deformation has to be addressed. Due to the area along the AOI edge where there are no data points in VIC-3D, the displacement measurement has to be done near the middle of the blade to ensure correct sampling of the surrounding region. In order to do so, a round tip dial gauge is used to get accurate measurements at a specific location.

A Mitutoyo Electronic Indicator model number 543-793 (Mitutoyo Corporation, Kawasaki, Japan) was used for static testing. It has \pm 1 μ m accuracy and a 0 – 12.7 mm displacement range, which is adequate for this particular application. The dial gauge is attached to a magnetic stand so it can be positioned anywhere and securely attached to the metallic support base.

Since the dial gauge cannot be placed on the back side of the blade as it faces the cameras, it is placed so that the tip is in the middle of the blade on the concave surface. Two points are drawn on the blade, at the same location on either surface of the blade. One is used as reference to place the dial gauge, the other used as reference for displacement calculations in VIC-3D.

Since the reference frame determined in VIC-3D is based on camera orientation, a displacement reference plane, visible in the stereo images, is needed to determine the orientation of the dial gauge with respect to the cameras. For this particular reason, a displacement reference plane was made by using a 4 mm speckle pattern which was printed

and attached to a flat piece of wood and placed normal to the dial gauge direction, as can be seen in Figures 5.1 and 5.3.

5.2. Testing Procedure

After the stick testing apparatus is in place, the FOV of both cameras is adjusted to encompass the full blade and the reference plane for the dial gauge indicator. The lighting is checked to make sure no shade or bright spots are visible on the blade surface. The camera settings are the same as for the speckle pattern dynamic testing, with a recording speed of 4000 FPS and shutter speed of 0.036 ms.

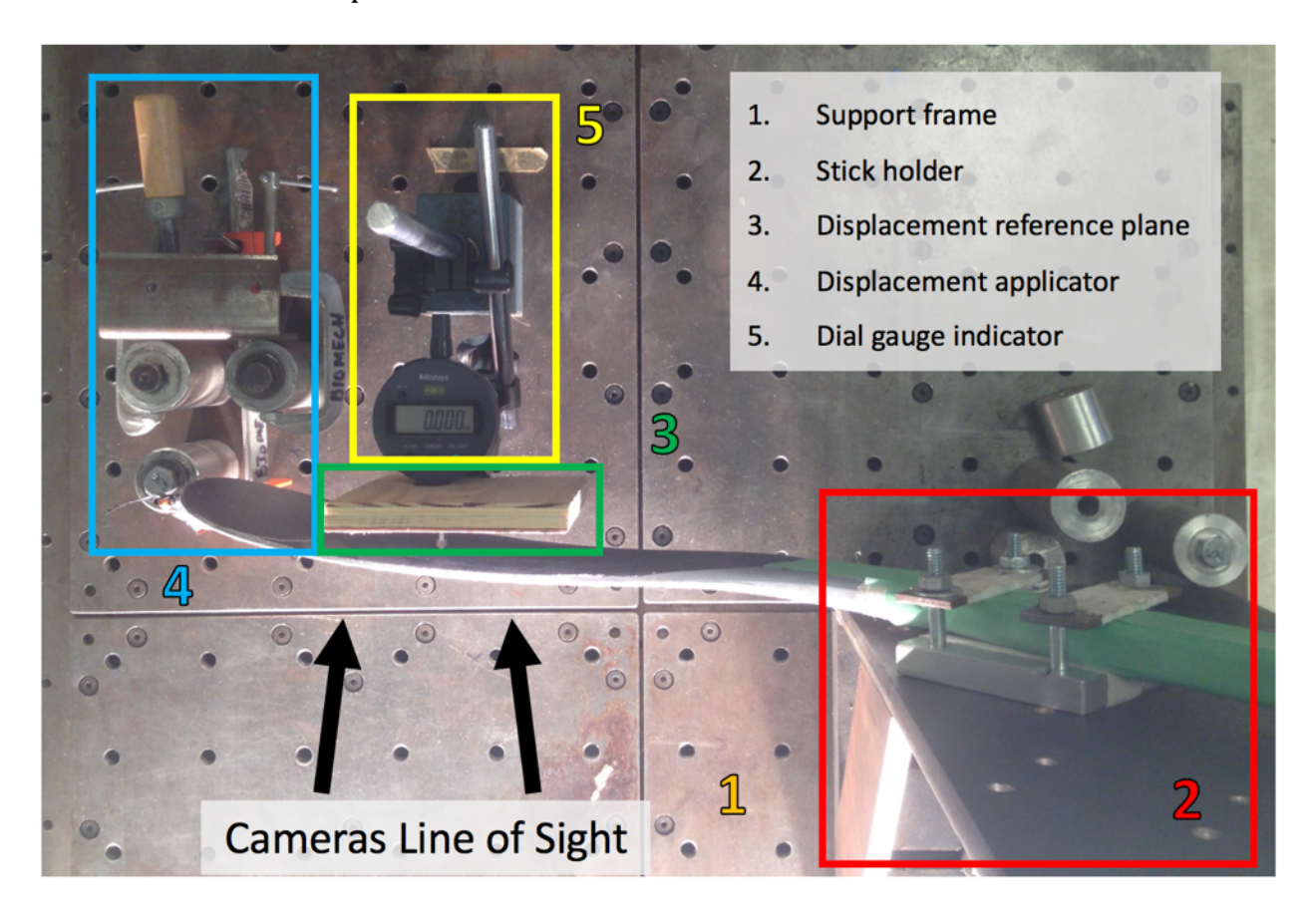


Figure 5.3: Stick with displacement applicator and dial gauge for static testing.

The first images to be recorded are the calibration images, and a new set of calibration images is required for each trial since there might be movement of the static testing jig or the camera support frame between trials. Once the calibration images have been taken, movements in the vicinity of the test area have to be kept to a minimum.

After calibration, the dial gauge indicator is set to zero and a reference image is taken of the undeformed blade at zero displacement. Following the reference image, displacement of the blade is applied.

The blade displacement was done in increments of about 1 mm and a total of 8 images were taken for a maximum displacement of around 10 mm. For each increment, displacement is applied and after the value has stabilized, a pair of images is captured and the dial gauge reading recorded.

After each trial, the displacement applicator is brought back to its initial position and the blade returns to its initial shape. Prior to the next trial, the displacement applicator, blade and dial gauge are checked to make sure they have returned to their initial position. After verifications, the next trial is done following the same procedure.

The images recorded can then be preprocessed as detailed in section 3.2 and imported into the VIC-3D software for data processing.

5.3. Data Processing & Results

The first step of data processing in VIC-3D is the calibration of the system. Using the same calibration grid as for previous testing, the system is calibrated and the calibration score and report are recorded. The calibration report gives information on camera settings and stereo setup, which can be useful to troubleshoot issues and to have a reference for other

trials. Once calibration is successful, the data processing is divided in three parts: first, the measured out-of-plane system accuracy, including the identification of the dial gauge orientation vector and the calculation of the blade displacement vector and norm, second, the VIC-3D measured system accuracy, and finally the comparison of the obtained results with the VIC-3D calculated system accuracy.

5.3.1. Measured Out-of-Plane System Accuracy

It has been previously determined that, due to the stereoscopic arrangement, the out-of-plane accuracy of the system is expected to be the greatest source of error for dynamic testing. In order to determine the out-of-plane accuracy of the system, a way to accurately compare the VIC-3D calculated blade displacement with the dial gauge measurements is required. A reference plane is used to define the orientation of the dial gauge with respect to the cameras. The point where displacement is measured with the dial gauge is also tracked using DIC and the displacement vector can be determined.

5.3.1.1. Dial Gauge Orientation Vector

As mentioned in section 5.1.3, a reference plane is required for the dial gauge indicator in order to identify the orientation of the gauge with respect to the reference frame of the cameras. The AOI is defined on the first image with zero displacement, and it is set so that it incorporates the majority of the blade as well as the dial gauge reference plane. This allows for extraction of data points along the reference plane surface and calculation of the normal vector to the surface. The suggested subset was used, the images were processed and the processing report, which details the number of data points and pixel error for each image, was saved.

After the collected images are processed, the data file corresponding to the first frame was opened, displaying the displacement data overlaid on the image, as can be seen in Figure 5.4 below. By placing the cursor over the image, it is possible to obtain the X and Y coordinates of the edges of the reference plane. Based on this information, six data points from the reference plane are defined using the metric node data export function, as shown in Figure 5.5. The data is then exported to an excel file, giving the X, Y & Z coordinates of each point in the cameras' reference frame for each image. The order of the data points and their approximate location is kept the same for each trial in order to facilitate data processing.

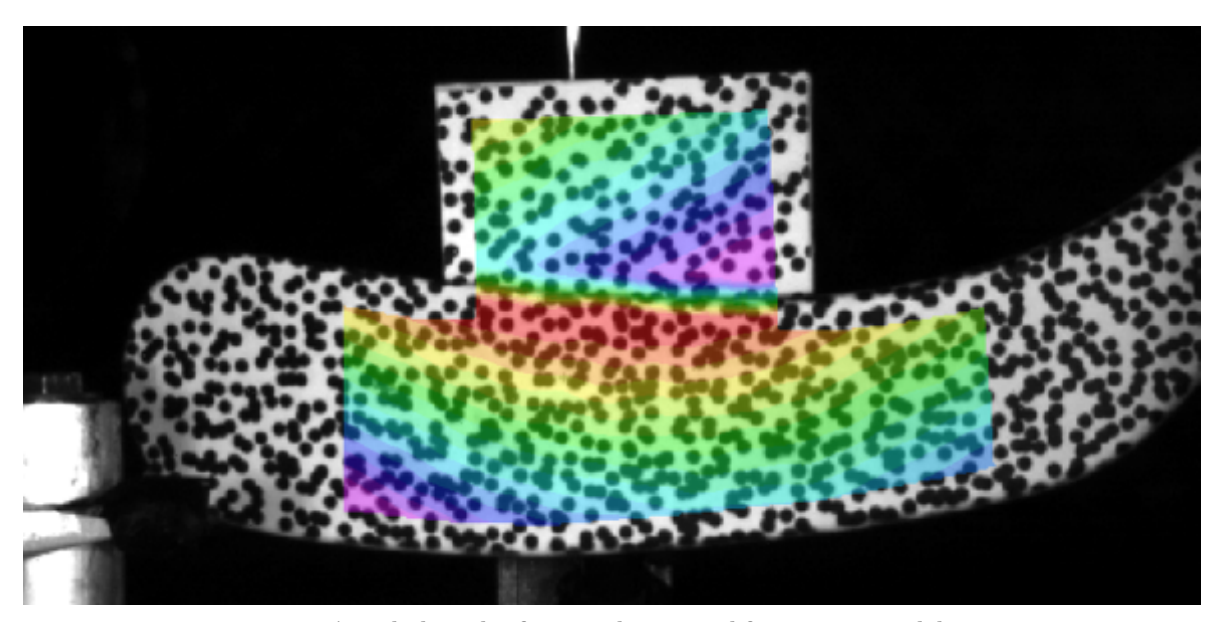


Figure 5.4: Blade and reference plane initial frame processed data.

As illustrated in Figure 5.5 below, the data points A to F are located at the four corners and in the middle of the reference plane. In order to get a more accurate representation of the reference plane orientation, the coordinates of the data points were extracted for each image and the X, Y and Z values were averaged independently to obtain the average location of each point over the length of the static test.

From these six points' average coordinates, ten plane direction vectors are defined. A cross product of the vectors is done to obtain seven vectors, normal to the reference plane, which are then scaled to unit length. The average of these vectors is used to define the direction of the dial gauge displacement. The calculations required to obtain the reference plane normal vector are detailed below, with a sample calculation using points A, B, D and E.

The coordinates for any point n are defined as X_n , Y_n and Z_n . The vectors \overrightarrow{AB} and \overrightarrow{ED} are obtained as follow.

$$\overrightarrow{AB} = [X_{AB}; Y_{AB}; Z_{AB}] = [X_B - X_A; Y_B - Y_A; Z_B - Z_A]$$

$$\overrightarrow{ED} = [X_{ED}; Y_{ED}; Z_{ED}] = [X_D - X_E; Y_D - Y_E; Z_D - Z_E]$$

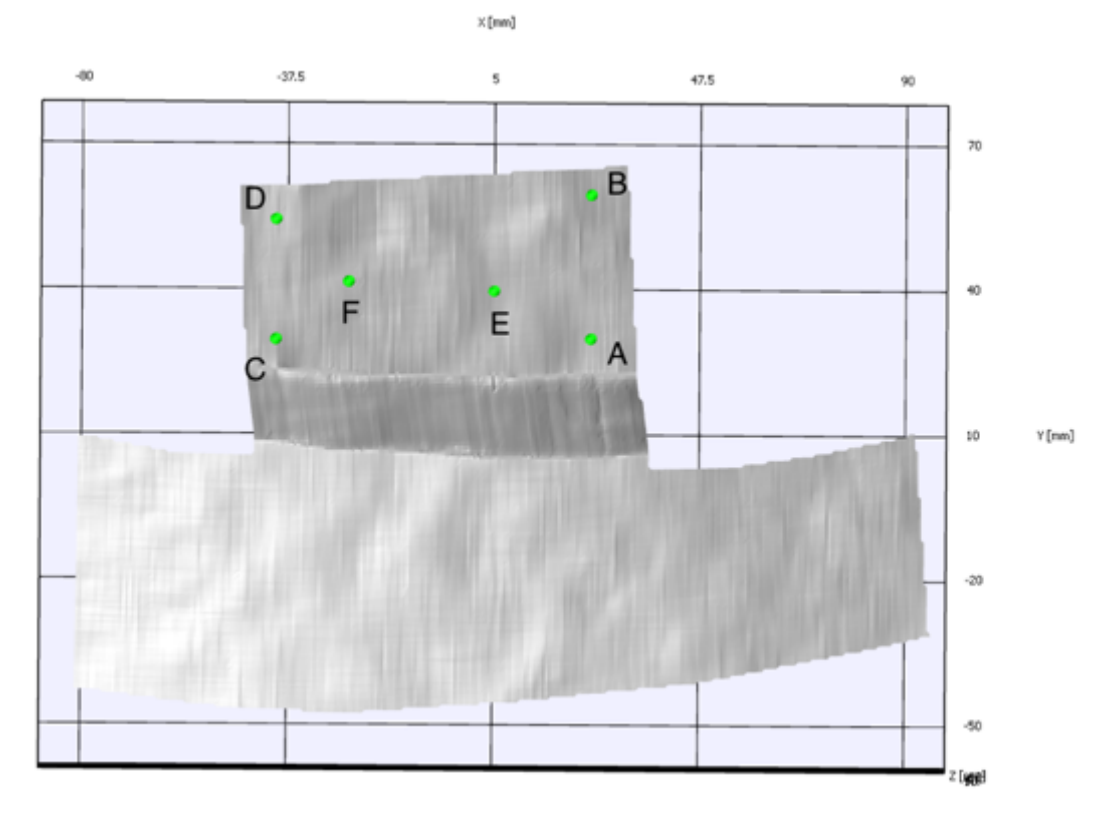


Figure 5.5: Reference plane data points metric node export.

Since the reference plane faces the cameras, the required normal vector has to be directed towards the camera in the out-of-plane direction. Based on the location of points A,

B, D and E, the cross product of \overrightarrow{AB} with \overrightarrow{ED} is calculated and the resulting vector, defined as $\overrightarrow{G_1}$, is normal to the reference plane surface.

$$\overrightarrow{G_1} = \begin{bmatrix} X_{G_1} ; Y_{G_1} ; Z_{G_1} \end{bmatrix} = \overrightarrow{AB} x \overrightarrow{ED}$$

$$X_{G_1} = Y_{AB} * Z_{ED} - Z_{AB} * Y_{ED}$$

$$Y_{G_1} = Z_{AB} * X_{ED} - X_{AB} * Z_{ED}$$

$$Z_{G_1} = X_{AB} * Y_{ED} - Y_{AB} * X_{ED}$$

Vectors $\overrightarrow{G_1}$ to $\overrightarrow{G_7}$ are calculated in the same way, and are defined by doing the cross product of different plane direction vectors. All $\overrightarrow{G_n}$ vectors are then brought to unit length and the X, Y and Z components are averaged to obtain the normal vector to the reference plane surface $\overrightarrow{G_{ava}}$.

$$\overrightarrow{G_{avg}} = \left[X_{G_{avg}} ; Y_{G_{avg}} ; Z_{G_{avg}} \right]$$

$$X_{G_{avg}} = \frac{\sum X_{G_n}}{n}$$

$$Y_{G_{avg}} = \frac{\sum Y_{G_n}}{n}$$

$$Z_{G_{avg}} = \frac{\sum Z_{G_n}}{n}$$

The vector \overrightarrow{G}_{avg} is then brought to unit length, giving the vector \overrightarrow{G} , which is the unit normal vector to the reference plane, providing the orientation of the dial gauge with respect to the cameras.

Although three points and two vectors would have been sufficient to obtain a normal vector to the surface, the use of numerous points and normal vectors allows for a better representation of the surface, avoiding any errors due to local inaccuracies in measurements or unevenness of the surface.

The calculation steps to obtain the reference plane unit normal vectors were defined in an excel file that was used as a template for all trial processing. Knowing the dial gauge direction vector, it is possible to project the measured VIC-3D blade displacement along the dial gauge direction to obtain a displacement value that is comparable to the dial gauge reading.

5.3.1.2. <u>Point Displacement Vector</u>

The VIC-3D displacement of the blade is obtained in a similar way as the reference plane data. By opening the captured image in VIC-3D, as seen in Figure 5.4, it is possible to identify the location of the displacement reference point on the speckle surface and extract the X & Y coordinates by placing the cursor over the point in the image. Using the metric node data export function, the X, Y & Z coordinates of the point are extracted for each of the images taken, including the reference image with no displacement.

Using the data points obtained, the displacement vectors of the point are calculated for each frame with respect to the points' coordinates in the reference image. The dot product of the point displacement vector and the dial gauge orientation vector is also calculated, which can then be compared to the dial gauge measurements. Below is a description of the calculations required to obtain the blade displacement along the dial gauge direction.

The initial coordinates of the point where displacement is measured is defined as X_0 , Y_0 and Z_0 . The coordinates of the point at frame N are X_N , Y_N and Z_N . The resulting displacement vector of the point at frame N is defined as $\overrightarrow{D_N}$.

$$\overrightarrow{D_N} = [\Delta X; \Delta Y; \Delta Z]_N = [X_N - X_0; Y_N - Y_0; Z_N - Z_0]$$

The unit vector \overrightarrow{DG} , defining the orientation of dial gauge measurement, as calculated in the previous section, is defined by $[X_{DG}; Y_{DG}; Z_{DG}]$. The displacement value for frame N, corrected to match the dial gauge orientation, is defined as D_{N-C} .

$$D_{N-C} = \overrightarrow{D_N} \cdot \overrightarrow{DG} = \Delta X_N * X_{DG} + \Delta Y_N * Y_{DG} + \Delta Z_N * Z_{DG}$$

The resulting value obtained for D_{N-C} can then be compared to the measured displacement obtained from the dial gauge reading. Once again, to simplify the data processing of the trials, the calculation steps were put in the same excel template used to obtain the dial gauge orientation vector.

The difference between the measured and VIC-3D corrected displacement is also calculated in the excel template, and the results are detailed in Table 5.1 in section 5.3.1.3 below. The comparison of the two values gives an estimate of the accuracy of the system in the out-of-plane direction. It can also be used later as a reference to compare the accuracy of the dynamic testing displacement measurements compared to what was obtained during the static testing.

5.3.1.3. <u>Measured out-of-plane system accuracy results</u>

The static tests were performed with the blade moving towards and away from the cameras. The two tests were conducted following the same testing procedures and the same data processing guidelines were applied. For each test, three practice trials were done to ensure proper setup of the displacement applicator and dial gauge indicator. Once the testing procedure was correctly executed, four trials were done and the results were recorded.

For each displacement increment, the difference between the dial gauge and VIC-3D corrected measurements are calculated in terms of absolute difference (in μm) and are

averaged for the entire trial. The average displacement difference is compared to the total blade displacement, giving a percentage displacement error with respect to the blade total displacement. The results for each trial, with the blade moving away and towards the cameras, are detailed in Table 5.1 below. For detailed results for each of the trials, please refer to Appendix A.

Table 5.1: Measured out-of-plane system accuracy results.

Blade Displacement Direction	Trial Number	Average Difference in Measurements [μm]	Percentage Error of Total Displacement
Avvov	1	142	1.73 %
Away from	2	178	2.17 %
	3	98	1.24 %
cameras	4	164	2.00 %
AVER	AGE	146	1.79 %
	1	178	2.47 %
Towards	2	216	2.55 %
cameras	3	172	1.85 %
	4	77	0.83 %
AVERAGE		161	1.93 %
ALL TRIALS AVERAGE		153	1.86 %

A statistical analysis was conducted and no statistically significant difference was identified between the blade displacement directions (M=12.48, SE=31.06 mm, p=0.691). The direction of the blade displacement will not significantly affect the results obtained, and the system does not display any bias in one direction for the displacement measurement.

Based on the average of all trials, the system accuracy for out-of-plane displacement measurements is $153\mu m$, representing below 2% error for total blade displacements

between 8 and 10 mm. It is important to note that the average blade displacement between images in the pilot dynamic testing is around 8 mm, which is consistent with the maximum blade displacement during static testing.

5.3.2. VIC-3D Measured System Accuracy

By taking multiple images of the reference plane, which is kept static, it is possible to estimate the noise in displacement and strain measurements. Since the plane is kept static, both displacement and strain values should theoretically be zero. Studying each of the reference points' displacement and strain values gives insight on the system accuracy and expected resolution of the measurements.

5.3.2.1. <u>Displacement Accuracy</u>

To calculate the displacement accuracy of the system, the data points extracted along the dial gauge reference plane can be used. The points' X and Y coordinates extracted for the first image are exact as they are defined as an input. The points' coordinates for the subsequent images are determined by tracking the points' location using DIC principles. Although the reference plane is kept static throughout all images, the points' coordinates will vary due to the limited accuracy of the system. Therefore, by comparing the X and Y coordinates of the points at each image with the reference coordinates defined in the first image, we can assess the measured in-plane accuracy of the system.

Since the initial Z coordinates of the points are determined by the system and not defined as an input, the initial Z coordinate is affected by the noise present in the system and cannot be used as an accurate reference point. Therefore, the VIC-3D measured out-of-plane

accuracy is not as reliable as the in-plane measurements. However, it does give some reference values to compare to the results obtained with the dial gauge measurements.

Below is an example of the calculations made to assess the VIC-3D measured system accuracy. The procedure is similar for point A as it is for points B to F. The coordinates of point A in the reference image are defined as $A_0 = [X_{A_0}; Y_{A_0}; Z_{A_0}]$. All subsequent images are defined as $A_n = [X_{A_n}; Y_{A_n}; Z_{A_n}]$, for which the following calculations were made, defining the error associated with point A and image n as $E_{A_n} = [\Delta X_{A_n}; \Delta Y_{A_n}; \Delta Z_{A_n}]$.

$$\Delta X_{A_n} = X_{A_n} - X_{A_0}$$

$$\Delta Y_{A_n} = Y_{A_n} - Y_{A_0}$$

$$\Delta Z_{A_n} = Z_{A_n} - Z_{A_0}$$

The error in X, Y and Z obtained for each point and image combination are averaged with respect to each coordinate direction, giving an average error in X, Y and Z, defined as ΔX_{avg} , ΔY_{avg} and ΔZ_{avg} . The results, representing the VIC-3D measured system displacement accuracy in both in-plane and out-of-plane directions, are detailed in Table 5.2 below.

For each trial, the average displacement error and standard deviation were calculated, and are represented in the grey and white rows respectively. With displacement away from the cameras, the average displacement error in the out-of-plane (Z-direction) direction is similar to what was found through measurements in section 5.3.1.3. For the trials with displacement towards the cameras, the average displacement error in the out-of-plane direction is noticeably greater. As mentioned previously, the VIC-3D measured displacement error in the out-of-plane direction is not as reliable as the in-plane measurements, and the values found in section 5.3.1.3 represent more accurately the system out-of-plane displacement accuracy.

The displacement error in the X and Y direction is similar for both away and towards camera displacement trials. It gives a good estimate of the expected in-plane system accuracy, around $31\mu m$ in X-direction and $57\mu m$ in the Y-direction.

Table 5.2: VIC-3D measured system displacement accuracy results.

For each trial the average displacement error (grey) and standard deviation (white) is shown.

Blade Displacement Direction	Trial	Displacement Error in X [µm]	Displacement Error in Y [µm]	Displacement Error in Z [μm]
	1	20	41	120
		17	36	112
Avvov	2	31	63	205
Away from		28	57	164
cameras	3	22	54	161
cameras		19	41	112
	4	28	65	191
		23	52	151
Average Disp	Average Displacement Error		56	169
Average Stan	Average Standard Deviation		46	135
	1	29	45	235
		24	29	174
	2	53	75	382
Towards		49	56	297
cameras	3	32	54	266
		25	35	194
	4	34	55	263
		20	36	166
Average Disp	Average Displacement Error		57	286
Average Standard Deviation		30	39	208
All Trials Avg Displacement Error		31	57	228
All Trials Avg Standard Deviation		26	43	171

5.3.2.2. <u>Strain Resolution</u>

To determine the strain resolution of the system, the AOI is modified to include only the reference plane, as no deformation is applied to it. The same processing parameters are used. In this case, the strain is calculated for each point along the reference plane, giving a bigger data set to evaluate the strain resolution of the system.

The ϵ_{xx} , ϵ_{yy} and ϵ_{xy} strain values for the entire reference are exported for each image. By looking at the mean and standard deviation associated with the strain measurements along the reference plane, we can estimate the strain resolution of the system.

Table 5.3: VIC-3D measured system strain resolution.

Blade Displacement Direction	Trial	E _{xx} resolution [μs]	E _{yy} resolution [μs]	E _{xy} resolution [μs]
Αννον	1	307	474	379
Away from	2	491	522	606
	3	436	480	449
cameras	4	721	626	735
Average Strain Resolution		489 μs	526 μs	542 μs
	1	1675	1215	1368
Towards	2	1244	837	1472
cameras	3	694	754	781
	4	617	519	585
Average Strain Resolution		1057 μs	831 μs	1052 μs
All Trials Average		773 μs	678 μs	797 μs

As there is no deformation or motion of the reference plane, the strain measurements should be zero for all the data points. The strain values obtained for each image are averaged together to obtain average values for the ϵ_{xx} , ϵ_{yy} and ϵ_{xy} strains for each trial. The results for

each trial, along with an average of all trials, is detailed in Table 5.3 above, giving an estimate of the strain resolution of the system.

As was noticed for the VIC-3D measured displacement accuracy, there is a noticeable difference between the *towards* and *away* from the cameras trials. Since the blade moves away from the cameras for the dynamic testing, the strain resolution of the system for this study can be taken as the average strain resolution for the trials with the blade moving away from the cameras. The strain resolution of the system can be estimated to be a little above 500 µstrain in the longitudinal and shear directions.

5.3.3. VIC-3D Calculated System Accuracy

The VIC-3D software allows for a number of pieces of information regarding the system accuracy to be exported for further study. Amongst other things, it allows for the statistics regarding displacement measurements to be studied for each processed image. The minimum, maximum, mean, median and standard deviation can be obtained for displacement measurements and sigma values. This information is useful to get a calculated estimate of the system accuracy.

The sigma values, which represent the 1-standard deviation confidence interval for the displacement data, can be used to assess the system displacement accuracy. The sigma values can be doubled to obtain a 95% confidence interval, providing an accurate estimate of the error associated with noise. Unfortunately, since the sigma values are calculation based, these results do not account for any error in calibration or issues with the experimental setup. Although the sigma values are not entirely representative of the system

accuracy, it still gives a set of reference data to compare to the static testing that was conducted and to the sigma values obtained for the dynamic testing.

For each image, the mean sigma values for the X, Y and Z axis are extracted, and the values are averaged to obtain an average sigma value for each trial. The values are doubled to obtain the 95% confidence interval and correctly assess the calculated displacement accuracy of the system. The results are shown in Table 5.4 below.

Table 5.4: VIC-3D calculated system displacement accuracy.

Blade Displacement Direction	Trial	Error in X- direction [µm]	Error in Y- direction [µm]	Error in Z- direction [µm]
A	1	5	14	119
Away	2	8	26	123
from	3	6	17	117
cameras	4	7	17	125
Average Displa	Average Displacement Error		18	121
	1	6	14	143
Towards	2	6	10	139
cameras	3	6	17	134
	4	9	14	144
Average Displacement Error		7	14	140
All Trials Average		7	16	131

The VIC-3D calculated displacement accuracy does not account for calibration errors or other issues with the experimental setup. The calculated displacement accuracy in the out-of-plane direction is slightly lower than what was measured with the dial gauge. Therefore, the sigma values extracted from each of the trial statistics gives an optimistic

estimate of the system accuracy, but can still be used as reference to ensure consistency between images taken from different trials.

5.4. Discussion

The displacement accuracy of the system is sufficient to track a hockey blade with great precision. The in-plane displacement measurements provide great accuracy, below $60\mu m$ error, which allows to track side to side motion of the blade precisely. The out-of-plane displacement accuracy is around $150\mu m$, which remains acceptable due to the large displacement of the blade throughout the shot (between 20 and 35 cm).

A possible source of error for the displacement measurements is the difference between the dial gauge on the concave side of the blade and the reference point for DIC on the convex side. Since the dial gauge is not visible in the images, it is assumed that there is no motion of the dial gauge with respect to the blade, which has not been proven. Moreover, there might be difference in the displacement of the inner surface of the blade compared to the outer surface, which can affect the results between dial gauge and DIC readings.

The accuracy of the system is not affected by the direction of the blade motion in the out-of-plane direction, as has been highlighted in the comparison of the VIC-3D displacement and dial gauge measurements. However, there are visible differences in accuracy and strain resolution when based on the VIC-3D data. This is surprising, but can be due to the increasing size of the speckles as the blade moves towards the cameras, decreasing the system accuracy and resolution. Since the speckle pattern was determined based on the blade moving away from the cameras, the static trials done with the blade moving away from the cameras are more representative of the dynamic testing trials to be conducted.

The static testing has allowed assessment of the displacement accuracy and strain resolution of the system, giving satisfying results. The displacement accuracy is around $150\mu m$ in the out-of-plane direction, and estimated to be below $60\mu m$ in the in-plane direction based on VIC-3D measurements. The strain resolution of the system is below $550\mu m$ in the in-plane and shear directions.

The displacement accuracy and strain resolution of the system can be improved by changing the camera system and focusing on a smaller region of the blade. For this study, the system accuracy and resolution is sufficient to identify blade dynamic behavior for a full-blade, and if more precision is required in a specific region, the experimental setup would have to be modified to improve the local accuracy.

6. Dynamic Testing

The use of DIC to study the deformation and displacement of the hockey blade is a new approach to a complex problem. Through static testing, it has been determined that the accuracy and resolution of the system allows for a precise study of the blade dynamic behavior. The dynamic testing portion of this study was done to obtain dynamic data on the different blade patterns and constructions and identify how these parameters may affect the blade behavior during a slap shot event.

This section details the steps taken to conduct the dynamic testing, from the participants and equipment used to the data processing and the results obtained. The testing setup as well as procedure to conduct the testing is also explained in this section.

6.1. Participants and Equipment

6.1.1.1. Participants

Participants for this study were recruited through word of mouth within the McGill community, focusing on high-level hockey players that were currently playing, or had recently played, at the university level.

A total of six male subjects participated in this study, all were right-handed and played with left-handed hockey sticks. The subjects' ages ranged from 22 to 31 years of age, with an average age of 28 years old. The players had between 17 to 29 years of hockey experience, with an average of 23.3 years. The subjects had not suffered major injuries, which would have prevented them from practicing hockey in the year prior to testing and considered themselves able to participate in the study.

6.1.1.2. <u>Equipment Tested</u>

To assess the effects of blade construction and geometry as well as the variability associated with human testing, four blades were tested, as mentioned in section 4.1.

Two blade patterns, denoted P1 and P2, were tested along with two blade constructions, denoted CA and CB. Two sticks with the same blade construction/pattern combination were tested to highlight the consistency, or inconsistency, associated with the slap shot technique and variation between shots.

The four sticks tested were defined as pattern-construction, as follow:

- P1-CA (pattern 1, construction A)
- P1-CB1 (pattern 1, construction B, stick 1)
- P1-CB2 (pattern 1, construction B, stick 2)
- P2-CA (pattern 2, construction A)

The stick testing order was randomized for each subject to reduce bias due to fatigue during testing. The sticks were also coded so that subjects were unaware of which blade construction and pattern was being tested.

6.2. Testing Setup

The DIC stereoscopic arrangement used for the dynamic testing is the same that has been detailed in previous sections and that has been used to conduct the static testing. For each subject, the cameras were adjusted to adapt to the blade displacement trajectory throughout the shot. Similarly, the lighting was adjusted to provide even lighting throughout the blade motion and keep light reflection off the blade to a minimum.

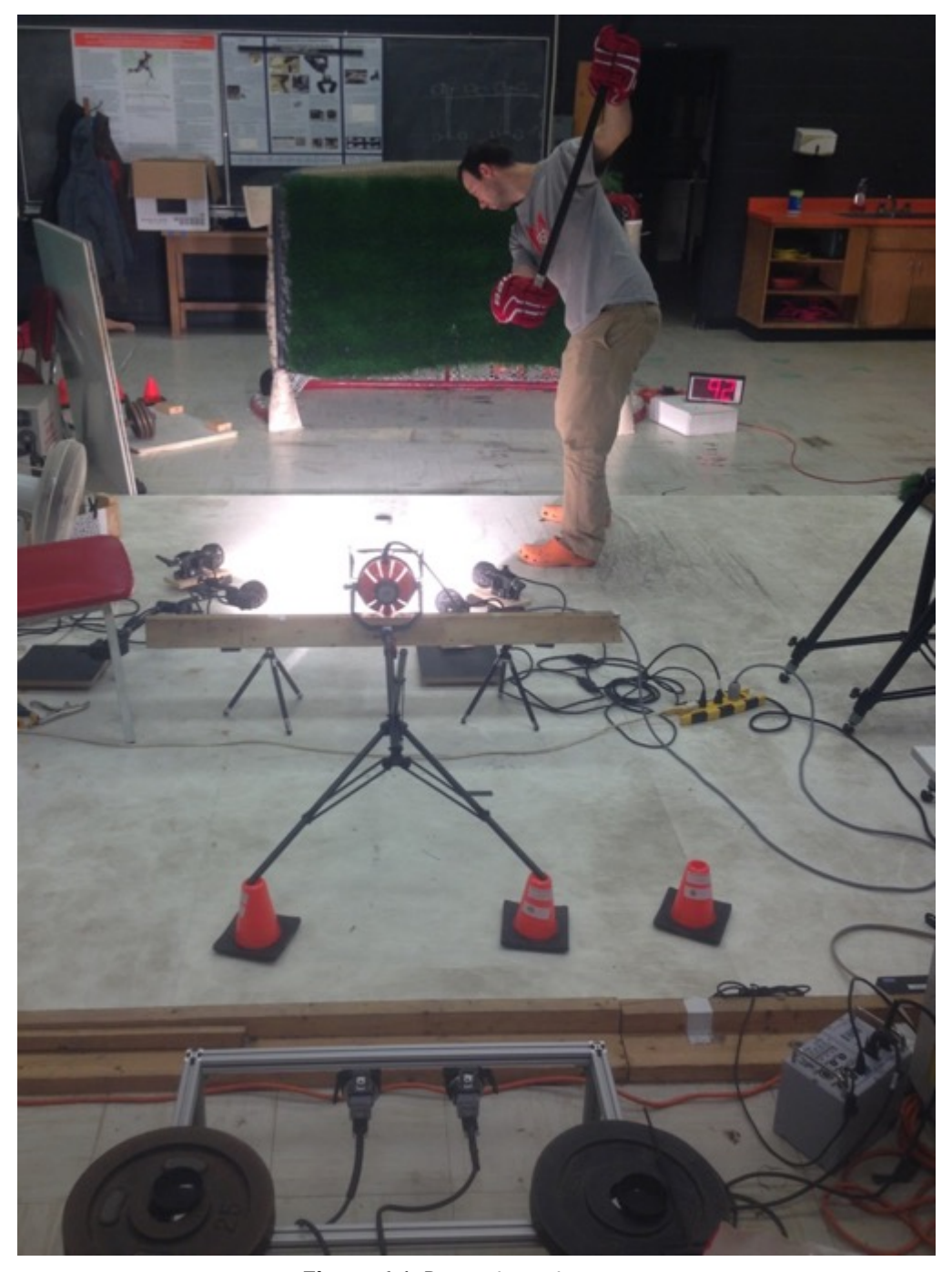


Figure 6.1: Dynamic testing setup.

The subject is positioned near the limit of the artificial ice surface, while leaving enough room for both feet to be on the surface. It is also ensured that the blade-puck contact ended prior to the end of the ice surface.

The puck is positioned three meters away from the camera, and a full size hockey net is set at a distance of 2.5 meters in front of the puck location. Some weights were added on the net to prevent any movement. A sheet of artificial turf is put on top of the net and left hanging in front in order to prevent the puck from bouncing back after the shots. A small gap is left at the bottom of the turf for the puck to go through and to allow the puck velocity to be measured by the radar gun. The radar gun is placed behind the net, aimed at the puck location and aligned with the shot direction. The radar gun display faces towards the computer so the shot velocity can be recorded after each shot.

6.3. Testing Procedure

Upon arrival, each subject is given explanations on the steps to be followed during testing as well as precautions to be taken to protect the equipment and ensure accurate results were obtained.

6.3.1. Paperwork

The subjects filled a pre-screening questionnaire to provide information regarding their age, hockey experience and handedness, amongst other information. An ethics certificate was obtained (REB #225-1115) for the study and the participants were given a consent form to be read and signed, in accordance with the Tri-Council Policy Statement on Ethical Conduct for Research Involving Humans. The two documents are presented in Appendix B.

6.3.2. Warm-Up

Each subject is given a minimum of 5 minutes to take some practice shots on the artificial ice surface in order to adapt to the shooting surface and the testing conditions. Simultaneously, the cameras and lighting are adjusted to obtain satisfying images. The shot direction was changed slightly depending on the subjects, directing them to aim for the right or left side of the net depending on their shooting technique and blade trajectory. Changing the shot direction allows for the blade to remain within the FOV of the cameras without having to move the camera's support frame.

The puck location is also adjusted throughout testing to ensure consistent images of the blade are obtained. The approximate location of the puck and of the subject's feet are marked on the ice surface to improve consistency between trials.

6.3.3. Dynamic Trials

Once the subject is comfortable with the testing environment and the recording system is adjusted, the dynamic trials are recorded.

6.3.3.1. <u>Systematic Calibration</u>

For each trial, a set of calibration images is taken. Snapshots of the calibration grid are saved in the same way as done for static testing, and the puck is positioned in the appropriate location. After each calibration, the subject is instructed to minimize his movements to reduce the vibrations, which can skew the system calibration.

6.3.3.2. Data Collection

The subject is handed a specific stick depending on the random stick order determined prior to testing. A shot is taken and the video captured is immediately played to verify the quality of the images obtained. If the blade remains within the FOV of both cameras prior to ice impact and throughout its motion, the shot is deemed good and the video is saved and the shot velocity is recorded. If an extremity of the blade goes out of the FOV, or if the subject is not satisfied with the shot, the trial is deemed unsuccessful and the data is not saved.

For each stick tested, 5 to 7 successful trials are recorded along with the corresponding set of calibration images.

6.3.3.3. <u>Data Pre-Processing</u>

Due to the time required to inspect each trial's video and export the images, these steps are done once all the trials have been recorded. The PFV software allows for any pair of video files to be opened and modified after they have been captured. The videos for each trial are therefore opened in PFV one by one, and the ice impact frame is identified along with the last frame where the blade is fully visible from both cameras' FOV. The first frame to be processed in VIC-3D is defined as 3 to 4 frames prior to blade ice impact in order to have a good reference image of the undeformed blade. All relevant images are then renamed in order to be compatible with the VIC-3D required filenames and are saved for further data processing.

6.4. Data Processing

In the case of dynamic testing, the displacement and strain data is extracted using the VIC-3D software and the data files obtained are subsequently processed using Matlab R2014b (MathWorks, Natick, MA, USA). Due to the amount of data obtained for each trial, a systematic approach is used for data processing and is applied to each dynamic trial. The processing steps done in VIC-3D, Matlab and the following statistical analysis of the data are detailed in this section.

6.4.1. VIC-3D Processing

As is required for all testing using VIC-3D, the first step of data processing is to calibrate the system using the calibration images obtained prior to each dynamic trial. The same $15\,\mathrm{x}$ 7 calibration grid is used and the calibration score and report are both recorded.

The AOI is then defined manually on the first image of the blade prior to puck impact, trying to match the blade outline while leaving a small region around the edges out of the AOI. Due to the round edges of the blade, the speckles near the edge are not as defined and are left out of the AOI to reduce inaccuracies in calculations.

From trial and error during processing of the static and dynamic trials, it was found that the size of the AOI, the step size and strain filter used have a great influence on the results obtained and the noise present in the data. The processing parameters do not affect significantly the displacement measurements, but have a great impact on the strain calculations. High vibrations were noticed at the tip of the blade, which could not be accurately captured at the camera sampling rate of 4000 FPS, which led to increased noise throughout the AOI. Cropping out the tip of the blade to focus on the puck impact region

leads to a reduction in noise in the data and a more accurate strain distribution. The step size, which defines the number of pixels between each data points, was found to give good results when its value is set to be around a quarter of the subset size, as is suggested by Correlated Solutions [53]. Reducing the step size increases the number of data points within the AOI, but also increases the error when associated with bigger subset sizes. Having a good ratio between subset size and step size was found to improve the results obtained. Moreover, using too small of a strain filter leads to high noises across the blade. The product of step size and strain filter defines the smoothing region for the strain calculations and corresponds to the size in pixels of the virtual strain gauge used for the calculations. It was found that the product of step size and strain filter should be between 50 to 65 pixels to reduce the strain noise. Finally, low-pass filtering and eighth order interpolation are used to further reduce the noise error.

Based on the guidelines mentioned above, the images are processed a first time and the results are inspected visually to ensure homogeneity in the strain calculations. The processing parameters are fine-tuned and some trials are re-processed until the strain distribution is acceptable with minimal error.

The processing parameters are adapted for each trial, and the final settings are compiled in an excel file. For all trials, the suggested subset size is used and varies between 19×19 to 37×37 pixels depending on blade orientation in the first image where the AOI is defined. The step size varies between 4 and 9 pixels and the strain filter is chosen to be between 7 and 15, depending on the step size used.

After successful data processing and visual inspection of the results, the processed data is exported. For each of the trials, the following data is exported in independent excel files, giving information for each of the images processed:

- Processing report: number of data points and pixel error.
- Strain statistics report: minimum, maximum, mean, median, standard deviation for the in-plane strains.
- Displacement error statistics report: minimum, maximum, mean, median, standard deviation for the displacement error (sigma).
- Full data set for each image: data point coordinates (X, Y, Z) with associated displacement in the X, Y and Z-direction and in-plane strains (ε_{xx} , ε_{yy} , ε_{xy}).

To study the blade velocity throughout the shot, nine points along the blade surface are defined using the metric node data export function, similar to reference plane data points extracted in the static testing portions of this study. For each frame of the trial, the nine points' coordinates and strain values are exported in individual excel files. The frame at which puck impact occurs is identified by analyzing the average blade velocity. The blade velocity for each frame is plotted on a graph and the frame at which puck velocity starts to decrease significantly is defined as the puck impact frame.

Along with the numerical data mentioned above, the approximate location of puck impact is estimated by visually identifying sudden deformation of the sample. Although the puck impact location may not be precise, it provides a reference region for strain data processing.

The data for each trial is then further processed using Matlab to extract the required information needed to assess the dynamic blade behavior.

6.4.2. Matlab Processing

Based on the VIC-3D output data and calibration results, the first step is to identify trials where calibration or image pixel error is deemed unacceptable. For all trial processing, the acceptable calibration error is set to 0.04 pixels while the acceptable average image error is set to 0.08 pixels. For each trial, the pixel error values for each image are averaged to obtain an average pixel error for the trial. The trials for which the average pixel error or the calibration score falls outside of the acceptable range are not considered for further processing. After this initial selection, a total of 87 trials were deemed acceptable out of a total of 140.

Using the approximate impact location, an area surrounding the impact region is determined and the maximum strain values within the region are extracted along with the location and frame at which the maximum strain occurs. This allows for identification of the maximum compressive and tensile strains used for statistical analysis. Moreover, based on the puck impact frame, the number of frames between puck impact and maximum strain is also calculated to identify possible differences in the speed of strain propagation within the blade.

The data from the nine points along the blade are used to calculate the blade velocity at each point and obtain an average blade velocity for each frame. The blade velocity is calculated by determining the distance between each point along the blade from one frame to the next and dividing it by the image capture rate of the camera. This allows the study of overall blade velocity, useful to compare to values previously found in literature. The blade velocity was also plotted using Matlab to study trends and visually identify differences between sticks.

Using the data compiled using Matlab, the information is then used for statistical analysis with the objective of identifying significant differences between blade patterns and constructions.

6.4.3. Statistics

For statistical analysis, the program IBM SPSS Statistics Version 19.0.0 (IBM, Armonk, NY, USA) was used and a Repeated Measures ANOVA analysis was used to conduct withinand between-subjects' comparisons.

The displacement error associated with each trial is investigated to ensure there is no significant difference in the displacement error for the trials for each stick.

The shot velocity is studied independently to identify any significant differences in puck velocity based on stick type or subject. The blade velocity at puck impact is studied to identify significant differences depending on stick type and subject. The shot velocity and average blade velocity at puck impact are also compared to identify any correlation between blade velocity and shot velocity.

The maximum tensile and compressive strain values are studied to identify significant differences depending on stick or subject. The values were also compared to shot velocity and blade velocity to identify any correlation between the results. Finally, the strain delay between puck impact frame and frame at maximum strain is investigated to highlight differences between sticks and subjects.

6.5. Results

6.5.1. Visual Representation

The analysis in VIC-3D of the sequential images captured during a trial allows the visualization of the blade deformation through time. Although the visual inspection of individual trials is time consuming and not a viable approach for data processing, it remains interesting to take a look at the images captured and the calculated strains throughout a shot.

Shown in Figure 6.2 below is the VIC-3D output for a specific trial, where ε_{xx} , the longitudinal strain data in the X-direction (along the blade length), is overlaid on the images captured by one of the cameras. Although it is impossible to reach a definitive conclusion by looking at an individual trial, it helps with the interpretation of the numerical data obtained.

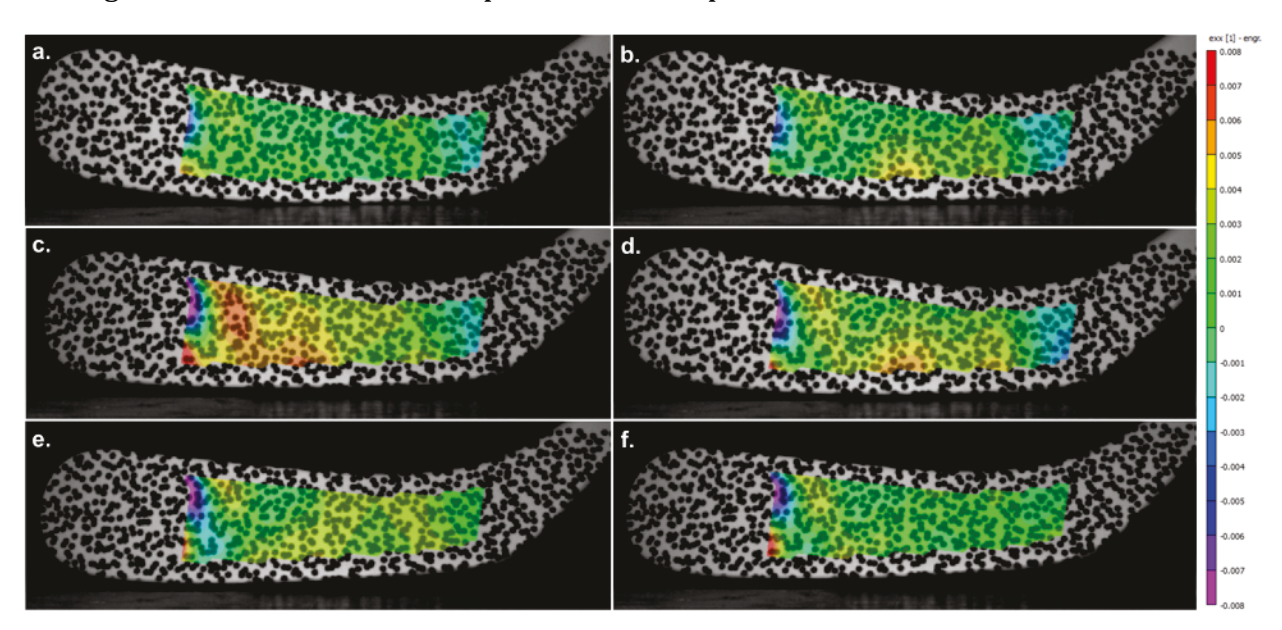


Figure 6.2: VIC-3D representation of the tensile strain along the X-direction (ε_{xx}) for blade P1-CB1.

a. Puck impact -1 frame. **b.** Puck impact frame. **c.** Puck impact +1 frame.

d. Puck impact +3 frames. e. Puck impact +6 frames. f. Puck impact +8 frames.

The visual output obtained via VIC-3D can be hard to visualize due to the strain errors along the edge of the AOI which stand out compared to the actual strain values due to blade

deformation. In order to obtain a more precise representation of the strain field in the puck impact region of the blade, the data for the specific trial shown in Figure 6.2 was exported in the form of an excel document and subsequently plotted using Matlab. The resulting strain distribution is shown in Figure 6.3 below.

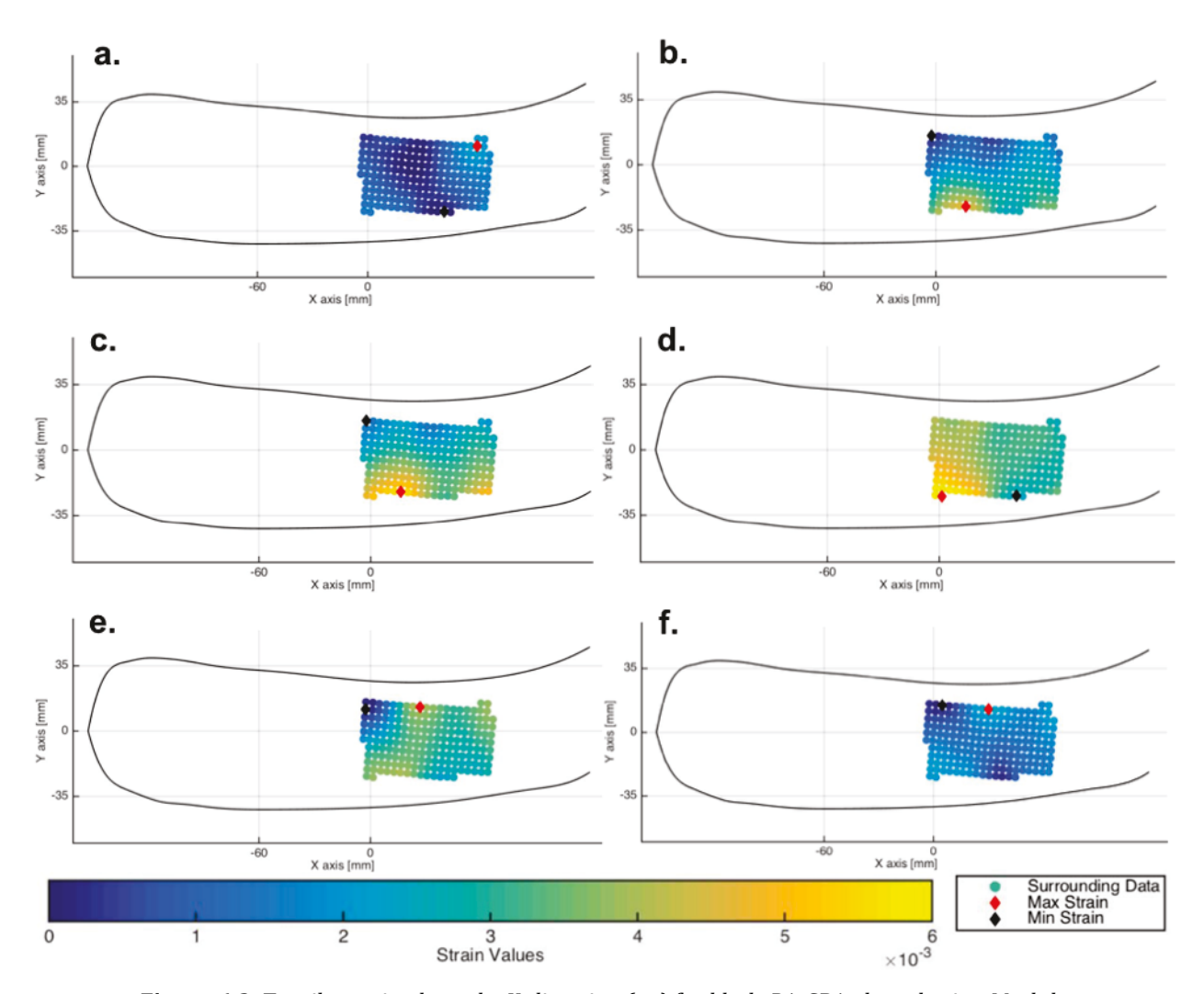


Figure 6.3: Tensile strain along the X-direction (ε_{xx}) for blade P1-CB1 plotted using Matlab.

a. Puck impact -1 frame. **b.** Puck impact frame. **c.** Puck impact +1 frame.

d. Puck impact +3 frames. e. Puck impact +6 frames. f. Puck impact +8 frames.

By looking at the visual representation of the strain distribution in the puck impact region for a number of frames before and after impact, it is possible to see how the strain propagates. It is interesting to see that there is very minimal strain prior to puck impact. This highlights the fact that preloading of the stick prior to puck impact, which is associated with a significant deformation of the shaft, does not significantly affect blade deformation. The peak strain (shown with a red diamond in Figure 6.3 above) along the X-direction occurs in the instants following puck impact. The strain increases near the bottom of the blade, where puck-blade contact occurs, until it reaches its peak value. It then decreases and moves towards the upper region of the blade before dissipating, leaving the blade with a similar strain distribution as prior to puck impact.

It is important to notice that this behavior occurs over a very short lapse of time, with Figures 6.2 and 6.3 above representing the strain distribution for a period of 2 milliseconds. The strain distribution along the blade throughout a shot can be studied alongside the blade velocity to identify possible multiple impacts between puck and blade. It is hypothesized that there is no contact between puck and blade at the instant where the blade reaches back its initial state as seen prior to puck impact.

The focus was put on puck impact as it is the instant where the maximum blade deformation is expected. The following puck impacts due to puck bounce are expected to be lower than the initial deformation highlighted in Figure 6.3 above.

6.5.2. Displacement Error

For each trial, the sigma statistics are averaged to obtain a Sigma X, Y and Z value. These values were compiled for each trial and averaged based on the stick number. The displacement error associated with each stick is shown in Table 6.1 below.

Table 6.1: Displacement error Sigma averaged for each stick.

Stick	Sigma X [µm]	Sigma Y [μm]	Sigma Z [μm]
P1-CA	17	37	193
P1-CB1	18	42	194
P1-CB2	12	33	168
P2-CA	21	52	194
Average	17	41	187

No statistically significant differences were identified between the sticks based on the displacement error values, F(3.613,100) = 0.411, p = 0.781, sphericity is not assumed and a Greenhouse-Geisser correction was used.

These results highlight that no bias in terms of displacement error occurred for any particular stick. Moreover, the results obtained are consistent with values found for the static testing, and therefore the data for all sticks can be compared with confidence.

6.5.3. Shot Velocity

The shot velocity, in kilometers per hour, was averaged for all trials and each stick and the following results were obtained.

Table 6.2: Average shot velocity per stick.

Stick	P1-CA	P1-CB1	P1-CB2	P2-CA
Average Shot Velocity [km.h ⁻¹]	118.72	116.03	118.88	121.19

Based on the average shot velocities, we can see that stick P2-CA has a greater overall average velocity than the three other sticks. Moreover, for 4 out of 6 subjects, stick P2-CA

produced the fastest average shot velocity, which shows that the blade pattern has an influence on the shot velocity.

For all trials combined, the P2-CA stick was found to provide significantly faster shots compared to the P1-CB1 stick (M = 5.16, SE = 1.34, p < 0.05). For stick P1-CA, no significant difference was identified (M = 2.47, SE = 1.31, p = 0.69), which is due to the error term and variability in the shot velocities. It is interesting to see that there is no significant difference between P2-CA and P1-CB2 (M = 2.31, SE = 1.37, p = 0.102), although it is the same blade pattern and construction as P1-CB1.

It is important to put this in perspective by mentioning that for one subject, a significant difference was found in the shot velocity between sticks P1-CB1 and P1-CB2 (M = -7.4, SE = 1.81, p < 0.05). This is a clear indication that the variability present with human testing of hockey stick is, in certain cases, more important than the differences in blade construction and pattern.

6.5.4. Blade Velocity

The blade velocity between each frame was calculated for each individual trial. An average of the trials was done for each stick, and the average blade velocity is presented in Figure 6.4 below.

By looking at the graph, we can see that the blade velocity throughout a shot seems consistent for all sticks. The blade velocity drops rapidly after puck impact and slowly increases afterwards. There are oscillations after the initial puck impact, which is attributed to the puck "bounce" on the blade, which has been observed in previous studies.

Unfortunately, the range of acceptable images is not long enough to reach the puck release event, which leads to a lack of data regarding the blade velocity at puck release.

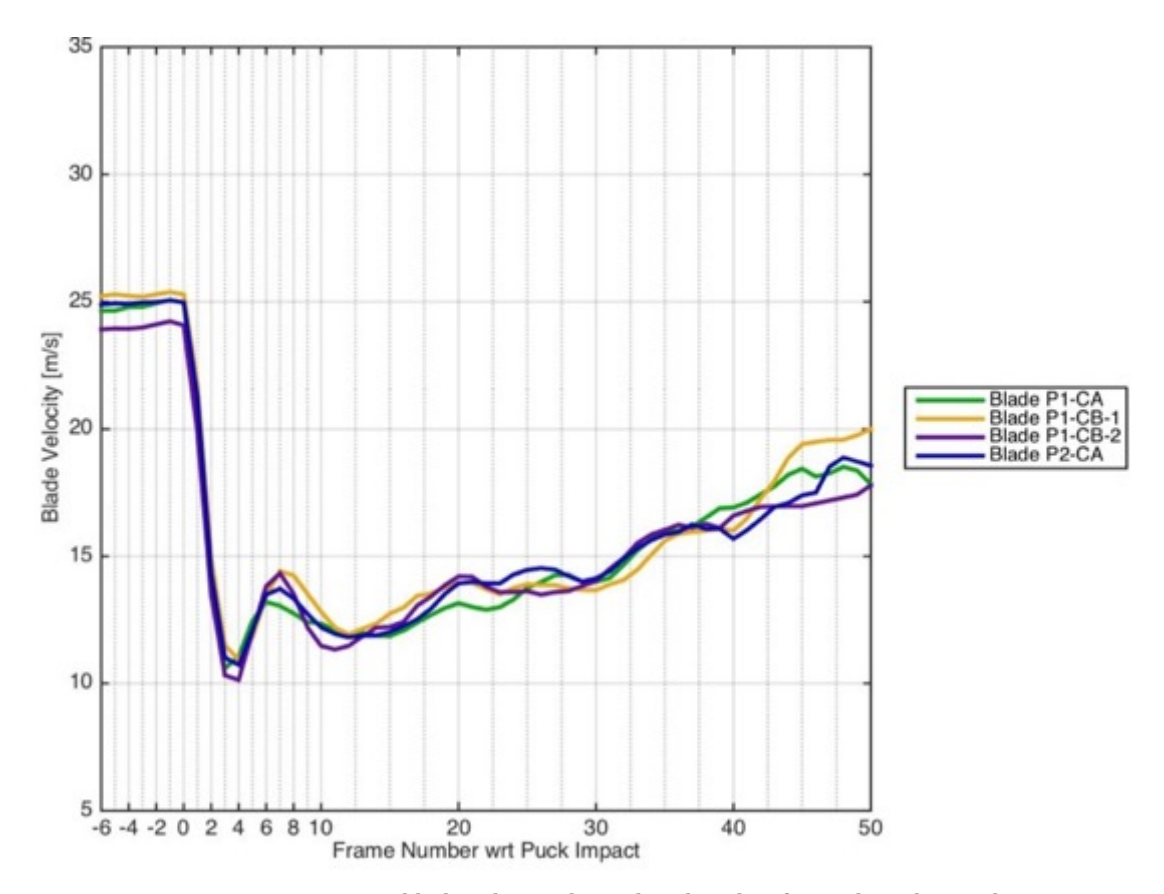


Figure 6.4: Average blade velocity through a slap shot for each stick tested.

The average blade velocity at puck impact (24.9 m.s⁻¹) is higher than what has been reported by Lomond et al. [22] (17.7 m.s⁻¹ for elite subjects), but can be justified in part by the difference in average puck velocity observed between the two studies (118.7 km.h⁻¹ and 73.7 km.h⁻¹ respectively).

A statistical analysis of the blade velocity at puck impact was done and the values for the four sticks were compared, the mean values are displayed in Table 6.3 below. It is interesting to notice that statistically significant differences were found between stick P1-CB2 and sticks P1-CA (M = -1.63, SE = 0.61, p < 0.05) and P1-CB1 (M = -2.19, SE = 0.50, p < 0.05)

0.0005). These differences in blade velocity can be due to both subject technique and blade properties, without a clear way to differentiate the individual effect of each factor.

Table 6.3: Average blade velocity at puck impact per stick.

Stick	P1-CA	P1-CB1	P1-CB2	P2-CA
Average Blade Velocity at Puck Impact [m.s ⁻¹]	25.71	26.26	24.07	24.87

The difference between maximum and minimum blade velocity was also calculated for each trial and represented as a percentage velocity loss with respect to the maximum value. No significant differences were identified based on stick type for the percentage blade velocity loss, F(3,48) = 0.966, p = 0.416.

6.5.5. Strain Values

The maximum strain values in the vicinity of the puck impact location were identified. It is of particular interest to identify the peak strains due to puck impact, the delay between puck impact and maximum strain as well as study the possible correlations between strain values and puck and blade velocity.

6.5.5.1. <u>Maximum strains</u>

The maximum strain values, compressive and tensile, were averaged per stick type and are detailed in Table 6.4 below, in terms of percentage strain. Both in-plane strains ϵ_{xx} and ϵ_{yy} and shear strain ϵ_{xy} were extracted from VIC-3D and the minimum and maximum values were used to identify the maximum compressive and tensile strains respectively.

Table 6.4: Maximum strain values averaged for each stick.

Sti	ick	P1-CA	P1-CB1	P1-CB2	P2-CA
	ε _{xx} [%]	- 0.698	- 0.679	- 0.734	- 0.872
Compressive Strain	ε _{yy} [%]	- 1.174	- 1.167	- 1.463	- 1.642
	ε _{xy} [%]	-2.123	-1.918	-1.718	-2.642
	ε _{xx} [%]	1.262	1.307	1.102	1.491
Tensile Strain	ε _{yy} [%]	1.415	1.594	1.474	1.848
	ε _{xy} [%]	1.152	1.560	1.736	1.631

In terms of compressive strain, the only significant difference was observed for the shear strain between sticks P1-CB2 and P2-CA (M = 0.009, SE = 0.003, p < 0.05). For the tensile strain, a significant difference was found for ϵ_{yy} , the strain along the Y-direction (the height of the blade) between sticks P1-CA and P2-CA (M = -0.004, SE = 0.002, p < 0.05). Based on these results, it can be said that there is an influence of the blade pattern is reflected in the shear strain and Y-direction strain of the blade.

For both compressive and tensile strain, ϵ_{xx} , the strain along the length of the blade, was found to be significantly smaller than ϵ_{yy} and ϵ_{xy} in absolute value. For the compressive strain, the shear strain was found to be significantly greater than both ϵ_{xx} and ϵ_{yy} , which is not the case for the tensile strains. The statistical results of the comparisons between strain types are detailed in Table 6.5 below. The average values for compressive strain for all trials

are -0.007, -0.013 and -0.021 for ϵ_{xx} , ϵ_{yy} and ϵ_{xy} respectively. The average values for tensile strain for all trials are 0.012, 0.016 and 0.015 for ϵ_{xx} , ϵ_{yy} and ϵ_{xy} respectively.

Table 6.5: Statistical results for comparison of strain types.

Strain Type	Strain I	Strain J	Mean Difference (I - J)	Standard Error	p value
	$\boldsymbol{\epsilon}_{\mathbf{x}\mathbf{x}}$	ϵ_{yy}	0.006	0.001	p < 0.0005
Compressive Strain	ε _{xx}	$\boldsymbol{\epsilon}_{\mathbf{x}\mathbf{y}}$	0.013	0.001	p < 0.0005
J. J. L.	ε _{yy}	$\boldsymbol{\epsilon}_{\mathrm{xy}}$	0.007	0.001	p < 0.0005
	ϵ_{xx}	ϵ_{yy}	- 0.004	0.001	p < 0.05
Tensile Strain	$\epsilon_{ ext{xx}}$	ϵ_{xy}	- 0.003	0.001	p < 0.05
	ε _{уу}	$oldsymbol{arepsilon}_{ ext{xy}}$	0.001	0.001	p = 0.257

It is interesting to see that when the back of the blade is under compression, the shear strain average value is three times as important as the in-plane strain along the length of the blade. The importance of the shear strain is not as significant when the blade is under tension, showing an intricate behavior of the blade which goes back and forth between tension and compression as the blade deforms after puck impact.

6.5.5.2. <u>Strain Delay</u>

The number of frames between puck impact and maximum strain was calculated for the three strains ϵ_{xx} , ϵ_{yy} and ϵ_{xy} , in both compression and tension. The average strain delays for each stick are detailed in Table 6.6 below.

In terms of compressive strains, the stick type was found to have no significant effect on ϵ_{xx} (F(3,48) = 0.181, p = 0.909), ϵ_{yy} (F(1.955,31.3) = 0.328, p = 0.718, Greenhouse-Geisser correction) or ϵ_{xy} (F(3,48) = 1.345, p = 0.271).

For tensile strains, the stick type was also found to have no significant effect on ϵ_{xx} (F(3,48) = 0.949, p = 0.424), ϵ_{yy} (F(3,48) = 1.914, p = 0.14) or ϵ_{xy} (F(3,48) = 0.558, p = 0.645). However, a significant difference was identified between sticks P1-CB1 and P1-CB2 (M = 3.471, SE = 1.422, p < 0.05), which highlights the effects of variability between and within subjects from shot to shot.

Table 6.6: Strain delay between frame at puck impact and frame at maximum strain.

All values are in number of frames. Multiply by 0.25 ms to obtain a time value.

Strain Type	Strain	P1-CA	P1-CB1	P1-CB2	P2-CA
	ϵ_{xx}	9.5	8.6	7.7	7.8
Compressive Strain	ε _{уу}	10.7	8.9	10.1	10.2
Strum	ϵ_{xy}	7.1	6.2	10.4	9.4
	ϵ_{xx}	5.9	7.5	5.2	8.1
Tensile Strain	ε _{уу}	9.0	12.4	8.9	11.5
	$oldsymbol{arepsilon}_{ ext{xy}}$	8.4	11.2	9.2	8.5

It is interesting to note that no statistically significant correlation (p > 0.05) was found between the strains for each type of sticks, except between ε_{xx} and ε_{yy} in compression for stick P1-CB2 (p < 0.05). Therefore, it can be said that there are no apparent relationships between the different maximum in-plane strains in the vicinity of the puck impact.

Moreover, it was found that the subject has a statistically significant effect on the strain delays for ϵ_{xx} and ϵ_{yy} , for both compressive and tensile strains.

• ε_{xx} Compressive: F(5,45) = 3.736, p < 0.05

• ε_{yy} Compressive: F(5,45) = 4.510, p < 0.05

• ε_{xx} Tensile: F(5,40) = 3.677, p < 0.05

• ε_{yy} Tensile: F(5,40) = 2.875, p < 0.05

6.5.5.3. <u>Correlation with puck and blade velocity</u>

A correlation analysis between the tensile and compressive strain values and the blade and shot velocities was done. The compressive strain in the Y-direction (ε_{yy}) was found to be positively correlated to the blade velocity (r = 0.476, p < 0.01), but not shot velocity (p > 0.05). The tensile strain in the Y-direction (ε_{yy}) was found to be correlated to shot velocity (p > 0.323, p < 0.01), but not blade velocity (p > 0.05).

These results once again highlight the complex dynamic behavior of the blade after puck impact, which leads to an absence of clear correlation between shot velocity, blade velocity and the in-plane strains present in the blade.

6.6. Discussion

The dynamic testing portion of this study was successful. Quality images of a hockey blade during a slap shot were captured and analyzed using DIC principles. The variability in players' technique and in consecutive shots proved challenging and led to a number of unsuccessful trials for some of the subjects. The processing of the images was successful

using the VIC-3D software, and extensive Matlab processing was required to extract the required information.

The displacement error associated with the dynamic tests is consistent with the values found for the static testing portion of this study, which proves the viability of this technique. The average velocity for stick P2-CA was higher than any other stick, and finding a significant difference in shot velocity for stick P2-CA compared to stick P1-CB1 highlights the influence of the blade pattern on shot velocity. The identification of a statistically significant difference between sticks P1-CB1 and P1-CB2 emphasizes the variability present with human testing.

Similar blade velocity profiles were identified for all sticks and the values found for blade velocity at puck impact are comparable to what was found in a previous study. The oscillation of the blade velocity profile, as illustrated in Figure 6.2, tends to support the "puck bounce" phenomenon noticed in previous studies.

The presence of a significant difference in the tensile strain along the Y-direction (ε_{yy}) between sticks P1-CA and P2-CA shows that a difference in dynamic behavior is identifiable depending on the blade pattern tested. Moreover, it has been found that the strain in the X-direction (ε_{xx}) is significantly lower, in absolute value, than ε_{yy} and ε_{xy} , both in compression and tension. This was not visually identifiable, as most of the deformation seemed to occur along the X-direction, and is an interesting consideration for further blade design.

Finally, the effect of subject technique and variability from shot to shot is undeniable. It has been found to have a significant effect on strain delays and has led to important variation in the results obtained.

The player technique has been a source of complication in the recording of quality images, and the angle at which the blade impacts the ice surface has had a great influence on

the results obtained. Despite having an adequate speckle pattern, the variability in blade trajectory and spatial orientation has led to significant error in certain trials, which had to be ignored.

To improve the dynamic testing and reduce image error and variability, the use of a shooting robot, to have consistent shooting technique and blade velocity, would be warranted. The use of such technology would help get consistent results and identify the effects of blade pattern and construction to a greater extent. Reducing the camera's FOV and focusing on a more specific region along the blade would also help increase the accuracy and resolution of the system.

7. Conclusion

To the author's knowledge, this study is the first of its kind to use DIC technique to analyze the dynamic behavior of a moving hockey blade. The study of blade deformation in a slapshot event allows for the stick and blade motion to be studied. No assumptions are made regarding stick or blade behavior, which is often the case in quasi-static test setups where a slapshot motion is replicated as best as possible. This is an important step forward in the study of hockey blade and of dynamic properties, which had not been investigated to this day.

The comparison of static and dynamic testing displacement error showed that they were in good agreement, which confirms the possibility of applying the DIC technique to a moving sample. The application of a specific pattern on a hockey blade was accomplished and great results were obtained, which shows the repeatability of the process and its possible application in and industrial setting. A static testing methodology was also created which allows for the assessment of the displacement accuracy and strain resolution of the imaging system.

Significant differences in blade behavior were noticed based on blade type, and the effects of subject technique on the obtained results were clearly identified. A significant difference in shot velocity was found for two of the sticks, which signifies that a specific blade was found to lead to higher performance for a slap shot event. The blade velocity profiles were similar for all blades, and the presence of "puck bounce" was identified based on oscillation in the blade velocity after puck impact. The strain along the length of the blade was found to be significantly smaller, in absolute value, than both shear strain and strain along the height of the blade. Moreover, the two blades with same construction but different

pattern displayed significantly different strain values along the height of the blade, emphasizing the effect of blade pattern on the blade's dynamic behavior.

7.1. Future Work

Based on the results of this study, a number of approaches can be taken to further improve the knowledge related to dynamic blade behavior:

- Shooting robot Shooting robots have been used in the stick testing industry to assess the durability of the sticks. This type of technology could be used to reduce the variability in technique and shots. It would allow for consistent shots to be taken, which would improve the quality of the results obtained, both in terms of images and extracted data.
- Camera Improving the resolution of the cameras used to capture the images of the blade would improve the displacement accuracy and strain resolution of the system. Increasing the recording speed of the cameras would help reduce the aliasing, which occurs near the toe of the blade. It would also help obtain better precision in the identification of the instant where maximum strains occur, which would make the strain delay measurements more precise as well.
- Region of Interest Focusing on the entire blade leads to a better understanding
 of the full blade behavior, but also reduces the accuracy of the measurements.

 By focusing on a smaller region of the blade, which is of particular interest, the
 accuracy of the system would improve and possibly allow for the identification
 of particular material behavior at a smaller scale.

References

- 1. Turcotte, R., P. Renaud, and D. Pearsall, *Ice Hockey Skate, Stick Design and Performance Measures*, in *The Engineering Approach to Winter Sports*. 2016, Springer. p. 311-326.
- 2. Hoerner, E.F., *The dynamic role played by the ice hockey stick*, in *Safety in ice hockey*. 1989, ASTM International.
- 3. Roy, B. and G. Delisle, Caractéristiques géométriques et dynamiques des bâtons de hockey en regard de leur performance (Geometric and dynamic characteristics of hockey sticks and their effect on performance). Canadian Journal of Applied Sport Sciences, 1984. 9: p. 214-219.
- 4. Bauer Vapor 1X Ice Hockey Stick. Bauer Hockey Corporation: https://www.bauer.com/player-ice-hockey-sticks/vapor/1x-composite-stick.
- 5. Feschuk, D., Evolution of the Hockey Stick, in Toronto Star. 2013.
- 6. Pearsall, D., et al., *The influence of stick stiffness on the performance of ice hockey slap shots.* Sports engineering, 1999. **2**: p. 3-12.
- 7. LeGault, M., Advanced Hockey Stick Design delivers Optimal Performance, in High Performance Composites. 2012, Composites World. p. 62-64.
- 8. Nazar, P.R., Comparison between the curved blade and straight blade hockey sticks on shooting velocity and accuracy in university varsity ice hockey players. 1971: University of Minnesota.
- 9. Marino, G. and C. VanNeck. Static and Dynamic Characteristics of Aluminum versus Wooden Hockey Sticks. in ISBS-Conference Proceedings Archive. 1992.
- 10. Marino, W.G. *Biomechanical investigations of performance characteristics of various types of ice hockey sticks.* in *ISBS-Conference Proceedings Archive.* 1998.
- 11. Kays, B. and L. Smith, *Numerical Simulation of the Ice Hockey Slap Shot*. Procedia Engineering, 2015. **112**: p. 22-27.
- 12. Baroud, G., D. Stefanyshyn, and T. Bellchamber. *Performance enhancements of hockey sticks using numerical simulation*. in *Proceedings of the XVIth Congress of the International Society of Biomechanics (eds Herzog, W. and Jihna, A.)*. 1999.

- 13. Sutton, M.A., J.J. Orteu, and H. Schreier, *Image correlation for shape, motion and deformation measurements: basic concepts, theory and applications.* 2009: Springer Science & Business Media.
- 14. Sutton, M., et al., *Determination of displacements using an improved digital correlation method.* Image and vision computing, 1983. **1**(3): p. 133-139.
- 15. Peters, W., et al., Application of digital correlation methods to rigid body mechanics.

 Optical Engineering, 1983. **22**(6): p. 226738-226738-.
- 16. Chu, T., W. Ranson, and M. Sutton, *Applications of digital-image-correlation techniques* to experimental mechanics. Experimental mechanics, 1985. **25**(3): p. 232-244.
- 17. Morimoto, Y. and M. Fujigaki, *Automated analysis of 3-D shape and surface strain distributions of a moving object using stereo vision*. Optics and lasers in engineering, 1993. **18**(3): p. 195-212.
- 18. Luo, P.F., et al., Accurate measurement of three-dimensional deformations in deformable and rigid bodies using computer vision. Experimental Mechanics, 1993. **33**(2): p. 123-132.
- 19. Robert, L., et al., *Use of 3-D digital image correlation to characterize the mechanical behavior of a fiber reinforced refractory castable.* Experimental Mechanics, 2007. **47**(6): p. 761-773.
- 20. Schmidt, T.E., et al. *Full-field dynamic deformation and strain measurements using high-speed digital cameras.* in *26th International Congress on High-Speed Photography and Photonics*. 2005. International Society for Optics and Photonics.
- 21. Pearsall, D., R. Turcotte, and S. Murphy, *Biomechanics of ice hockey*. Exercise and sport science, 2000. **1**: p. 675-692.
- 22. Lomond, K., R. Turcotte, and D. Pearsall, *Three-dimensional analysis of blade contact in an ice hockey slap shot, in relation to player skill.* Sports Engineering, 2007. **10**(2): p. 87-100.
- 23. Hannon, A., et al., *Dynamic strain profile of the ice hockey stick: comparisons of player calibre and stick shaft stiffness.* Sports Engineering, 2011. **14**(2-4): p. 57-65.
- 24. Wu, T.-C., et al., *The performance of the ice hockey slap and wrist shots: the effects of stick construction and player skill.* Sports Engineering, 2003. **6**(1): p. 31-39.

- 25. Villaseñor, A., R. Turcotte, and D. Pearsall, *Recoil effect of the ice hockey stick during a slap shot*. Journal of applied biomechanics, 2006. **22**(3): p. 202.
- 26. NHL, National Hockey League Official Rules 2015-2016. 2015.
- 27. Anderson, R.L. and L.V. Smith. *Experimental Characterization of Ice Hockey Sticks and Pucks*. in *26th IMAC: Conference and Exposition on Structural Dynamics 2008: IMAC XXVI*. 2008. Orlando, Florida, USA: Society for Experimental Mechanics (SEM).
- 28. Simard, E., et al. *Static and Dynamic Characteristics of Composite One Piece Hockey Sticks*. in *ISBS-Conference Proceedings Archive*. 2004.
- 29. Smith, L. and R. Bigford, Laboratory measurements of ice hockey stick performance. 2009.
- 30. Russell, D. and L. Hunt, Spring Constants for Hockey Sticks. 2009.
- 31. Behrmann, L., et al., *Evaluation of Bending and Torsional Properties of Different Ice Hockey Sticks.* Procedia Engineering, 2014. **72**: p. 332-337.
- 32. Worobets, J., J. Fairbairn, and D. Stefanyshyn, *The influence of shaft stiffness on potential energy and puck speed during wrist and slap shots in ice hockey.* Sports Engineering, 2006. **9**(4): p. 191-200.
- 33. Kays, B. and L. Smith, *Field Measurements of Ice Hockey Stick Performance and Player Motion*. Procedia Engineering, 2014. **72**: p. 563-568.
- 34. Roy, B. and R. Doré. Kinematics of the slap shot in ice hockey as executed by players of different age classifications. in Proceedings of the Fifth International Congress on Biomechanics, Biomechanics VB. 1976.
- 35. Magee, P., et al., Portable strain measurement system for ice hockey sticks 2008.
- 36. Blade Characteristics. Bauer Hockey Corporation: http://issuu.com/bauer-hockey/docs/bauer_stick_fit_guide_2015_en.
- 37. Zane, L., Grip force measures during ice hockey slap and wrist shots, in 17th Biennoal Meeting of the Canadian Society of Biomechanics 2012: Simon Fraser University Burnaby Campus.
- 38. Flemming, A., The dynamic interaction of hand grip and ice hockey stick flexion during slap shots and wrist shots, in Department of Kinesiology and Physical Education. 2014, McGill University.

- 39. *Minimizing Noise and Bias in DIC*. 2013, Correlated Solutions Inc.: http://www.correlatedsolutions.com/support/index.php?/Knowledgebase/Article/View/31/1/minimizing-noise-and-bias-in-dic.
- 40. Lecompte, D., et al., *Quality assessment of speckle patterns for digital image correlation.*Optics and Lasers in Engineering, 2006. **44**(11): p. 1132-1145.
- 41. Reu, P.L. and T.J. Miller, *The application of high-speed digital image correlation*. The Journal of Strain Analysis for Engineering Design, 2008. **43**(8): p. 673-688.
- 42. Tiwari, V., M. Sutton, and S. McNeill, Assessment of high speed imaging systems for 2D and 3D deformation measurements: methodology development and validation. Experimental mechanics, 2007. **47**(4): p. 561-579.
- 43. Miller, T., H. Schreier, and P. Reu. *High-speed DIC data analysis from a shaking camera system.* in *SEM Conference and Exposition on Experimental and Applied Mechanics, Springfield, MA, June.* 2007.
- 44. Siebert, T. and M.J. Crompton. *Application of high speed digital image correlation for vibration mode shape analysis.* in *SEM Annual Conference*. 2010. Indianapolis, IN, USA: Society for Experimental Mechanics Inc.
- 45. *CSI Application Note AN-525 Speckle Pattern Fundamentals*. Correlated Solutions Inc.: https://melab.wikischolars.columbia.edu/file/view/AN525 Speckle Pattern Fundamentals.pdf.
- 46. Lecompte, D., et al. Study and generation of optimal speckle patterns for DIC. in Proceedings of the annual conference and exposition on experimental and applied mechanics. 2007.
- 47. Selezneva, M., Experimental and Theoretical Investigations of Mechanical Properties of Randomly-Oriented Strand (ROS) Composites, in Mechanical Engineering. 2015, McGill University.
- 48. *Photron FASTCAM Mini UX100*. Photron USA, Inc.: http://photron.com/high-speed/cameras/fastcam-mini-ux-100/.

- 49. Kirugulige, M.S., H.V. Tippur, and T.S. Denney, *Measurement of transient deformations using digital image correlation method and high-speed photography: application to dynamic fracture*. Applied Optics, 2007. **46**(22): p. 5083-5096.
- 50. Tiwari, V., et al. Application of digital image correlation in impact testing. in SEM Annual Conference and Exposition on Experimental and Applied Mechanics, Portland, OR, June. 2005.
- 51. Siebert, T., et al., *Error estimations in digital image correlation technique*. Applied Mechanics and Materials, 2007. **7**: p. 265-270.
- 52. *Photron FASTCAM MC2 cube cameras and processor*. Photron USA, Inc.: http://photron.com/wp-content/uploads/2014/10/FASTCAM-MC2-with-2-cubes-and-1-pencil-copy.jpg.
- 53. *Subset, Step Size and Strain Filter Selection* 2014, Correlated Solutions Inc.: http://www.correlatedsolutions.com/support/index.php?/Knowledgebase/Article/View/10/1/subset-step-size-and-strain-filter-selection.

Appendix A: Static Testing Detailed Results

• Blade displacement away from the cameras.

TRIAL 1					
Calibration Score	0.021				
AVG Pixel Error	0.008				
Displacement	Dial Gauge [mm]	VIC-3D [mm]	Difference [µm]	% displacement	
1	-1.805	-1.821	16	-0.88	
2	-2.987	-2.997	10	-0.35	
3	-4.043	-4.238	195	-4.82	
4	-5.136	-5.008	128	-2.50	
5	-6.141	-5.980	161	-2.62	
6	-7.294	-7.117	177	-2.42	
7	-8.192	-7.887	305	-3.72	
		Average	142	2.47	
% Error of Total Displacement			1.73		

TRIAL 2					
Calibration Score	0.03		_		
AVG Pixel Error	0.015				
Displacement	Dial Gauge [mm]	VIC-3D [mm]	Difference [µm]	% displacement	
1	-1.35	-1.626	276	-20.44	
2	-2.188	-2.179	9	-0.40	
3	-3.679	-3.792	113	-3.06	
4	-4.865	-5.196	331	-6.79	
5	-6.023	-6.370	347	-5.76	
6	-7.103	-7.177	74	-1.05	
7	-8.223	-8.125	98	-1.19	
		Average	178	5.53	
% Error of Total Displacement			2.17		

TRIAL 3					
Calibration Score	0.03				
AVG Pixel Error	0.028				
Displacement	Dial Gauge [mm]	VIC-3D [mm]	Difference [µm]	% displacement	
1	-1.369	-1.543	174	-12.74	
2	-2.448	-2.396	52	-2.11	
3	-3.539	-3.621	82	-2.33	
4	-4.585	-4.677	92	-2.01	
5	-5.752	-5.977	225	-3.91	
6	-6.917	-6.879	38	-0.55	
7	-7.885	-7.904	19	-0.24	
		Average	98	3.41	
		% Error of Total Displacement		1.24	

TRIAL 4					
Calibration Score	0.03				
AVG Pixel Error	0.016				
Displacement	Dial Gauge [mm]	VIC-3D [mm]	Difference [µm]	% displacement	
1	-1.458	-1.512	54	-3.73	
2	-2.539	-2.331	208	-8.19	
3	-3.596	-3.109	487	-13.54	
4	-4.617	-4.587	30	-0.64	
5	-5.696	-5.889	193	-3.39	
6	-6.659	-6.574	85	-1.28	
7	-8.204	-8.109	95	-1.15	
		Average	164	4.56	
	% Error of Total Displacement			2.00	

• Blade displacement towards the cameras.

TRIAL 1						
Calibration Score	0.032					
AVG Pixel Error	0.014					
Displacement	Dial Gauge [mm]	VIC-3D [mm]	Difference [μm]	% displacement		
1	1.777	1.527	250	14.09		
2	3.181	3.057	124	3.89		
3	4.153	4.518	365	8.79		
4	5.173	5.323	150	2.90		
5	6.123	6.113	10	0.16		
6	7.182	7.348	166	2.31		
			178	5.36		
		% Error of Tot	2.47			

TRIAL 2						
Calibration Score	0.023					
AVG Pixel Error	0.017					
Displacement	Dial Gauge [mm]	VIC-3D [mm]	Difference [µm]	% displacement		
1	2.008	1.762	246	12.26		
2	3.017	2.639	378	12.54		
3	4.072	4.107	35	0.85		
4	5.095	4.780	315	6.19		
5	6.239	6.344	105	1.69		
6	7.499	7.591	92	1.22		
7	8.448	8.109	339	4.01		
		Average	216	5.54		
% Error of Total Displacement			2.55			

TRIAL 3				
Calibration Score	0.03			
AVG Pixel Error	0.022			
Displacement	Dial Gauge [mm]	VIC-3D [mm]	Difference [µm]	% displacement
1	1.91	2.120	210	10.97
2	3.096	2.773	323	10.44
3	4.385	4.577	192	4.38
4	5.302	5.128	174	3.28
5	6.675	6.477	198	2.96
6	8.137	8.085	52	0.64
7	9.309	9.254	55	0.59
		Average	172	4.75
		% Error of Tot	al Displacement	1.85

TRIAL 4				
Calibration Score	0.034		_	
AVG Pixel Error	0.012			
Displacement	Dial Gauge [mm]	VIC-3D [mm]	Difference [μm]	% displacement
1	1.978	1.999	21	1.08
2	3.027	2.928	99	3.27
3	4.293	4.313	20	0.47
4	5.582	5.717	135	2.42
5	6.759	6.572	187	2.77
6	7.474	7.449	25	0.33
7	9.245	9.295	50	0.54
		Average	77	1.56
		% Error of Tot	tal Displacement	0.83

Appendix B: Pre-Screening Questionnaire and Consent Form

	Subject Number: Testing Time: PRE-SCI	REENING QUESTIONNAIRE	
	Name:		
	Date of Birth:		
	Hockey Experience (years):		
	Highest Level Played:		
	Current Team:		
	Stick Model:		
	Stick Size:		
	Stick Flex:		
	Blade Pattern:		
	Hand that you write with?:		
-	In the past year have you experienced ligaments, groin strain etc.) Have the		
2.	In the past year have you suffered a nerve, numbness or pins and needle explain.	any nervous system injury? (E.g. es, etc.) Has it prevented you from	Concussion, damage to a playing hockey? Please
3.	Is there any other reason why you be	lieve you shouldn't participate in th	nis study? Please explain.



McGill University 475 Pine Avenue West Montreal, Quebec H2W 1S4

ent of Kinesiology and Physical Education Département de kinésiologie et d'éducation physique Université McGill 475 avenue des Pins Ouest Montréal, Québec H2W 154

Tel./Tél.: (514) 398-4184 x0583 Fax/Télécopieur (514) 398-4186

INFORMATION AND CONSENT DOCUMENT

Investigator: Adrien Gerbé, M.Eng. (Mechanical Engineering) Candidate

adrien.gerbe@mail.mcgill.ca

David Pearsall, Ph.D.

david.pearsall@mcgill.ca

Biomechanics Laboratory, Currie Gym Room 402

Department of Kinesiology and Physical Education, McGill University

Statement of Invitation

You are invited to participate in a research project conducted by the above named investigators. This research project will be performed in the Ice Hockey Research Group Laboratory of the Department of Kinesiology and Physical Education, McGill University, located at 475 Pine Ave West, Montréal, Québec H2W 1S4. You will receive no compensation for your participation in this project. You are asked to come to one experimental session that will last approximately 2 hours. We greatly appreciate your interest in our work.

Purpose of the Study

The purpose of this study is to examine the effects of different hockey stick blade construction and geometry on blade deformation and dynamic behavior during a stationary slapshot. specifically, the maximum deformation and its location along the blade, the strain along the major and minor axis of the blade as well as the direction of propagation of the deformation wave along the blade will be studied. In addition, major similarities and differences in shooting techniques will be highlighted.

In order to conduct the research mentioned above, all slapshots executed will be filmed using a custom filming apparatus. The cameras will be focused on the blade, and at no time will your face face, or body, be present in the field of view (within the frame).

The videos and images collected in this study will be published in a research thesis as part of the requirements needed to obtain a Master of Engineering Degree in Mechanical Engineering. The results will also be disseminated through publications in scientific journals and possibly as presentations in conferences.

Your participation in this study involves:

- Providing informed consent prior to the experimental session.
- 2. Providing data concerning your hockey experience and past injuries.
- Carrying out several slap shot trials wearing ice hockey gloves on an artificial ice surface while manipulating a specifically painted hockey stick and a puck.

Risks and Discomforts

It is anticipated that you will encounter no significant discomfort during these experiments. There are no risks associated with these experiments.

There are no personal benefits to be derived from participating in this study. Observations from this study will offer insights as to the effects of different blade constructions and patterns on blade

Research Ethics Board Office (REB I,II, III), James Admin. Bldg. Rm 429, Montreal, QC H3A OG4 tel:514-398-6193 fax:514-398-4644 ;www.mcgill.ca/research/researchers/compliance/human/

(version 01-2013)

deformation during a slapshot. Findings may help developers optimize the construction of the hockey stick, as well as proper stick fitting for players.

Confidentiality

All the personal information collected during the study concerning you will be encoded in order to keep their confidentiality. These records will be maintained at the Biomechanics Laboratory by Dr. David Pearsall for 5 years after the end of the project, and will be destroyed upon the expiration of this time frame. Only members of the research team will be able to access them. In case of presentation, your personal information will remain completely confidential.

Inquiries Concerning this Study

If you require information concerning the study (experimental procedures or other details), please do not hesitate to contact *Adrien Gerbé* at the address or e-mail listed at the top of this document.

Responsibility clause

In accepting to participate in this study, you will not relinquish any of your rights and you will not liberate the researchers nor their sponsors or the institutions involved from any of their legal or professional obligations.

Consent

Please be advised that your participation in this research undertaking is strictly on a voluntary basis, and you may withdraw at any time.

A copy of this form will be given to you before the end of the experimental session.

If you have any questions or concerns regarding your rights or welfare as a participant in this research study, please contact the McGill Ethics Officer at 514-398-6831 or lynda.mcneil@mcgill.ca.

CONSENT

CUDIECT

Analysis of Hockey Blade Deformation Using Digital Image Correlation (DIC)

YOU HAVE RECEIVED AND READ A DETAILED DESCRIPTION OF THE EXPERIMENTAL PROTOCOL. YOU ARE FULLY SATISFIED WITH THE EXPLANATIONS THAT WERE GIVEN TO YOU REGARDING THE NATURE OF THIS RESEARCH PROJECT, INCLUDING THE POTENTIAL RISKS AND DISCOMFORTS RELATED TO YOUR PARTICIPATION IN THIS STUDY.

You are aware that you have the right to withdraw your consent and discontinue your participation at any time without any prejudices.

Please sign below if you agree to participate in this study.		
(Print Name)		
(Signature) Research Ethics Board Office (REB I,II, III), James Admin. Bldg. Rm 429, 1	(Date) Montreal, QC H3A OG4	

Research Ethics Board Office (REB I,II, III), James Admin. Bldg. Rm 429, Montreal, QC H3A OC tel:514-398-6193 fax:514-398-4644; www.mcgill.ca/research/researchers/compliance/human/

(version 01-2013)

RESEARCHER	
(Print Name)	
(Signature)	(Date)